GEOPHYSICS, VOL. 47, NO. 5 (MAY 1982); P. 819–824, 7 FIGS., 4 TABLES.

GL01324

Seismic wave velocity investigation at The Geysers-Clear Lake geothermal field, California

Harsh K. Gupta*, Ronald W. Ward*, and Tzeu-Lie Lin*

ABSTRACT

Analysis of *P*- and *S*-waves from shallow microearthquakes in the vicinity of The Geysers geothermal area, California, recorded by a dense, telemetered seismic array operated by the U.S. Geological Survey (USGS) shows that these phases are easily recognized and traced on record sections to distances of 80 km. Regional average velocities for the upper crust are estimated to be 5.49 ± 0.07 and 2.98 ± 0.07 km/sec for *P*- and *S*-waves, respectively. Poisson's ratio is estimated at 23 locations using Wadati diagrams and is found to vary from 0.13 to 0.32. In general, the Poisson's ratio is found to be lower at the locations close to the steam production zones at The Geysers and Clear Lake volcanic field to the northeast. The low Poisson ratio corresponds to a decrease in *P*-wave velocity in areas of high heat flow. The decrease may be caused by fracturing of the rock and saturation with gas or steam.

INTRODUCTION

The Geysers geothermal area, with current production of 950 MW, is the largest geothermal power producing installation in the world. It is located in northern California in the vicinity of the Clear Lake volcanic system where igneous activity is believed to have occurred in the recent past (Donnelly et al, 1977). The earliest microearthquake investigations at The Geysers geothermal area were carried out by Hamilton and Muffler (1972). They located 53 microearthquakes within 10 km of The Geysers during a three-week period of operation of eight seismograph stations. Most of these earthquakes were located in a 4-km long and 1-km wide zone passing through the geothermal field with the focal depth varying from near-surface to 4 km. Marks et al (1978), using the USGS seismic array, identified two clusters of microearthquakes probably related to two independent pressure sinks resulting from steam production. They found that the earthquakes at The Geysers are confined to depths of less than 5 km, whereas earthquakes along Rodgers Creek and Mayacama faults south and west of The Geysers occur at depths greater than 5 km. In another, more recent seismic study, Bufe et al (1980) deduced tectonic stress orientation and the deep pattern of faulting. From the spatial distribution of earthquakes and their continuous occurrence in The Geysers in contrast to their episodic occurrence outside the production zone, Bufe et al (1980) strongly suggest that The Geysers's seismicity is induced. These observations are consistent with the surface deformation (Lofgren, 1978) and temporal changes in gravity (Isherwood, 1980) reported for the region.

Iyer et al (1979), on the basis of teleseismic delays, inferred molten rocks beneath Mount Hannah and a highly fractured steam reservoir beneath The Geysers. Ward and Young (1980) and Young and Ward (1981) obtained a two-dimensional (2-D) *Q* model of The Geysers-Clear Lake geothermal area using attenuation data of teleseismic events. They found a zone of high attenuation located in the middle crust centered southeast of Mount Hannah. Majer and McEvilly (1979) obtained a regional upper crustal *P*-wave traveltime curve extending to a distance of 45 km using data recorded from two explosions at several seismic stations operating in the vicinity of The Geysers-Clear Lake geothermal field. However, no *S*-wave velocity structure has been determined for the region. We report here our results of *P*- and *S*-wave velocity structure and estimation of the Poisson ratio using microearthquake data recorded by the USGS seismic stations.

THE DATA

The seismic stations and microearthquakes used in the present study are listed in Tables 1 and 2, respectively, and shown in Figure 1. The earthquake magnitude threshold for obtaining a hypocenter is approximately $M = 1.2$, and the location error for a blast fired south of plant no. 12 was only 200 m (Marks et al, 1978). Figure 2 shows a seismogram record section arranged at increasing epicentral distances from top to bottom for event no. 5. Figure 3, a segment of record section for event no. 6, shows *S*-phases.

Identification of *S*-phases on the vertical component instruments requires considerable care to make reliable picks. It is only possible by using dense array data and picking the clear *S*-phase arrivals on the best seismograms. It is then possible to correlate this arrival with those at other stations. The change in amplitude and/or frequency of the arrival aids in making a positive identification. The consistency of these picks for events with nearby hypocenters further supports this approach.

Manuscript received by the Editor August 14, 1980; revised manuscript received July 20, 1981.
*Center for Energy Studies, University of Texas at Dallas, P.O. Box 688, Dallas, TX 75080.

Table 1. Station parameters.

Station		Name	Latitude		Longitude		Elevation (m)
			Degrees	Minutes	Degrees	Minutes	
			North		West		
1	GCM	Cobb Mountain	38	48.45	122	45.31	1286
2	GSS	Skagg Springs	38	42.12	123	.81	282
3	GCV	Cloverdale	38	46.14	123	.89	150
4	GDC	Dry Creek	38	46.03	123	14.31	772
5	GML	McLaughlin Ranch	38	47.56	123	7.80	428
6	GMO	Moffitt Ranch	38	42.61	123	8.59	802
7	GHC	House Creek	38	36.36	123	11.81	518
8	GSM	Socrates Mine	38	46.15	122	46.87	1017
9	GGP	Geyser Park	38	45.88	122	50.65	1054
10	GHL	Highland Springs	39	2.43	123	1.12	956
11	GGL	Glenview	38	53.80	122	46.58	893
12	GPM	Pine Mountains	38	50.85	122	56.78	783
13	GBO	Black Oak	38	49.60	122	50.57	879
14	GMK	Mt. Konoctii	38	58.17	122	47.22	906
15	GSN	Snow Mountain	38	56.43	123	11.50	870
16	GHG	Hog Mountain	39	7.70	122	49.47	903
17	GAX	Alexander Valley	38	42.65	122	45.30	379
18	GRT	Round Top Mountain	38	56.32	122	40.18	619
19	GBG	Boggs	38	48.84	122	40.76	1125
20	GRM	Round Mountain	39	1.23	122	35.06	783
21	GSG	Seigler Mountain	38	52.30	122	42.58	1080
22	GAF	Pt. Arens A.F.B.	38	53.59	123	32.28	710
23	NBR	Beebe Ranch	38	15.65	122	32.99	137
24	NMW	Mi Wuk Village	38	33.03	122	43.37	134
25	NWR	Wright Ranch	38	27.42	122	53.26	50
26	NTM	Taylor Mountain	38	23.15	122	40.83	105
27	NCF	Cornfield Road	38	19.28	122	47.73	98
28	NLN	Lincoln School	38	9.15	122	42.75	120
29	NSH	St. Helena Road	38	31.20	122	36.43	328
30	NSP	Sears Point	38	10.96	122	27.20	88
31	NNX	Mix Canyon	38	24.60	122	3.44	177
32	NHM	Hamilton Ranch	38	9.28	121	48.02	65
33	NCD	Cavedale Road	38	22.19	122	27.70	620
34	CDU	Duarte Ranch	38	1.78	122	.05	168
35	NGV	Green Valley Ranch	38	16.84	122	12.89	257
36	CBW	Brookwood Road	37	55.45	122	6.40	221
37	CAC	Antioch	37	58.57	121	45.62	74
38	NFR	Fort Ross	38	31.36	123	9.66	528
39	NHB	Healdsburg	38	35.36	122	54.54	165
40	NMH	Mt. St. Helens	38	40.17	122	37.93	1311
41	NMT	Middletown	38	48.34	122	26.76	422
42	CRA	San Ramon	37	46.03	121	56.25	171
43	CNC	Norris Canyon Road	37	45.36	121	59.40	306

Table 2. Events used in study.

Event no.	Origin date	Time	Epicenter		Focal depth (km)	Magnitude
			Latitude	Longitude		
	(YYMMDD)		NORTH	EAST		
1	750701	1444	38°41.00′	122°48.80′	6.8	1.1
2	750912	1833	38°43.80′	122°39.00′	5.0	1.1
3	770208	1919	38°56.82′	122°35.35′	4.87	1.12
4	770303	0153	38°42.07′	122°55.40′	5.23	1.27
5	770309	1400	38°47.39′	122°58.38′	5.3	1.40
6	770521	2252	38°45.84′	122°56.56′	5.92	0.86
8	770817	0337	38°47.68′	122°39.00′	7.72	1.05
9	770831	0240	38°40.87′	122°54.15′	6.06	1.20
11	770916	1053	38°39.92′	122°46.32′	5.44	1.31
12	770918	0044	38°39.85′	122°46.30′	5.29	1.00
13	770918	0242	38°40.00′	122°46.23′	5.24	1.17
14	770920	0110	38°47.02′	122°37.85′	7.88	1.46
15	770923	1400	38°39.76′	122°46.27′	5.50	1.24
16	771012	1501	38°40.60′	122°46.25′	5.18	1.44

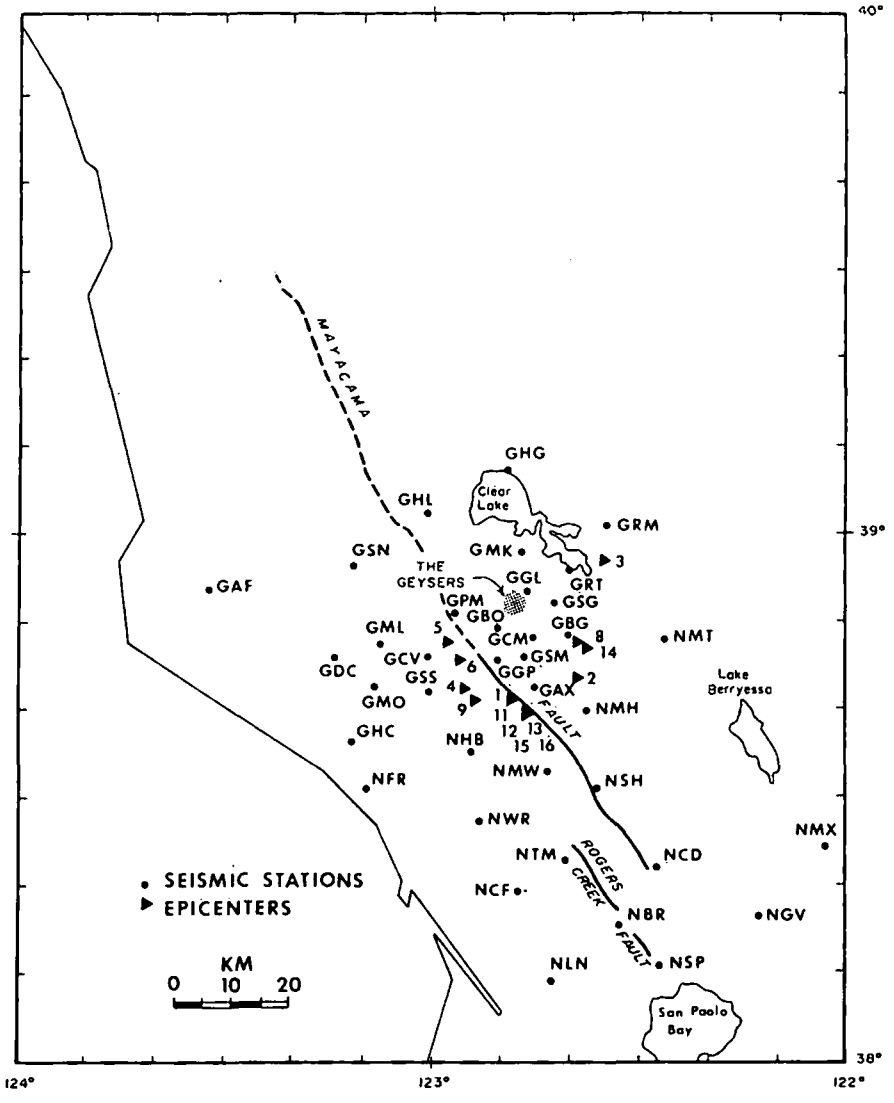

FIG. 1. Map of seismic stations and epicenters used in this study.

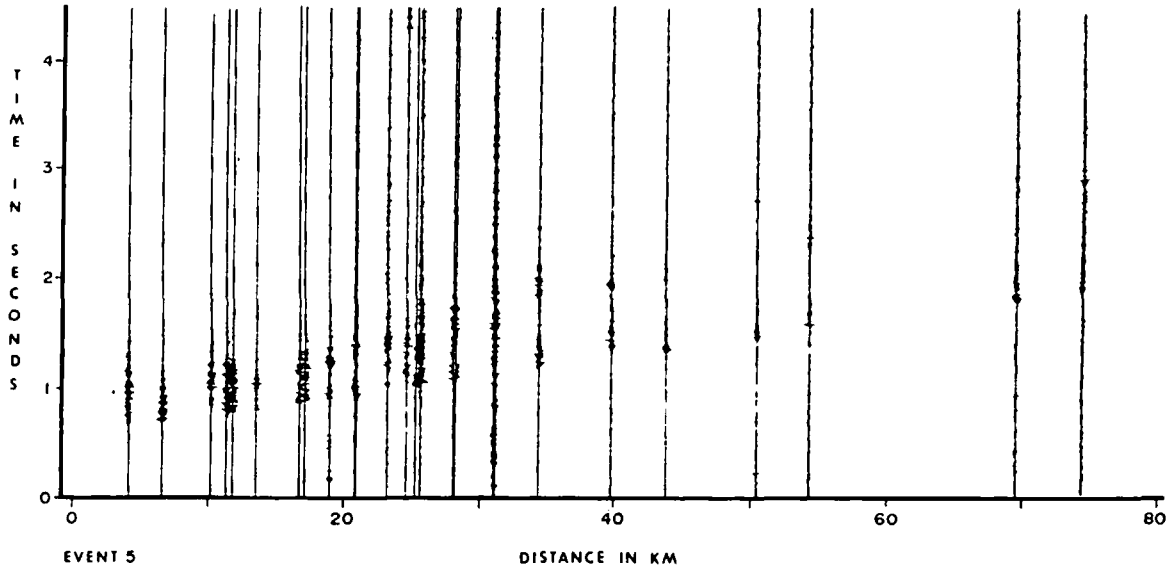

FIG. 2. Typical seismogram record section versus distance for event no. 5.

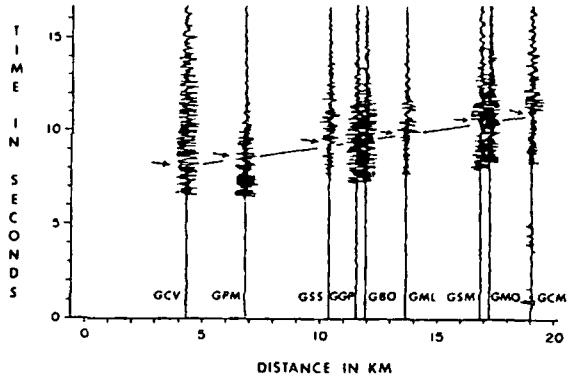

FIG. 3. Segment of seismogram record section versus distance for event no. 6 showing the clarity of the *S*-wave arrival.

REGIONAL *P*- AND *S*-WAVE VELOCITIES

As may be noted from Table 1, seismic stations used in the present study have a considerable variation in their elevations. The highest station NMH (Mount St. Helen) has an elevation of 1311 m, while the lowest station NWR (Wright Ranch) has an elevation of 50 m. Majer and McEvilly (1979) corrected *P*-wave traveltimes to various stations for elevation with respect to a reference station using 4.0 km/sec velocity. We investigated the effect of using various velocities for elevation correction of both *P*- and *S*-wave traveltimes. After a linear least-squares fit of the traveltime residuals, we found that the best results (lowest traveltime residuals) were obtained when no elevation correction was applied. Bufe (personal communication) reached a similar conclusion. Figures 4 and 5 show *P*- and *S*-wave traveltimes versus distance plots for all the events. Most of the data for *P*-waves (159 out of a total population of 166) and all the data for *S*-waves lie in the epicentral distance range of 6 to 45 km. The average velocities for *P*- and *S*-waves, obtained by linear least-squares fit (with focal depth consideration in epicentral distance calculations) are 5.49 ± 0.07 and 2.98 ± 0.07 km/sec, respectively. Majer and McEvilly's (1979) regional traveltime plot shows a break at about 15 km. We divided our traveltime data into two groups, i.e., for epicentral distances less than 15 km and greater than 15 km. Linear least-squares fits were made to these two sets of data. As can be noted in Table 3, for epicentral distances greater than 15 km, the errors are less than 0.10 and 0.12 km/sec for *P*- and *S*-waves, respectively. The large standard deviations of the velocity estimates for distances less than 15 km indicate lateral heterogeneity at shallow depths.

POISSON'S RATIO

Poisson's ratio has been estimated at a few geothermal areas. Combs and Rotstein (1976) estimated a low Poisson's ratio of 0.16 at the Coso Geothermal area, China Lake, California, and inferred that the shallow subsurface is either deficient in liquid water saturation or, more likely, the void spaces are filled with steam. Gupta and Nyman (1977) estimated Poisson's ratio at the East Mesa geothermal field, California. Majer and McEvilly (1979) reported Poisson's ratio at four seismic stations in The Geysers area varying from 0.15 to 0.27.

In this study, Poisson's ratio was estimated for a number of seismic stations using multiple events as well as at a number of hypocenters using multiple seismic station data. The technique used is the construction of a Wadati diagram of *S-P* traveltimes with *P*-wave traveltime (e.g., Majer and McEvilly, 1979). In Figure 6, *S-P* intervals are plotted against *P*-wave traveltime for event no. 5. A straight line is fitted to the data, minimizing the square error. The slope of the line $K - 1$ where $K = V_p/V_s$ gives Poisson's ratio σ by

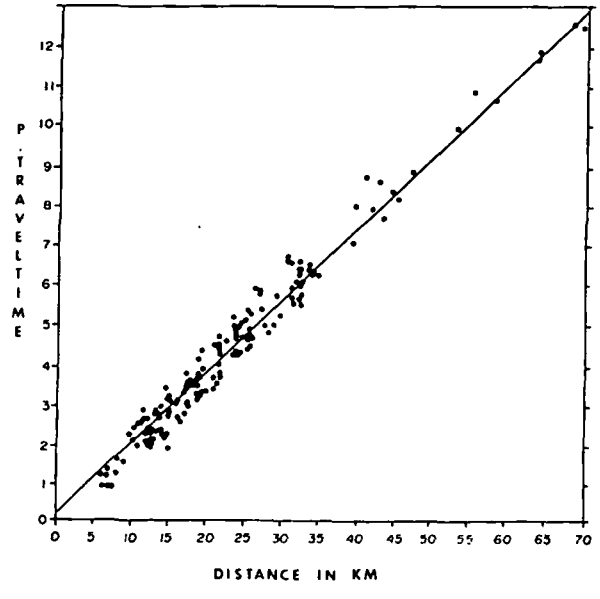

FIG. 4. *P*-wave traveltime versus epicentral distance for all events.

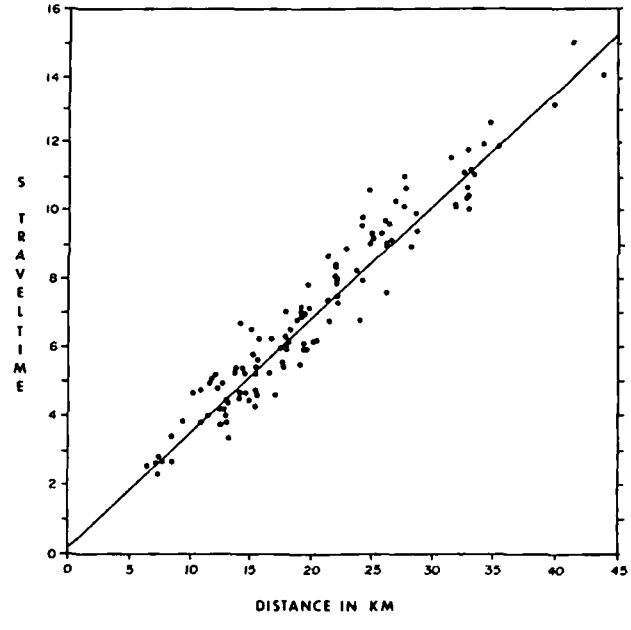

FIG. 5. *S*-wave traveltime versus epicentral distance for all events.

Table 3. Estimates of *P*- and *S*-wave velocities at The Geysers-Clear Lake geothermal field.

P-wave velocities (km/sec)		
Total	$\Delta < 15$ km	$\Delta > 15$ km
5.4945 ± 0.0718	5.2509 ± 0.4665	5.5894 ± 0.0973
S-wave velocities (km/sec)		
Total	$\Delta < 15$ km	$\Delta > 15$ km
2.9867 ± 0.0719	3.1542 ± 0.3392	2.9648 ± 0.1149

Note: The entire data set and subsets of epicentral distances of <15 km and >15 km were used.

Table 4. Poisson's ratio at various locations at The Geysers (Figure 7).

Location	Poisson's ratio	Location	Poisson's ratio
GSM	0.17 (0.11)	NSH	0.123 (−0.06)
GBG	0.13 (0.32)	NMW	0.32 (0.00)
GSG	0.13 (0.63)	NHB	0.28 (−0.06)
GBO	0.15 (0.68)	no. 4	0.22
GCM	0.16 (0.25)	no. 5	0.30
GGP	0.27 (−0.1)	no. 6	0.24
GAX	0.27 (−0.04)	no. 9	0.27
GSS	0.32 (−0.04)	no. 11	0.20
GPM	0.29 (0.12)	no. 12	0.28
GML	0.32	no. 13	0.26
NMH	0.30 (−0.003)	no. 14	0.26
NMT	0.22 (0.12)	no. 15	0.32
		no. 16	0.28

Note: The values within parentheses are average traveltime residuals calculated by Iyer et al (1979).

$$\sigma = \frac{K^2 - 2}{2(K^2 - 1)}.$$

From Figure 6, K is found to be 1.8685, and Poisson's ratio is estimated to be 0.29 from 19 samples, with a goodness of fit of 0.947 and correlation coefficient of 0.973. Poisson's ratio is also estimated using the slope of a linear least-squares error fit of *P*- and *S*-wave traveltime data. Our results are given in Table 4, and the locations of Poisson's ratio estimates are shown in Figure 7. In general, Poisson's ratio is found to be lower at the locations close to the steam production zones at The Geysers and beneath the Clear Lake volcanic field to the northeast. Specifically, the Mercuryville fault separates the zone of low Poisson's ratio to the northeast side from the normal zone on the southwest side of the fault.

CONCLUSIONS

Several interesting and important features of *P*- and *S*-wave traveltimes in the vicinity of The Geysers are presented here. The regional *P*-wave velocity reported here (5.49 ± 0.07 km/sec) is higher than 5.04 km/sec reported by Majer and McEvilly (1979). The *S*-wave velocity for the region, reported for the first time, is 2.98 ± 0.07 km/sec. We used a set of well-distributed earthquakes for these velocity estimates. Poisson's ratios were estimated at 23 locations and found to vary from

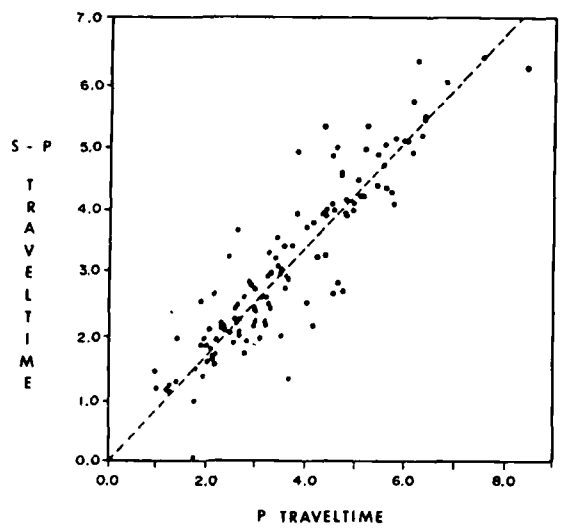

FIG. 6. Wadati diagram of *S-P* traveltime difference versus *P*-wave traveltime for event no. 5.

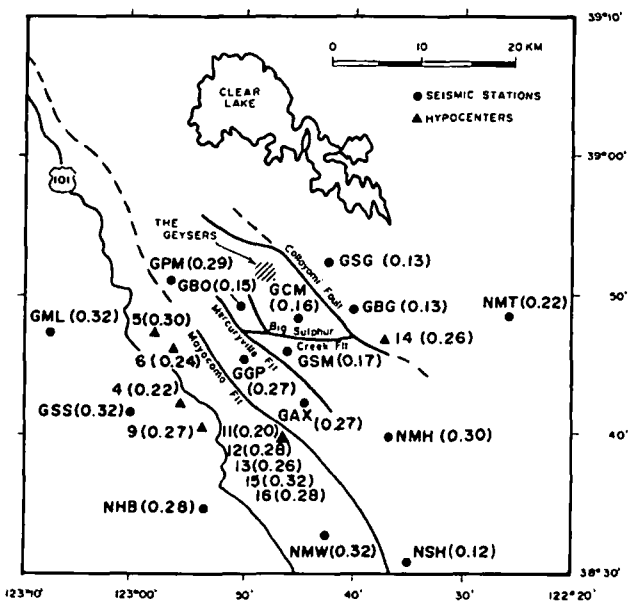

FIG. 7. Map showing Poisson's ratio estimates at seismic stations and epicenters in The Geysers-Clear Lake region.

0.13 to 0.32. Poisson's ratios at locations GBO, GSM, GCM, GSG, and GBG are low (less than 0.2), while at other locations they are normal (larger than 0.2). The low Poisson's ratios appear to be associated with zones of steam production. The Mercuryville fault appears to limit the boundary of the steam reservoir on the southwest. It is interesting to note that seismic stations having low Poisson's ratio are associated, in general, with large teleseismic *P*-wave delays, as reported by Iyer et al (1979), while stations with normal Poisson's ratios do not show significant delays (Table 4). This implies that a local decrease in *P*-velocity is probably responsible for the observed decrease in the Poisson's ratio.

A decrease in *P*-wave velocity with constant *S*-wave velocity results from a change in the compressibility of the rock. Intense fracturing of the upper crust in areas of high heat flow is a plausible explanation based upon analysis of these data. The recording of three-component, more densely spaced arrays may corroborate this preliminary interpretation of the variation of Poisson's ratio.

ACKNOWLEDGMENTS

The data analyzed in this study were provided by W. H. Bakun of the U.S. Geological Survey in Menlo Park, California. Useful discussions were held with Chuck Bufe and H. M. Iyer, also of USGS. Dr. Iyer made several useful suggestions on the manuscript. The calculations were performed at UTD on the Geosciences Program PRIME 550 computer. The assistance of Belle Koblentz, Del Hunt, Janet Garlow, and Elizabeth Partlow in preparing the manuscript is gratefully acknowledged. This research was supported by the U.S. Geological Survey, Dept. of the Interior, under USGS grant no. 14-08-0001-G-426 and the National Science Foundation grant EAR-78-23422.

REFERENCES

Bufe, C. G., Marks, S. M., Lester, F. W., Ludwin, R. S., and Stickney, M. C., 1980, Seismicity of The Geysers-Clear Lake region: U.S.G.S. open file rep.

Combs, J., and Rotstein, Y., 1976, Microearthquake studies at the Coso geothermal area, China Lake, California: Proc. 2nd UN Symp. on the dev. and use of geothermal resources, v. 2, p. 909.

Donnelly, J. M., Hearn, B. C., Jr., and Goff, F. E., 1977, The Clear Lake volcanics, California: Geol. and Field Trip Guide, p. 25.

Gupta, H. K., and Nyman, D., 1977, Short period surface wave dispersion studies in the East Mesa geothermal field, California: Geothermal Res. Council Trans. v. 1, p. 123.

Hamilton, R. M., and Muffler, L. J. P., 1972, Microearthquakes at The Geyser Geothermal Area, California: J. Geophys. Res., v. 77, p. 2081.

Isherwood, W. F., 1980, Geophysical overview of The Geysers, California: U.S.G.S. open file report.

Iyer, H. M., Oppenheimer, D. H., and Hitchcock, T., 1979, Abnormal *P*-wave delays in The Geysers-Clear Lake geothermal area, California: Science, v. 204, p. 495.

Lofgren, B., 1978, Monitoring crustal information in The Geysers-Clear Lake geothermal area, California: U.S.G.S. open file rep.

Majer, E. L., and McEvilly, T. M., 1979, Seismological investigations at The Geysers geothermal field: Geophysics, v. 44, p. 246.

Marks, S. M., Ludwin, R. S., Louie, K. B., and Bufe, C. G., 1978, Seismic monitoring at The Geysers geothermal field, California: U.S.G.S. open file report, no. 78-798, p. 26.

Ward, R. W., and Young, C. Y., 1980, Mapping seismic attenuation within geothermal systems using teleseisms with application to The Geysers-Clear Lake region: J. Geophys. Res., v. 85, p. 5227–5236.

Young, C. Y., and Ward, R. W., 1981, Attenuation of teleseismic *P*-waves in The Geysers-Clear Lake region, California: U.S.G.S. Prof. Paper, no. 1141.

GEOPHYSICS, VOL. 44, NO. 6 (JUNE 1979); P. 1097–1115, 15 FIGS.

Same

Microseisms in geothermal exploration—studies in Grass Valley, Nevada

Alfred L. Liaw* and T. V. McEvilly‡

Frequency(f)-wavenumber(k) spectra of seismic noise in the bands $1 \leq f \leq 10$ Hz in frequency and $|k| \leq 35.7$ cycles/km in wavenumber, measured at several places in Grass Valley, Nevada, exhibit numerous features which can be correlated with variations in surface geology and sources associated with hot spring activity. Exploration techniques for geothermal reservoirs, based upon the spatial distribution of the amplitude and frequency characteristics of short-period seismic noise, are applied and evaluated in a field program at this potential geothermal area.

A detailed investigation of the spatial and temporal characteristics of the noise field was made to guide subsequent data acquisition and processing. Contour maps of normalized noise level derived from judiciously sampled data are dominated by the hot spring noise source and the generally high noise levels outlining the regions of thick alluvium. Major faults are evident when they produce a shallow lateral contrast in rock properties. Conventional seismic noise mapping techniques cannot differentiate noise anomalies due to buried seismic sources from those due to shallow geologic effects. The noise radiating from a deep reservoir ought to be evident as body waves of high-phase velocity with time-invariant source azimuth. A small two-dimensional (2-D) array was placed at 16 locations in the region to map propagation parameters. The f-k spectra reveal shallow local sources, but no evidence for a significant body wave component in the noise field was found.

With proper data sampling, array processing provides a powerful method for mapping the horizontal component of the vector wavenumber of the noise field. This information, along with the accurate velocity structure, will allow ray tracing to locate a source region of radiating microseisms. In Grass Valley, and probably in most areas of sedimentary cover, the 2–10 Hz microseismic field is predominantly fundamental-mode Rayleigh waves controlled by the very shallow structure.

INTRODUCTION

Two methods have been proposed to utilize microseisms for delineating geothermal reservoirs. The first is based on the speculation that hydrothermal processes deep in the reservoir radiate seismic wave energy in the frequency band 1 to 100 Hz. If this phenomenon exists, the exploration method becomes a rather straightforward "listening" survey, using stations on a 0.5- to 2-km grid. Contours of noise power on the surface should delineate noise sources. This is the "standard" noise survey used widely in geothermal exploration. A second approach interprets the noise field as propagating elastic waves of appropriate type, e.g., fundamental-mode Rayleigh waves, and inverts their propagation characteristics to obtain the distribution of medium properties, i.e., velocity and attenuation, both laterally and vertically. The propagation parameters of ambient microseisms

Presented at the 46th Annual International SEG Meeting October 28, 1976 in Houston, Texas. Manuscript received by the Editor July 19, 1977; revised manuscript received November 10, 1978.
*Res. and Dev. Dept., ARCO Oil and Gas Co., P.O. Box 2819, Dallas, TX 75221; formerly Engineering Geoscience, University of California, Berkeley, CA 94720.
‡Seismograph Station, Dept. of Geology and Geophysics, University of California, Berkeley, CA 94620.
0016-8033/79/0601—1097$03.00.

so measured will also locate distinctive radiation sources. With sufficient knowledge of the wave nature of the microseisms and a reasonably accurate velocity-depth model, a fixed nonaliased array can be used in a beam-steering mode to define the source region of radiated noise. Both approaches, as used in typical surveys, suffer greatly when data are contaminated by nongeothermal seismic noise, by interfering seismic wave trains, or by improper temporal and spatial data sampling. These pervasive problems have combined to render noise analysis at best a qualitative geophysical method and have substantially limited the acceptance of the seismic noise survey as an integral element in geothermal exploration.

This study attempts to avoid such problems through careful analysis of microseismic data in an evaluation of the feasibility of ground noise studies in geothermal site delineation. We report a series of investigations undertaken near Leach Hot Springs in Grass Valley, within the region of generally high heat flow in northern Nevada. We first quantify the spatial and temporal variations of ground noise in the region and find that the seismic noise spectrum is strongly affected by near-surface sedimentary layers at the recording site. In fact, with broadband seismic sensors in a mapping technique using amplitudes and frequencies, one can outline lateral variations in alluvial thickness. This standard mapping technique cannot differentiate noise enhancement due to shallow structure from noise enhancement due to a buried seismic source. On the other hand, we find that the mapping of wave propagation parameters provides additional information about the noise field. However, the successful application of this technique requires some understanding of the wave nature of microseisms. We used multiple-sensor arrays to study the seismic coherency as a function of frequency and spatial separation. Based on this information, an array was designed to record propagating microseismic data. The array data were processed by both the frequency domain beamforming method (BFM) and the maximum-likelihood method (MLM). From the dispersion curves obtained in the array study, it was verified that the seismic noise consists primarily of fundamental-mode Rayleigh waves.

This paper consists of several sections describing the methodology, the area studied, the data, its interpretation, and recommendations. This study together with other detailed geologic, geochemical, and geophysical studies carried out in the area provide all the ingredients, except the test wells, for a complete case history on a geothermal prospect.

GEOTHERMAL GROUND NOISE

Clacy (1968) first suggested that seismic noise increased near geothermal reservoirs. His first results northeast of Lake Taupo, New Zealand, were based on contours of total noise amplitude in the frequency band of 1 to 20 Hz. In subsequent surveys at Wairakei, Waiotapu, and Broadlands geothermal areas, he found that the local noise amplitude anomalies were characterized by a dominant frequency of 2 Hz, whereas, away from the area of the anomaly, frequencies higher than 3 Hz predominated. On the other hand, Whiteford (1970) found in repeat surveys of the same areas that neither the shape of the frequency spectrum nor its dominant frequency conformed to any regional pattern. Whiteford measured the absolute ground motion in the Waiotapu geothermal area and found that, within a distance of 1 to 2 km of the high heat flow area, the average minimum ground particle velocity was greater than 150×10^{-9} m/sec, while farther away the amplitude of the ground movement decreased by a factor of about 3 and, in addition, exhibited pronounced diurnal variations.

In the United States, a similar survey was first carried out southeast of the Salton Sea by Goforth et al (1972) who suggested for geothermal reservoirs an empirical relationship between high-temperature gradient and high seismic noise level. Their results showed a significant increase in the noise power in the frequency band of 1 to 3 Hz at sites above the reservoir. They estimated the power spectrum at each site from ten 200-sec data segments taken over eight hours of nighttime recording. The contour map of the total power in the frequency band of 1 to 3 Hz was similar to the temperature gradient contour map. Douze and Sorrells (1972) conducted a similar survey over the nearby East Mesa area, where they found that the total seismic power in the 3 to 5 Hz band exhibited spatial variations similar, in general, to gravity and heat flow fields. East Mesa was later surveyed by Iyer (1974) with significantly different results. Iyer measured seismic noise by averaging 20 of the lowest values of the root-mean-square (rms) amplitude in several narrow frequency bands, using data blocks of 81.92 sec selected from four hours of digital data. He did not find an anomaly in seismic noise associated with geothermal activity but only the noise from canals and freeway traffic.

The seismic pulsation associated with several geysers in Yellowstone National Park is believed to be indicative of the heating of water in the underground reservoir and the eruption triggered by the

superheated system. Nicholls and Rinehart (1967) have studied the seismic signature of several geysers in the park and inferred that their predominant pulse frequencies are quite similar, in the range of 20–60 Hz, presumably due to steam action. The very low-frequency seismic pulses recorded at Old Faithful, Castle, Bead, Plume, and Jewel geysers are believed to be associated with some type of water movement. The maximum amplitude of seismic pulses recorded in Yellowstone Park is 5.08×10^{-5} m/sec. At Old Faithful Geyser, the maximum amplitude is 2.54×10^{-5} m/sec at 30–50 Hz.

Iyer and Hitchcock (1974) also found good correlation between geothermal activity and high seismic noise levels in the 1 to 26 Hz range in the Park. The ground noise level in nongeothermal areas of the Park is approximately 13 to 15×10^{-9} m/sec at 1 to 26 Hz. In the Lower and Upper Geyser Basins where there are numerous geysers and hot springs, the average noise level is in general higher than $50 \times$

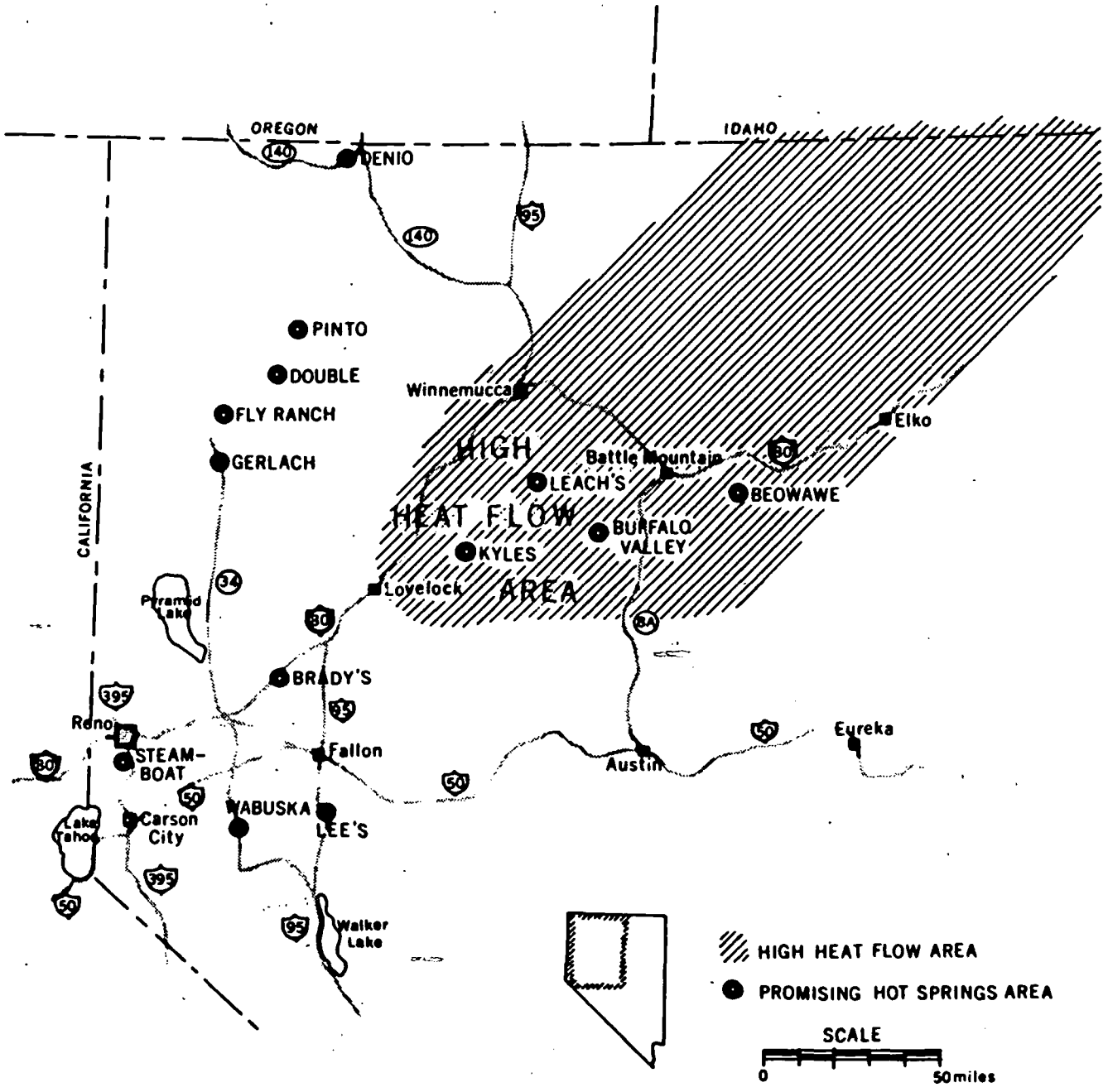

FIG. 1. Prominent thermal springs areas and the Battle Mountain high heat flow region in Northwestern Nevada. Shaded area indicates high heat flow area.

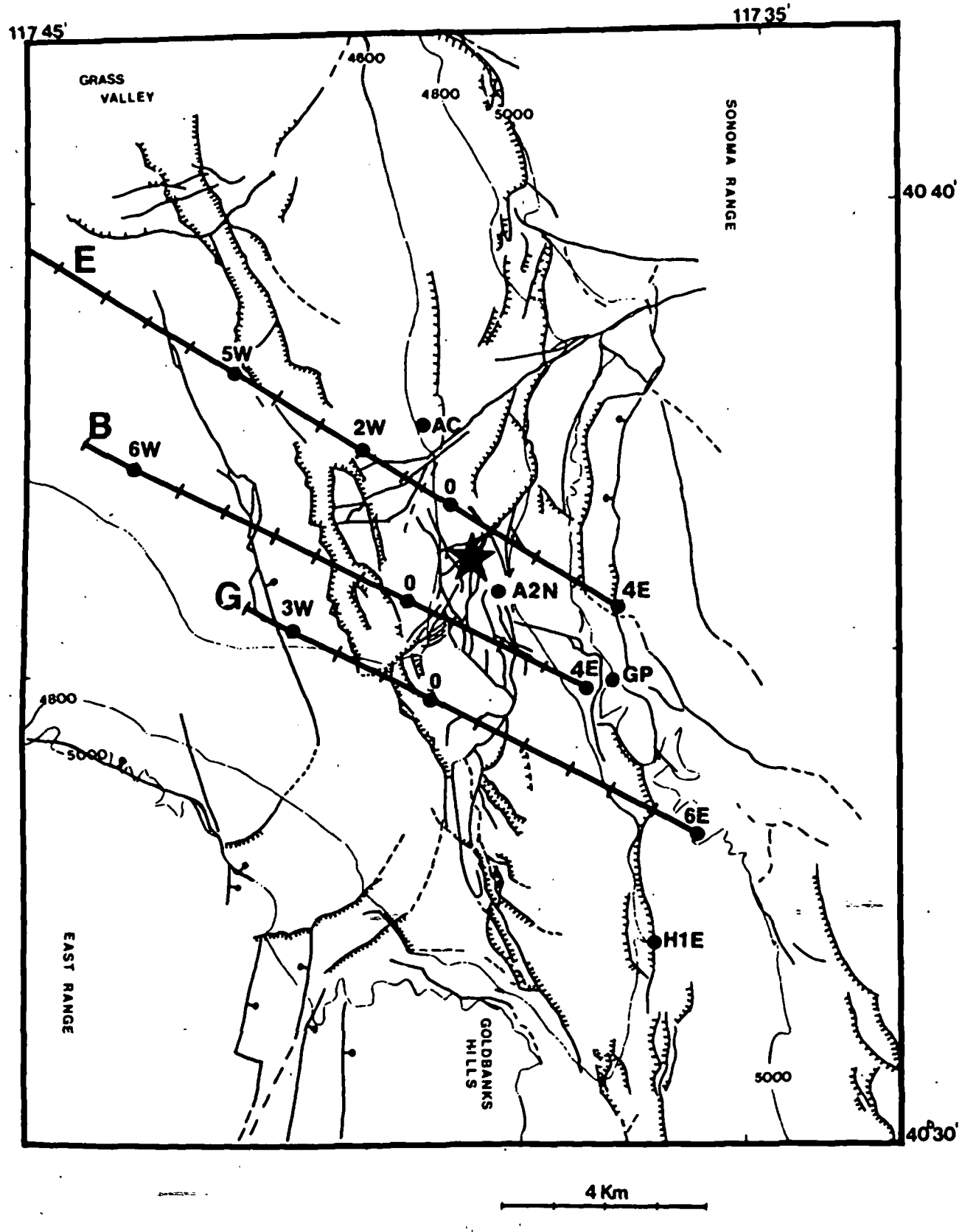

FIG. 2. Mapped faults and pertinent geophysical traverses in the Leach Hot Springs area. Hachured lines indicate down-faulted sides of scarplets; ball symbols indicate downthrown side of other faults. Star shows location of Leach Hot Springs. Heavy solid lines are survey lines E, B, and G with tick marks every 1 km.

10^{-9} m/sec and reaches a value of 672×10^{-9} m/sec near Old Faithful. In the Norris Basin, another highly active geyser basin in the Park, the noise level varies from 50 to 500×10^{-9} m/sec. Part of the observed noise in the Lower, Upper, and Norris Geyser Basins is no doubt generated by the hydrothermal activity at the surface. The measurements near Old Faithful indicate that high-frequency noise, in the 8 to 16 Hz band, is generated during geyser eruptions; the noise level of lower frequencies is not affected by the eruption cycles. Noise levels around Mammoth Hot Springs are two to five times higher than in the surrounding area. There is no geyser or fumarole here, and the geothermal water is relatively cooler than at Norris and the other geyser basins. Hence, it is very unlikely that the seismic noise observed here is generated near the surface. The noise anomaly observed in the area between Lower Falls and Mud Volcano could be caused by ground amplification effects in the soft sedimentary deposits.

Correlations have also been reported between geothermal activity and high seismic ground noise in the Vulcano Islands, Italy (Luongo and Rapolla, 1973), the Coso geothermal area, China Lake, California (Combs and Rotstein, 1975), and Long Valley, California (Iyer and Hitchcock, 1976). High-frequency noise ($f > 8$ Hz) in the vicinity of geysers. fumaroles, and hot springs is associated with hydrothermal activity near the surface and during the geyser eruption. Low-frequency noise ($f < 8$ Hz) is not affected by geyser eruption cycles and is probably generated at depth.

It is evident that a noise power anomaly may result not only from an active seismic source, but also from lateral variation in near-surface velocity, particularly where low-velocity alluvium is involved. In order to identify a buried radiating source, the direction of propagation and the apparent phase velocity of the coherent noise field must be utilized. Whiteford (1975) successfully located the noise source in the Wairakei area using tripartite geophone array measurements. Iyer and Hitchcock (1976) used an L-shaped array with 106-m geophone spacing in Long Valley and found that propagation azimuths for the high-velocity waves defined the area of surface geothermal phenomena, but they found that random directions of propagation were characteristic of low-velocity waves.

Azimuth and apparent velocity measurements are complicated for microseisms because of multipath arrivals and nonstationary characteristics. In addition, very short wavelengths (10–20 m) can characterize the noise field in areas of low-velocity surface materials, and these are often aliased to lower wavenumber (longer wavelengths, higher velocities) and misinterpreted if array geophone spacing is too large.

MICROSEISMS

The study of microseisms, or earth noise, has been directed primarily toward frequencies less than 0.5 Hz, where the source is either ocean waves associated with storms (Longuet-Higgins, 1950; Gutenberg, 1958; Oliver, 1962; Oliver and Ewing, 1957; Oliver and Page, 1963; Haubrich and Mackenzie, 1965; Haubrich and McCamy, 1969; Fix, 1972) or atmospheric disturbances (Sorrells et al, 1971; Savino et al, 1972). Background microseism spectra for the range 0.02 to 1 Hz are characterized by two maxima at frequencies near 0.071 and 0.143 Hz (periods of 14 and 7 sec), both apparently due to coastal storm effects. In the period range beyond about 3 sec, local atmospheric pressure changes contribute primarily to the microseisms observed.

High-frequency microseisms ($f > 0.5$ Hz) observed away from the coast are generated locally by cultural activity, traffic, wind, rivers (Wilson, 1953; Robertson, 1965; Iyer and Hitchcock, 1974), by geothermal processes, and by distant sources (Lacoss et al, 1969). Noise observed at the ground surface usually consists principally of fundamental-mode Rayleigh waves. At depths where the fundamental mode has decreased to negligible amplitude, the noise consists of Rayleigh modes of order higher than third, or of body waves (Douze, 1967). Sharp spectral peaks and troughs can be related to shallow geologic structure. Low-velocity alluvium or weathering can produce a significant amplitude increase of seismic noise over that observed at a bedrock site. Thus, the shallow section can provide a waveguide for microseisms at particular frequencies (Kanai and Tanaka, 1961; Sax and Hartenberger, 1965; Katz, 1976; Iyer and Hitchcock, 1976). Certain sources of microseisms, such as waterfalls or pipelines, can produce narrow-band radiation. Near the Owens River at Long Valley, California, Iyer and Hitchcock (1976) report that the flowing river generates noise at frequencies above 6 Hz, attenuated by about 12 dB at 1 km from the river. At East Mesa, California, the canals seem to be continuous wide-band sources of seismic noise which drops off rapidly with distance, reaching a fairly steady level at 3 km. At the power drops (small waterfalls) along the canal, however,

intense noise is seen in a narrow frequency band around 2.5 Hz (Iyer, 1974).

AREA OF STUDY

Leach Hot Springs in Grass Valley, Nevada is located 30 km south of Winnemucca (Figure 1). Grass Valley is a typical valley of the Basin and Range province with normal faulting, major earthquakes, and hot springs occurring along the valley margins. The valley is bounded by the Sonoma and Tobin Ranges to the east and the basalt-capped East Range to the west. The valley narrows south of the hot springs as it approaches the Goldbanks Hills (Figure 2). These ranges are composed of Paleozoic sedimentary rocks or Triassic siliceous clastic and carbonate rocks. Some granitic intrusions, probably of

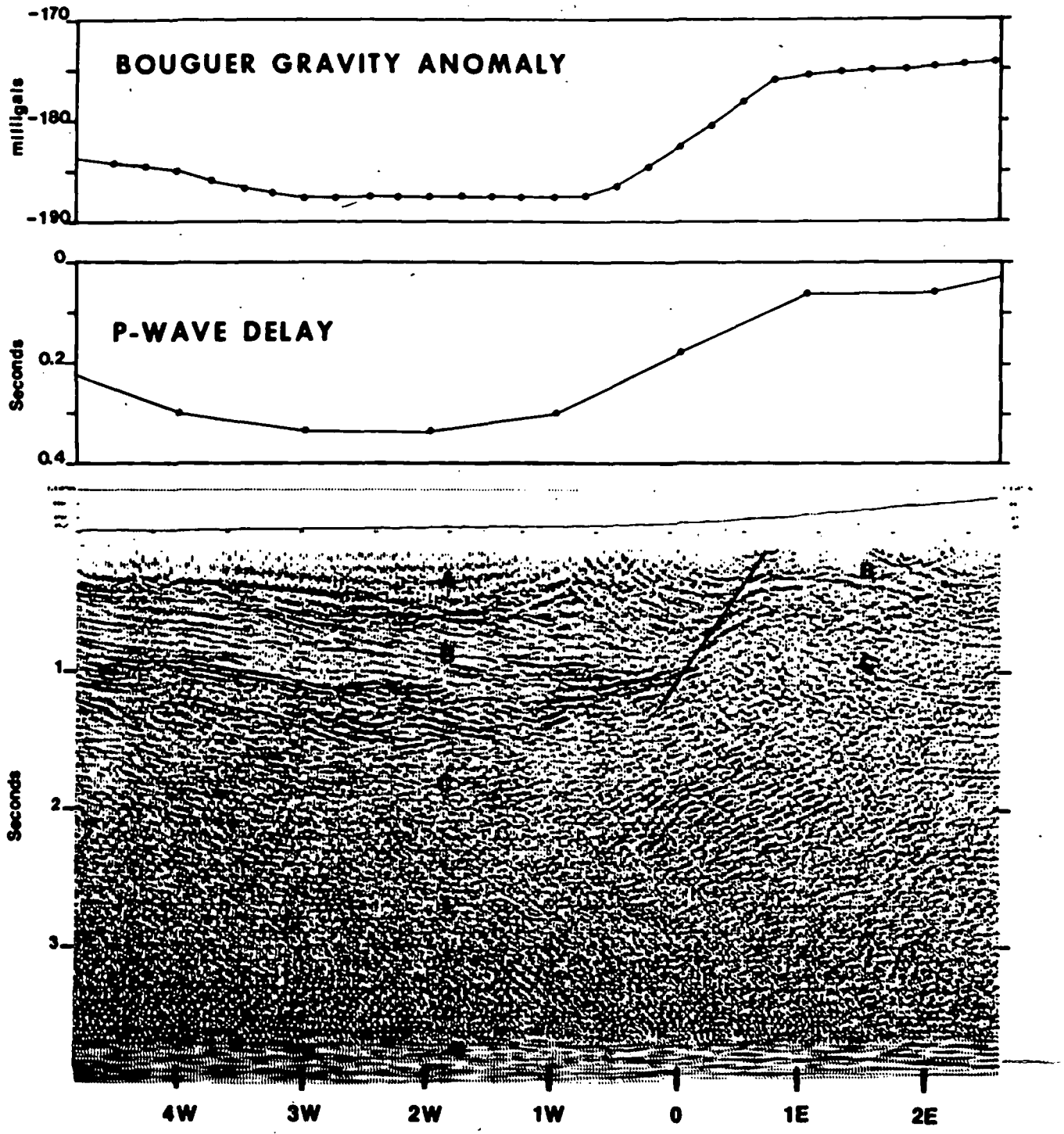

FIG. 3. Profiles for line E, 5W to 3E, of Bouguer gravity anomaly, *P*-wave delay, and migrated seismic reflection section, showing east margin fault (trace at 1E) and maximum sediment thickness near 2W. Averaged section velocities are: (a) 1.8 km/sec, Quaternary alluvium; (b) 2.9 km/sec, Tertiary sediments; and (c) 4.0 km/sec, Paleozoic rocks.

Triassic origin, have offset rock units of several tens to several hundreds of meters measured vertically. As shown on the fault and lineament map (Figure 2), the present day hot springs occur at the intersection of a major northeast-trending fault and the more common north-northwest/south-southeast trending lineament on the eastern side of the valley.

Leach Hot Springs is within the high heat flow area of northern Nevada indicated in Figure 1. This high heat flow area is often called the "Battle Mountain high" (Sass et al, 1971) and exhibits heat flow values in the range of 1.5 to 3.5 HFU (1 HFU = 10 cal/m^2 sec). The diffuse region of elevated heat flow over the Basin and Range province is generally thought to be an expression of high temperature in the lower crust and upper mantle, and it seems reasonable to interpret the localized Battle Mountain high as an effect of fairly recent intrusion of magma into the earth's crust. Quaternary volcanism within the province supports this hypothesis.

Geophysical data were obtained primarily along 17 survey lines, although not all methods were employed on every line. Line E (Figure 2) is typical. Bouguer gravity anomaly, P-wave delay data, and seismic reflection data, presented in Figure 3 for line E, indicate that the greatest thickness of sediments and major faulting occur near the eastern valley margin. The major lithologic units from the seismic reflection section are Quaternary alluvium (1.8 km/sec), Tertiary sedimentary and volcanic rocks (2.9 km/sec), Paleozoic rocks (4.0 km/sec), and deep basement (5.0 km/sec), respectively. The basement surface rises gently to the west but is apparently upthrown at the eastern boundary faults.

A low apparent resistivity zone beneath 2W–4W on Line E (Figure 2) (Beyer et al, 1976), found in the dipole-dipole resistivity survey, has been identified with Tertiary sediments. Since the heat flow value in this zone is not high by Battle Mountain standards (2.24 HFU), the accumulation of conductive sediments, such as ancient playa deposits in the deepest portion of the valley, is probably responsible for the resistivity anomaly. More details of the geophysical data obtained in the Grass Valley area are given by Beyer et al (1976).

DATA ACQUISITION AND PROCESSING

A portable seismic network, with up to 12 stations linked by radio telemetry to a recording system mounted in a small, two-wheeled trailer, was designed for simplicity, flexibility, and ease of installation. It proved possible for two men to deploy the sensors and test the telemetry in about one day. Ease of network emplacement made it possible to modify the array as data were collected and to design field experiments with multiple objectives.

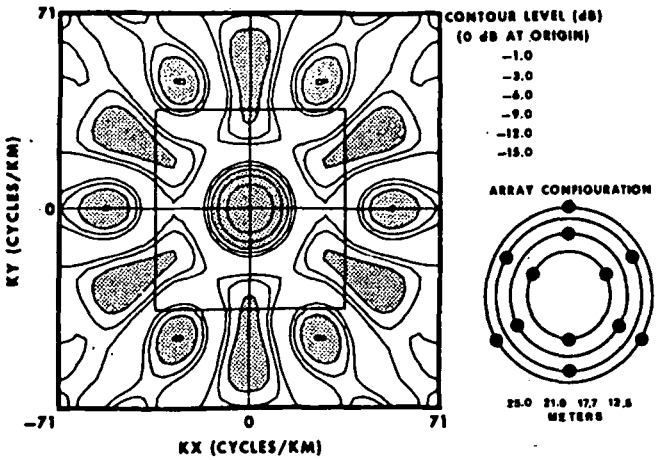

FIG. 4. Array configuration and its contoured impulse response in wavenumber space, plotted to k_x and $k_y = 71$ cycles/km. The effective Nyquist wavenumber can be seen to vary with azimuth in the range of approximately 50–70 cycles/km. The interior square outlines the standard wavenumber plot range of 35.7 cycles/km used in subsequent figures. Radii of the array concentric circles are given.

A 4.5-Hz vertical-component geophone, a high-gain amplifier (60–120 dB), a voltage controlled oscillator, and a radio transmitter constituted the station site equipment. A 0.1-watt transmitter gave a range of about 20 km for average topography. In applications using all 12 geophones spaced over a small aperture array (50-m diameter), the radio links were eliminated and signals were transmitted by cable to the recording trailer. The trailer housed the radio receivers, FM discriminators, a 14-channel slow-speed FM tape recorder (0.12 ips, 0–40 Hz; or 0.24 ips, 0–80 Hz), timing system, and batteries. A slow-speed smoked-paper recorder was used as a monitor. The system had about 40 dB dynamic range (peak-to-peak measurement), limited primarily by the tape recorder.

To study the spatial variations of ground noise amplitude, we occupied a reference site at E2W (line E, station 2W in Figure 2) throughout the survey period. Normally we recorded overnight, with stations spaced at 1-km intervals along the survey lines. The smoked-paper monitor record was observed every morning to verify the occurrence of low seismic noise level at the reference site; otherwise, the sites were reoccupied another night, until low-noise conditions prevailed. Geophones were buried about one

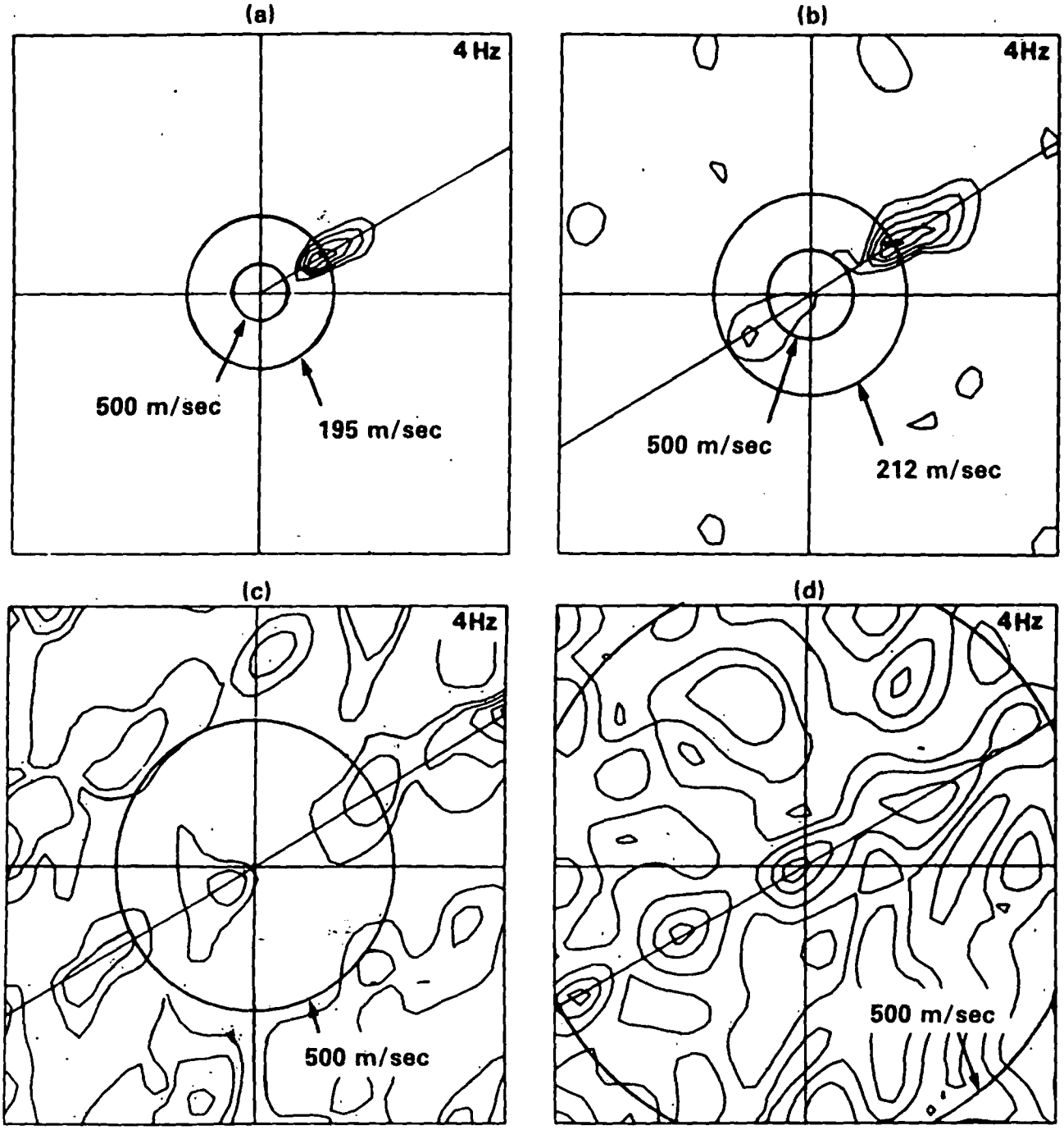

FIG. 5. High-resolution f-k power spectral density estimates for a simulated 4-Hz plane wave signal propagating N60° E across the array at phase velocity 200 m/sec (k = 20 cycles/km) to illustrate spatial aliasing. The array configuration is as shown in Figure 4, with dimensions scaled (a) 1, (b) 1.5, (c) 5, and (d) 10 times the radii values indicated in Figure 4. The maximum k_x and k_y values in the plots are (a) 71.4, (b) 47.6, (c) 14.3, and (d) 7.1 cycles/km corresponding approximately to the effective Nyquist wavenumbers for the arrays. The f-k power spectral density contours are −1.0, −3.0, −6.0, −9.0, and −12.0 dB below the main peak. Circles indicate the constant velocities shown, expanding with array size. Aliasing is apparent in the high phase velocities in (b), (c), and (d), easily misinterpreted as detected body waves.

foot below the surface. Before and after a survey, all geophones were buried in a common hole to verify uniformity of their responses.

For determination of spatial variation of wavenumber, an array of 12 closely spaced geophones was emplaced at a site each evening. Data were transmitted by cable to the recording vehicle some 500 m from the array. The array configuration and its impulse response in wavenumber space are shown in Figure 4. The existence of short-wavelength noise components and the low coherence seen at large geophone separation both dictated the tight array spacing used. An array of 100-m element separation or more, commonly used in ground noise studies elsewhere, would give spurious results because spatial aliasing folds the high-wavenumber noise components (which we have seen dominant in the valley alluvium) into low-wavenumber noise components. The spatial aliasing results in the appearance of erroneously high-velocity ground noise, which is interpreted as body waves. The effect of spatial aliasing due to inadequate element separation is illustrated in Figure 5, where we processed a simulated 4 Hz plane wave with 50-m wavelength, propagating with phase velocity of 200 m/sec in the direction N60°E across four arrays. Those arrays have identical array shapes and numbers of sensors but different sensor spacing. The diameters of the arrays are 50, 75, 250, and 500 m, such that the sensor spacing for each array is proportional to the array size. Since the plane waves are propagating at an azimuth of 60 degrees, the folding effects are evident along the directions of 60 degrees and 240 degrees. Many interpretations of microseisms as body waves, based on coarse sensor separation, may well be incorrect due to aliased low-velocity surface waves as seen, for example, in Figure 5c. It is true, of course, that when the array is made small enough to accommodate the short-wavelength noise characteristics, resolution for near-vertically incident body waves is degraded seriously; however, they could be enhanced by appropriate array expansion and spatial filtering.

For determination of the spatial variation of amplitude, data were selected judiciously from the quietest recording period in the early morning hours. At least 28 simultaneously recorded blocks of data were chosen from each of the recording stations, avoiding any spurious transient signals. Each data block of 12.8 sec length was filtered and digitized. The resulting 512-point records were tapered to zero at each end over 51 points and Fourier transformed. The Fourier transform was multiplied by its complex conjugate to produce power spectral density. The estimated power spectral density at each location is the average over at least 28 data blocks, to increase statistical confidence. The ground velocity spectral density (VSD) in $m\mu/\text{sec}/\sqrt{\text{Hz}}$ was obtained by taking the square root of the power spectral density estimate and correcting it for system response. The relative intrinsic noise level, in dB, for a particular frequency band at a station is obtained by integrating the velocity spectral density over the frequency band and normalizing by that quantity at the reference station.

For estimation of the frequency(f)-wavenumber (k) power spectral density, array data were processed by using both the frequency domain beam-forming method (BFM) (Lacoss et al, 1969) and the maximum-likelihood method (MLM) (Capon, 1969). The BFM estimates f-k power spectral density by the formula

$$\hat{P}(f,\mathbf{k}) = \frac{1}{N^2}\,\mathbf{a}'\cdot\hat{\mathbf{S}}\cdot\mathbf{a}, \tag{1}$$

where $\hat{P}(f,\mathbf{k})$ is BFM f-k power spectral density estimate, N is the number of geophones in the array, $\mathbf{S}$ is the estimate of the coherent power spectral density matrix between sensors, and $\mathbf{a}'$, the conjugate transpose of $\mathbf{a}$, is given by

$$[\exp(i2\pi\mathbf{k}\cdot\mathbf{r}),\ \exp(i2\pi\mathbf{k}\cdot\mathbf{r}_2),\ \ldots,\ \exp(i2\pi\mathbf{k}\cdot\mathbf{r}_N)], \tag{2}$$

where $\mathbf{r}_n$ is the coordinate of the nth geophone location. Each entry of $\hat{\mathbf{S}}$, $\hat{S}_{ln}(f)$, is obtained from

$$S_{ln}(f) = \frac{1}{M}\sum_{m=1}^{M}\Phi_{lm}(f)\,\Phi^*_{nm}(f), \tag{3}$$

by the normalization

$$\hat{S}_{ln}(f) = \frac{S_{ln}(f)}{\sqrt{S_{ll}(f)S_{nn}(f)}}, \tag{4}$$

where $\Phi_{lm}(f)$ are the Fourier coefficients of the mth block time series from the lth geophone, and * indicates complex conjugate.

BFM is commonly called a conventional method, whose operation can be seen by rearranging equation (1) to be

$$P(f,\mathbf{k}) = \frac{1}{N^2}\sum_{n=1}^{N}\sum_{l=1}^{N}\hat{S}_{ln}(f)\cdot \cdot\exp[-i2\pi\mathbf{k}\cdot(\mathbf{r}_l-\mathbf{r}_n)]. \tag{5}$$

For BFM, a uniform weighting function is applied

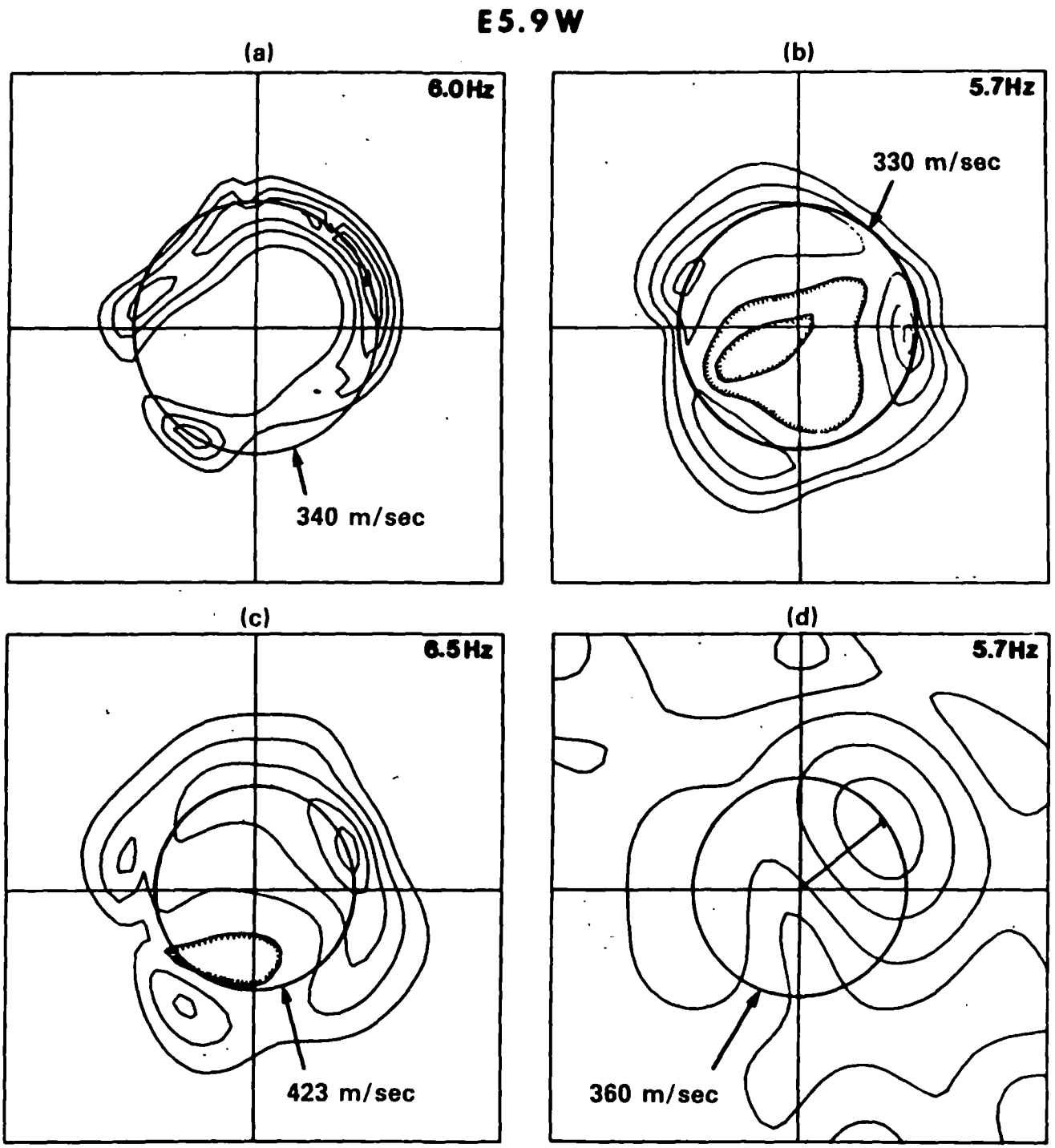

FIG. 6. Results of *f-k* analysis for site E5.9W (line E, station 5.9W) for different data block lengths, comparing MLM and BFM: (a) 12 data blocks, each with 128 points, processed by MLM, (b) 24 data blocks, each with 64 points, processed by MLM, (c) 48 data blocks, each with 32 points, processed by MLM, (d) 24 data blocks, each with 64 points, processed by BFM. The frequency on each frame corresponds to a maximum *f-k* power spectral density estimate. The range of wavenumber plotted is 35.7 cycles/km in both k_x and k_y.

to each array element and then a delay-and-sum operation is performed. The resolution in wavenumber space is therefore strongly characterized by the impulse response of the array (Figure 4) with prominent side lobes. In the presence of multipath propagation, the large side-lobe effects are not clearly recognizable, resulting in an ambiguous pattern of peaks in wavenumber space with loss of resolution due to smearing of the true spectrum.

MLM, sometimes called the high-resolution method, calculates the f-k power spectral density estimate by

$$\tilde{P}(f, \mathbf{k}) = (\mathbf{a}' \cdot \hat{\mathbf{S}}^{-1} \cdot \mathbf{a})^{-1}. \tag{6}$$

To motivate this operation, equation (6) can be written as

$$\begin{aligned}\tilde{P}(f, \mathbf{k}) &= \sum_{l=1}^{N} \sum_{n=1}^{N} A_l(f, \mathbf{k}) A_n^*(f, \mathbf{k}) \hat{S}_{ln}(f) \cdot \\ &\quad \cdot \exp[-i2\pi \mathbf{k} \cdot (\boldsymbol{\ell} - \mathbf{r}_n)] \\ &= \frac{1}{M} \sum_{m=1}^{M} \left| \sum_{l=1}^{N} A_l(f, \mathbf{k})\, \Phi_{lm}(f) \cdot \right. \\ &\quad \left. \cdot \exp[-i2\pi \mathbf{k} \cdot \mathbf{r}_l] \right|^2, \end{aligned} \tag{7}$$

where $A_l(f, \mathbf{k})$ are optimal complex weighting functions, known as maximum-likelihood filters, applied to each sensor's output. The procedure for finding $A_l(f, \mathbf{k})$ involves the inversion of the signal-plus-noise coherent power spectral matrix, such that

$$A_l(f, \mathbf{k}) = \frac{\sum_{n=1}^{N} q_{ln}(f, \mathbf{k})}{\sum_{n=1}^{N} \sum_{l=1}^{N} q_{ln}(f, \mathbf{k})} \tag{8}$$

and $[q_{ln}(f, \mathbf{k})]$ is the inverse of the matrix $\{\hat{S}_{ln}(f) \exp[-i2\pi \mathbf{k} \cdot (\mathbf{r}_l - \mathbf{r}_n)]\}$. Application of the maximum-likelihood filters allows the array processor to pass an undistorted monochromatic plane wave with a given velocity corresponding to a peak in f-k power spectral density and to suppress, in an optimal least-squares sense, the power of waves traveling at different velocities. The MLM impulse response, without noise, is ideally sharp; with noise, it depends on the characteristics of the data.

Theoretically, MLM has a disadvantage relative to BFM in terms of its sensitivity to measurement errors, especially in a case of channel mismatch (Cox, 1973). Mismatch may result from distortion in the waveform during propagation, or from amplitude, phase, and position errors in the sensors (geophones), sampling, and digitization. However, MLM spectra from the array data of Grass Valley seldom showed evidence of serious degradation. Regarding resolution of two separate waves, BFM depends on the array impulse response, while MLM depends not only on array response but also on the signal-to-noise ratio (Cox, 1973).

The maximum entropy method (MEM) would theoretically provide higher resolution estimates than the above two methods. Unfortunately, this method is developed only for equally-spaced (Barnard, 1969) and nonuniform-spaced (McDonough, 1974) linear arrays. It appears that, at present, MLM is the best method for processing 2-D array data for high resolution in the presence of multipath interference, the normal situation in ground noise studies.

Data blocks without sporadic noise pulses (i.e., transient-free) from each of the 12 geophones of the array were selected for processing. The number and length of the data blocks were selected for resolution and statistical stability of the estimated power spectral density. A MLM comparison of different numbers and lengths, holding the total number of data points constant, is illustrated with the array data from the site E5.9W by processing the identical data in three different lengths. The results are shown in Figure 6a for 12 blocks × 128 points, in Figure 6b for 24 blocks × 64 points, and in Figure 6c for 48 blocks × 32 points. We find that the use of either 12 blocks × 128 data points, or 24 blocks × 64 data points provides adequate resolution in wavenumber space and realistic direction estimates, especially in situations of multipath propagation. In Figure 6, the f-k power spectral densities are estimated at each of 41 × 41 grid points in a 2-D wavenumber space at a desired frequency component. The frequencies selected for processing are maxima in the power spectral density curves. The wavenumber of the peak value in the wavenumber plot, along with the frequency, provides the estimate of apparent phase velocity and the direction of propagation for the most coherent propagation in the data sample.

A comparison of BFM and MLM is provided in Figures 6b and 6d for the 24 block × 64 point case. The resolution improvement in MLM is quite apparent. Consequently, our processing method was normally MLM.

Based on these studies, data were processed for the Grass Valley area using the large network spacing for studying spatial variations in ground noise

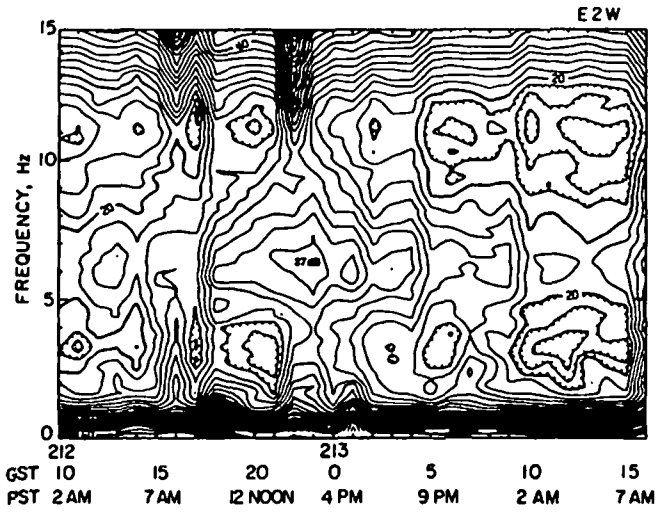

FIG. 7. Diurnal variation of ground noise level at reference site E2W, with respect to 10^{-11} m/sec/$\sqrt{\text{Hz}}$, (0 dB), from day 212, hour 10 to day 213, hour 16 of 1976. Contour interval is 2 dB. Note the minimum noise level at 2–4 AM for all frequencies.

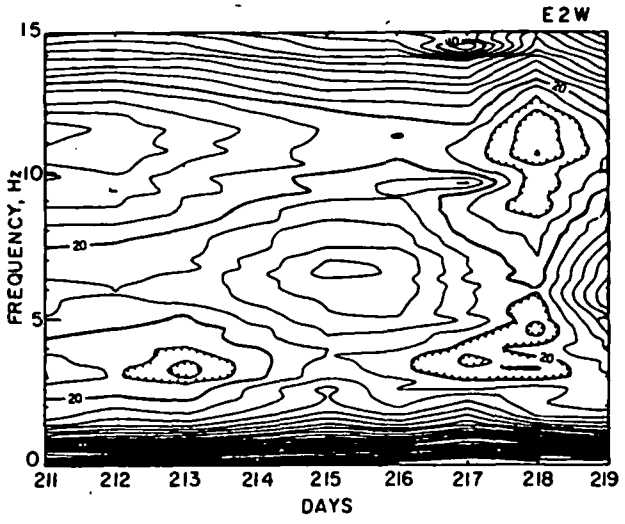

FIG. 8. Secular variation of early morning quiet ground noise level at E2W with respect to 10^{-11} m/sec/$\sqrt{\text{Hz}}$, (0 dB), from day 211 to day 219 of 1976. Contour interval is 2 dB. Thunderstorms and unsettled regional weather characterized days 214–216.

and utilizing the 25-m radius array with MLM for ground noise propagation (f-k) parameters.

DATA AND INTERPRETATION

Temporal variation of ground noise

The total seismic noise amplitude $\sigma(x, y, t, f)$ can be modeled very generally by

$$\sigma(x, y, t, f) = \sigma_i(x, y, t, f) + \sigma_m(x, y, t, f) + \sigma_l(x, y, t, f),$$

where

(1) $\sigma_i(x, y, t, f)$ is the intrinsic noise at the site, including geothermal noise,
(2) $\sigma_m(x, y, t, f)$ is the microseismic component from distant sources, and
(3) $\sigma_l(x, y, t, f)$ is the noise generated locally at the surface by human activity and atmospheric disturbances.

If we are interested only in intrinsic noise, the sampling and processing procedures must exclude the effect of the other two noise sources. To minimize local noise, $\sigma_l(x, y, t, f)$, the data must be taken between midnight and dawn, because normally the noise level is low. Figure 7 presents the diurnal variation of seismic noise at the reference site E2W. To construct this figure, transient-free noise data were chosen to estimate VSD every hour for a 30-hour period. Roughly 6 minutes of seismic noise actually went into each hourly average. The spectral density then was contoured as a function of time and frequency. The figure shows the typical wide-band, high-diurnal noise level, extending from 9 AM to 7 PM, the result of more disturbed daytime meteorological conditions and cultural activity in the area. This suggests that we record only between 2 and 4 AM to minimize contamination of the VSD estimate by unwanted diurnal noise sources.

A typical survey is carried out over a period of several days, so that long-term secular variations are apparent in the data. The nature of this variation over a 9-day period at the reference site E2W is shown in Figure 8. We estimate one VSD every 24 hours, using the quietest data during early morning hours, and contour the VSD from day 211 to day 219. In this figure, the high-amplitude seismic noise which appears from day 214 to day 216 is related to regional weather conditions. On those three days there were thunderstorms starting in the afternoon and ending in the early evening throughout the region. To eliminate temporal variations of the observed microseisms, the band-limited power of seismic noise at each site, obtained by integrating VSD over the frequency band of interest, is normalized by the simultaneous power in the same frequency band at the reference site, provided that data are sampled from the quiet period in early morning. Mapping the normalized power gives the spatial distribution of relative intrinsic noise power level.

Spatial variation of ground noise

Estimation of ground noise VSD from simul-

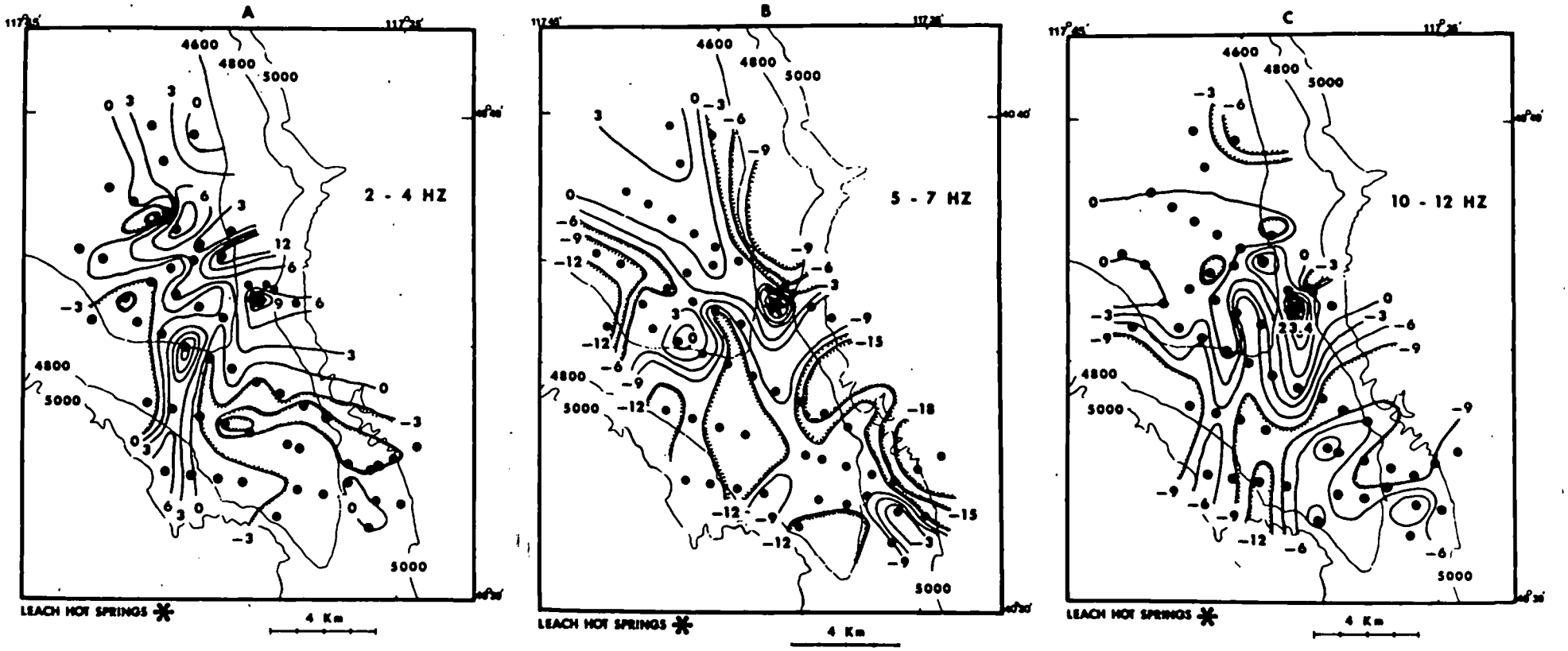

FIG. 9. Relative intrinsic noise power contours with respect to reference site E2W in three different frequency bands, namely (a) 2–4 Hz, (b) 5–7 Hz, and (c) 10–12 Hz. Contoured interval is 3 dB. Solid circles indicate geophone sites. Elevations are in feet. The star indicates Leach Hot Springs location.

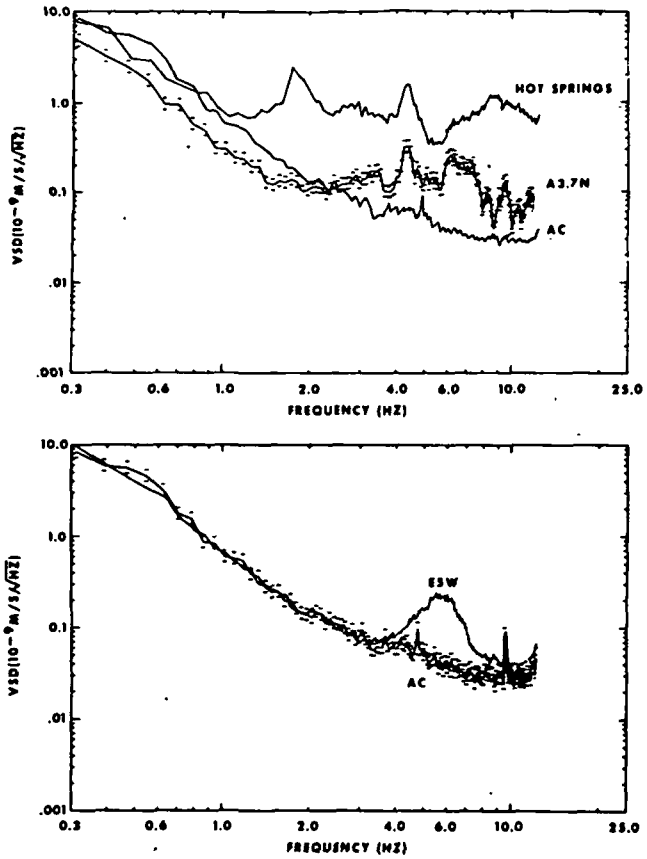

FIG. 10. Velocity spectral density (VSD) of ground noise at Leach Hot Springs and at site A3.7N, 500 m northwest of the hot springs (upper) and at site E5W in the center of the valley (lower) compared to bedrock site AC, at the valley edge (Figure 2). The horizontal bars show typical 95 percent confidence limits for A3.7N (upper) and AC (lower) sites.

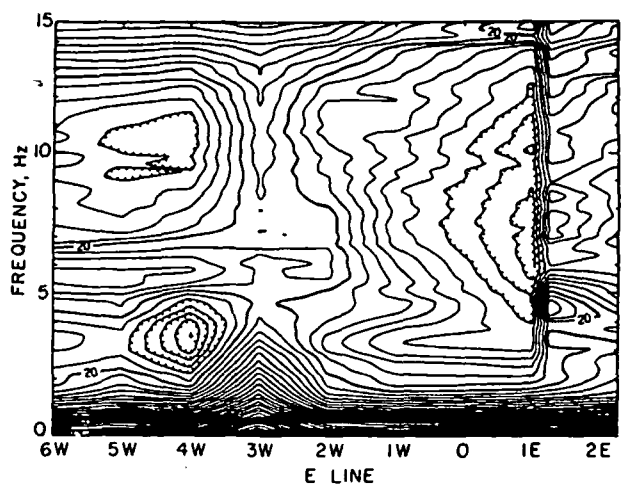

FIG. 11. Instantaneous noise field along survey line E. Abscissa is station location, with 1 km spacing and ordinate is frequency. Contour interval is 2 dB. Note high wide-band noise level at 3W, the region of thickest alluvial cover, and the sharp gradient across the valley margin fault trace at 1E.

taneous sampling in the early morning, with stations at 1-km intervals, yields relative intrinsic noise power contour maps as illustrated for the frequency band of 2–4 Hz (Figure 9a), 5–7 Hz (Figure 9b), and 10–12 Hz (Figure 9c). High noise levels are found at Leach Hot Springs and near the center of Grass Valley, as anticipated, but there are also local anomalies such as in the areas around G2W and G3W, H1E and H2E (see Figure 2 for site locations). Those ground noise anomalies, especially in the 5–7 Hz band, correlating spatially with the occurrence of Bouguer gravity anomalies, imply the occurrence of thickest alluvial deposits. The long-term stability of these anomalies is reproducible as indicated by close agreement with the results of a preliminary survey carried out in the summer of 1975, a year earlier than the survey for the data shown here.

Leach Hot Springs clearly generates seismic noise, but the noise is localized and does not propagate unattenuated more than a few km. In the vicinity of the springs, noise spectra show the high-amplitude seismic noise over a wide-frequency band; 500 m northwest of the hot springs (A3.7N) the amplitude of the noise at all frequencies greater than 1 Hz has attenuated nearly 20 dB. The noise spectrum at the Hot Springs site, at site A3.7N (500 m northwest of the Hot Springs site), and at a bedrock valley edge site AC (Figure 2) are shown in Figure 10. Note the wideband nature of the hot springs noise.

In the valley center, station E5W, the noise has a distinctive broad peak around 5.5 Hz, as can be seen at the bottom of Figure 10. The character of the broad valley peak varies from site to site, probably as a consequence of changes in near-surface properties. In Figure 9b, the areas of high-amplitude seismic noise in the 5–7 Hz band generally correspond to the areas of thick alluvium. The details of noise variation across the valley are illustrated by data for three typical survey lines, E. B, and G, shown respectively in Figures 11, 12, and 13.

The instantaneous ground noise level along 8.25 km of line E is presented in Figure 11. Data blocks were taken simultaneously from sites at E6W, 5W, 4W, 3W, 2W, 1W, 1E, 1.25E, and 2.25E. In this figure there is a clear peak at 5.5 Hz extending westward. The source of this well defined and band-limited peak is not clearly understood, though it is doubtless related to near-surface properties and is a surface wave with a wavelength of about 50 m. A wide-band ridge of rather high-amplitude noise appears at E3W and is frequently seen to extend to 1W. Maximum thickness of alluvium and the lowest

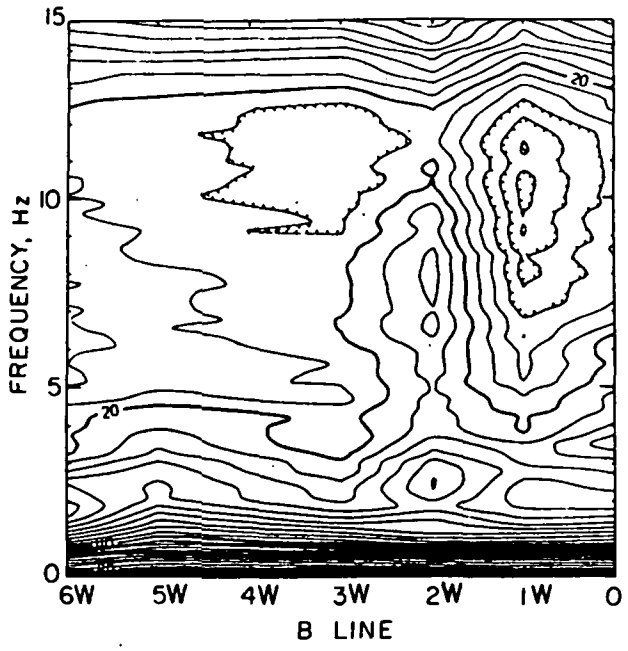

FIG. 12. Instantaneous noise field along survey line B. Abscissa is station location with 1 km spacing and ordinate is frequency. Contour interval is 2 dB. Note high wide-band noise level at valley center near 2W. Sharp gradients may indicate valley faults.

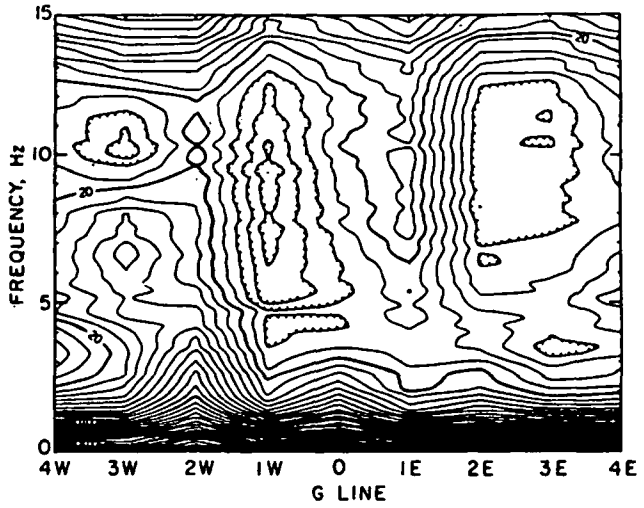

FIG. 13. Instantaneous noise field along survey line G. Abscissa is station location with 1 km spacing and ordinate is frequency. Contour interval is 2 dB. Note high wide-band noise level at valley center near 1E. Sharp gradients may indicate valley faults.

topography occurs around 2W. A remarkable feature seen in the figure is the dramatic 10 dB contrast between points 1E and 1.25E, spanning the Hot Springs fault (Figure 2). It seems the local noise field, generated by hot springs, is less attenuated east of the fault than west of it, probably due to high-Q surface rocks on the east being in faulted contact with alluvium west of the fault. This geologic feature can be seen in the faults anomaly (Figure 2) as well as in the Bouguer gravity map, the P-wave delay profiles, and the seismic reflection section; in addition, it is indicated by surface scarps.

Asymmetrical ridges of wide-band noise with sharp gradients to the east are seen near 2W on line B (Figure 12) and near 1E on line G (Figure 13). These ridges in the noise contours, as was the case for line E, correspond in position to the location of the minimum Bouguer gravity anomaly along each line and to the location of the thickest alluvium (Beyer et al, 1976). The positions of high gradients in ground noise east of the noise ridge on line B near 2W and on line G near 1E apparently correlate with locations of shallow faults. The prominent broad peak of 6.5 to 7 Hz, seen at G3W in Figure 13, is probably also related to properties of shallow alluvium. At the south end of Grass Valley, the ground noise level is generally lower than at the north end, and this contrast is presumably due to larger distance from the Leach Hot Springs and thinner alluvial deposits to the south.

Propagation characteristics

The most effective parameters for discriminating noise due to a buried localized source from that due to distributed surface sources and variations in local subsurface properties are the direction of propagation and the apparent phase velocity of the microseisms. Above a deeply buried source, we expect time-invariant direction of propagation associated with high-phase velocity across the array.

Time-invariant azimuths of propagating noise fields are seen at sites in the vicinity of Leach Hot Springs. Typical noise data recorded in this area show highly coherent energy, as seen in the array data from site A2N, 1 km southeast of Leach Hot Springs, shown in Figure 14. The dominant frequency of the propagating noise field in the area is 4.4 Hz. The result of f-k analysis at the dominant frequency indicates that the noise field propagates across the array at azimuth 149 degrees, with phase velocity of 422 m/sec. The azimuth in the plot is in a direction away from the Hot Springs. In the frequency band near 2.5 Hz shown in Figure 14b, the coherent noise propagating at 904 m/sec at an azimuth of 207 degrees also is away from the Hot Springs.

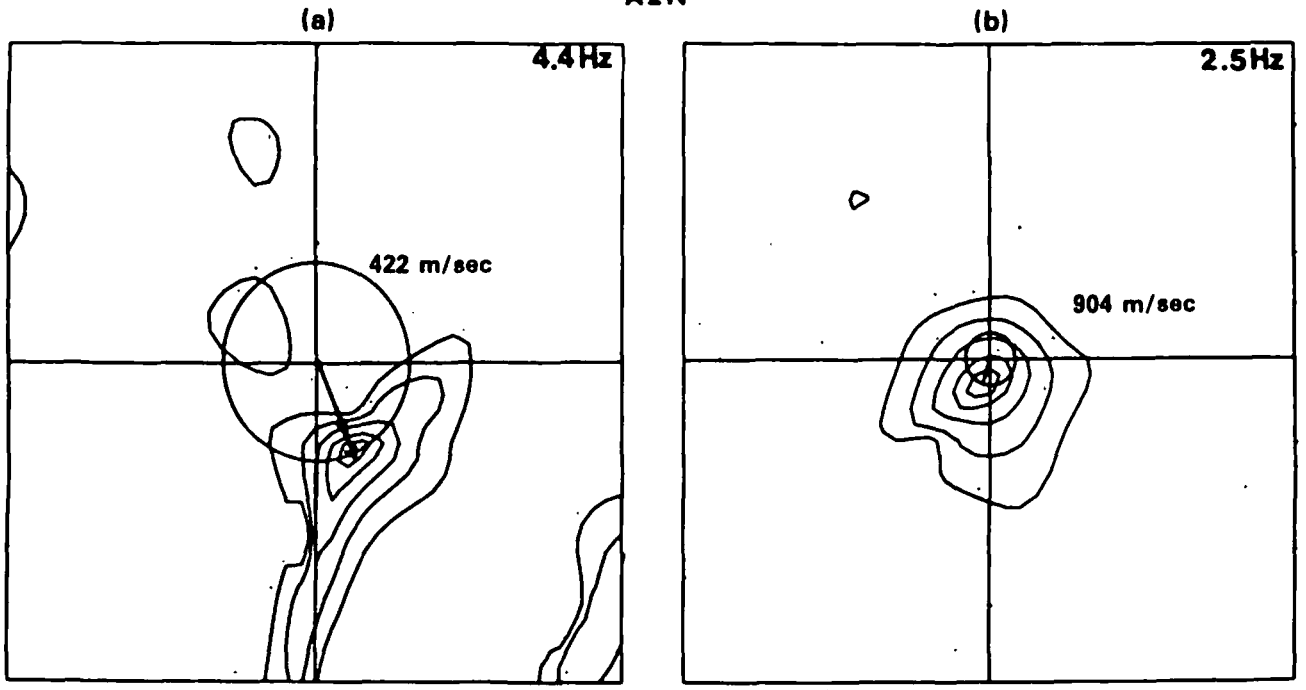

FIG. 14. High-resolution *f-k* results at site A2N, 1 km southeast of Leach Hot Springs. The microseismic field consists of (a) 4.4 Hz noise propagating in the direction 149 degrees with apparent phase velocity of 422 m/sec and (b) 2.5 Hz noise propagating in the direction 207 degrees with apparent phase velocity 904 m/sec. The maximum wavenumber plotted is 35.7 cycles/km. These noise components are apparently fundamental-mode Rayleigh waves generated at the hot springs, where near-surface velocities exceed 2.9 km/sec.

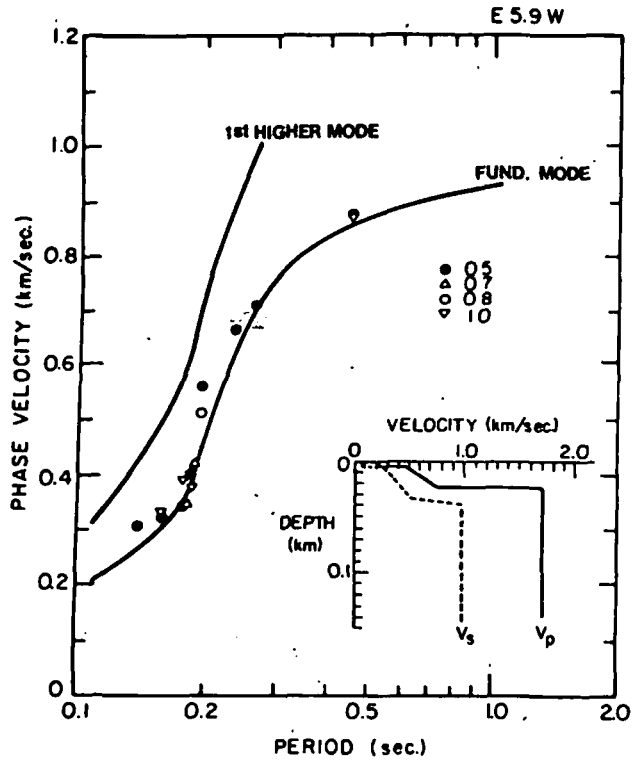

FIG. 15. Rayleigh wave dispersion curves for fundamental and first higher mode computed for the model shown, compared with observed ground noise phase velocities at site E5.9W. The observed phase velocities were determined at various times of the day by *f-k* analysis, the hour indicated by symbol type.

The noise anomaly in the center of the valley, for example, E5.9W at 5 to 7 Hz (Figure 9b), can be explained by the superposition of multipath surface waves propagating in the shallow alluvial section. The absence of a unique and time-invariant propagation direction, as seen, for example, in Figure 6a, indicates clearly that the high-amplitude ground noise at this site is not due to a local buried source. Further, the uniform propagation velocity, 340 m/sec in Figure 6a, seen at all azimuths suggests a surface wave nature of the noise field. Similar multiazimuth surface waves are seen also in the results of *f-k* analysis at 5.71 Hz for the array data at other sites. The phase velocities estimated from these plots indicate that the microseisms are apparently fundamental-mode Rayleigh waves.

Dispersion characteristics and shallow structure

On the assumption that the microseismic field consists of surface waves, the *f-k* analysis technique allows direct measurement of the local dispersion curve by selecting phase velocities corresponding to the frequencies at peak *f-k* power spectral densities. As an example, in Figure 15 we show phase velocities so estimated, along with computed fundamental and first higher-mode Rayleigh wave dispersion curves

for a model based on P-wave velocities from a shallow refraction survey in the area. The effect of the very shallow velocity structure is illustrated clearly. Lateral variations in the upper 10 to 20 m will control the surface wave propagation characteristics. In estimating dispersion curves, we do not restrict sampling to the quiet periods, since larger microseisms are very coherent across the array. The dispersion measurements, besides providing local observations of phase velocity for shallow structure mapping, also provide a method of verifying the wave nature of the microseisms. It is clear that waves with periods of 1 sec and greater must be analyzed for structural information at geothermal target depths, if the microseisms are fundamental-mode Rayleigh waves (see, for example, McEvilly and Stauder, 1965).

CONCLUSIONS

The spatial distribution of the amplitude, frequency, and wavenumber characteristics of background microseisms, or ground noise, contains information on the variation of subsurface properties and the location of buried sources of seismic waves. Extraction of the information requires careful sampling of the microseismic field in time and space. A simple field system, utilizing FM telemetry of data to a small, trailer-mounted, central recording site, was fabricated for one- or two-man installation and operation in a study of the methodology in a potential geothermal area in Grass Valley, Nevada.

Diurnal variation in the 2–20 Hz noise field is regular. A consistent diurnal variation that repeats from day to day is due apparently to meteorological and cultural sources, with typically 15 dB variation seen from the midday high noise level to the low noise level in the early morning hours of 2–4 AM. Secular variations, due to regional weather patterns, can produce a 5–10 dB range in the early morning minimum noise levels over a duration of a few days.

For spectral stability in investigating spatial variation of noise, at least 28 quiet data blocks, each 12.8 sec long, were taken simultaneously at the network stations, and the spectra were averaged for each site. This procedure produced consistent results throughout the area, revealing a characteristically low-amplitude smooth noise spectrum at hard rock sites, a prominent peak at 4–6 Hz at valley sites, and wide-band high-amplitude noise, apparently due to very shallow sources, at hot springs sites. Contour maps of noise level, normalized to a reference site, are dominated by the hot springs noise levels outlining the regions of maximum alluvium thickness. Major faults are evident when they produce a shallow lateral contrast in rock properties.

Microseisms in the 2–10 Hz band are predominantly fundamental-mode Rayleigh waves, characterized by low velocities and wavelengths as small as 20 m, requiring arrays of closely spaced geophones for adequate spatial sampling.

High-resolution f-k processing, with proper data sampling, provides a powerful technique for mapping the phase velocity and the direction of propagation of the noise field, revealing local sources and lateral changes in shallow subsurface structure.

No evidence for a significant body wave component in the noise field was found, although it becomes clear that improper spatial sampling can give a false indication through aliasing. Noise emanating from a deep reservoir would be evident as body waves and could be traced to its source given a reasonably accurate velocity model.

RECOMMENDATIONS

Conventional seismic ground noise surveys, conducted as outlined in this study, require a large number of stations for economical implementation. With 100 stations, for example, a week-long survey could provide maps of noise amplitude distribution, P-wave delay time, and microearthquake locations, as well as f-k analyses at many sites, utilizing a 2–3 man crew. It is not clear, however, that such data will be of significant value in delineating a geothermal reservoir.

The amplitude mapping of ground noise in certain frequency bands is a poor exploration technique for delineating buried geothermal systems. The results of the amplitude mapping indicate that the amplitude variations of microseisms in an area are controlled by the near-surface geology, especially lateral variations in thickness of the alluvial layer. The large amplitude surface wave generated by surface sources and propagating horizontally will mask weak seismic waves emitted from a buried source. Therefore, amplitude mapping only reveals information on the very shallow structure.

On the other hand, the technique of f-k analysis can, theoretically, map the wavenumber of the microseisms, discriminating the vertically incident body waves from the surface waves. The yet open question of whether a reservoir acts as a radiator of seismic body waves can be answered through careful f-k analyses in existent geothermal areas. The array to be used for further study must be a nonaliased array of larger diameter than that used in this study. The ex-

pansion in array size will improve the resolution around the origin of the $k_x - k_y$ diagram. This improvement would provide a more accurate estimate for power at the small wavenumbers, so that the azimuth and the apparent velocity of the long-wavelength body waves are estimated more accurately. The amplitudes of body waves radiating from a source at depth are apparently much smaller than those of the ambient surface waves. In order to extract useful information from the body waves, a sophisticated signal detection and processing scheme is required. However, the *f-k* analysis technique may fail to detect the geothermal system at depth if our assumption of body wave radiation from the reservoir is not valid, or if the emanating body waves are either attenuated or completely masked by the ambient surface waves. It is fortunate that the ambient surface waves have shorter wavelengths than the anticipated body waves; because of this, the detection of weak body waves can be improved by a more sophisticated array, as is commonly done in conventional seismic reflection surveying.

If the assumption of radiated body waves is indeed valid, and if such body waves are detectable, we can trace the recorded wavefronts to their source, given a reasonably accurate velocity model. There are two schemes which have been used for projecting waves observed at the surface back into the earth and locating the source region, and these methods may be applicable to the geothermal reservoir delineation problem.

The first method is seismic ray tracing described by Julian (1970) and Engdahl and Lee (1976). If the array diameter is much smaller than the distance to the buried source, the microseismic field propagates as a plane wave across the array. Estimation of the azimuth and the apparent velocity of the propagating noise field from *f-k* analysis, along with the knowledge of the near-surface velocity distribution, can give us the incident angle of the coherent body wave noise. Given a reasonable velocity structure in the area and simultaneously occupied array sites, we can reconstruct raypaths to each site. The intersection of these raypaths indicates the region of the radiating source.

Another approach is much like that used in a conventional reflection survey with 2-D surface coverage but without a surface-controlled source. The coherent noise fields recorded by a 2-D surface array are projected downward into the assumed subsurface model. The reconstruction of the coherent noise field propagating in an upward direction can be carried out by the wave equation migration technique, using a finite-difference approximation such as the one described by Claerbout (1976). The restriction of this approach to microseismic data is that the noise field must propagate as a spherical wavefront across the geophone array. The spherical wavefront exists in the situation where the array dimension is greater than the distance to the source. In this case, we can determine the region of radiating sources in terms of the convergent pattern of the extrapolated wave fields.

It is clear that ray tracing and the wave equation migration are applicable at different source-array distances in the application of delineating geothermal reservoirs. In a practical exploration program, we do not know the depth of geothermal reservoirs, nor do we know the shape of the wavefront across the array. One way of solving the problem is to place a non-aliased array at several sites and search for the evidence of time-invariant, high-velocity body waves. As soon as the body waves are detected, one may compare several results of *f-k* analysis, using data of identical recording periods but of different sizes of subarray. The deterioration of the resolution in the *f-k* diagrams, as we expand the size of the subarray, indicates that the plane wave assumption is violated and the wavefront migration techniques should be applied. On the other hand, if the noise fields propagate as plane waves across the large array, the resolution in the *f-k* diagrams will be improved as we expand the size of subarrays, and the *f-k* analysis with seismic ray tracing is the proper technique to locate the noise source.

Based on this study, we suggest that if the geothermal system is indeed emanating detectable body waves, the analysis of ambient ground motion or seismic noise can be applied to the delineation of geothermal reservoirs. In fact, if the radiated body waves exist, the method can be one of the most effective geophysical methods in geothermal explorations. Clearly, a few carefully executed and strategically located experiments are warranted.

ACKNOWLEDGMENTS

This study has been supported by the U.S. Energy Research and Development Administration under contract no. W-7405-ENG-48 with the Lawrence Berkeley Laboratory.

The authors are grateful to Steven Palmer, Jack Yatou, Glen Melosh, and Ernie Majer of the University of California at Berkeley and geothermal field crews of Lawrence Berkeley Laboratory for field assistance in various stages of study.

REFERENCES

Barnard, T. E., 1969, Analytical studies of techniques for the computation of high resolution wavenumber spectra: Advanced Array Research, special report no. 9, Dallas, Texas, Texas Instruments, Inc.

Beyer, A., Dey, A., Liaw, A., Majer, E., McEvilly, T. V., Morrison, H. F., and Wollenberg, H., 1976, Geological and geophysical studies in Grass Valley, Nevada: Preliminary open file rep. LBL-5262.

Capon, J., 1969, High-resolution frequency-wavenumber spectrum analysis: Proc. IEEE, v. 57, p. 1408–1418.

Clacy, G. R. T., 1968, Geothermal ground noise amplitude and frequency spectra in New Zealand volcanic region: J. Geophys. Res., v. 73, p. 5377–5383.

Claerbout, J. F., 1976, Fundamentals of geophysical data processing: New York, McGraw-Hill Book Co., Inc., p. 184–226.

Combs, J., and Rotstein, Y., 1975, Microearthquake studies at the Coso geothermal area, China Lake, California: 2nd U.N. Symps. on the Dev. and Use of Geothermal Resources, San Francisco, p. 909–916.

Cox, H., 1973, Resolving power and sensitivity to mismatch of optimum array processors: J. Acous. Soc. of Am., v. 54, no. 3, p. 771–785.

Douze, E. J., 1967, Short-period seismic noise: SSA Bull., v. 57, p. 55–81.

Douze, E. J., and Sorrells, G. G., 1972, Geothermal ground-noise surveys: Geophysics, v. 37, p. 813–824.

Engdahl, E. R., and Lee, W. H. K., 1976, Relocation of local earthquake by seismic ray tracing: J. Geophys. Res., v. 81, p. 4400–4406.

Fix, J. E., 1972, Ambient earth motion in the period range from 0.1 to 2560 sec.: SSA Bull., v. 62, p. 1753–1760.

Goforth, T. T., Douze, E. J., and Sorrells, G. G., 1972, Seismic noise measurements in a geothermal area: Geophys. Prosp., v. 20, p. 76–82.

Guttenberg, B., 1958, Microseisms, *in* Advances in Geophysics: New York. Academic Press, v. 5, p. 53–97.

Haubrich, R. A., and Mackenzie, G. S., 1965, Earth noise 5–500 millicycles per second; 2. Reaction of the earth to oceans and the atmosphere: J. Geophys. Res., v. 70, p. 1429–1440.

Haubrich, R. A., and McCamy, K., 1969, Microseisms: Coastal and pelagic sources: Rev. of Geophys. v. 7, p. 539–571.

Iyer, H. M., 1974, Search for geothermal seismic noise in the East Mesa area, Imperial Valley, California: U.S.G.S. open-file rep. no. 74–96, 52 p.

Iyer, H. M., and Hitchcock, T., 1974, Seismic noise measurements in Yellowstone National Park: Geophysics, v. 39, p. 389–400.

——— 1976, Seismic noise survey in Long Valley, California: J. Geophys. Res., v. 81, p. 821–840.

Julian, B. R., 1970, Ray tracing in arbitrary heterogeneous media: Tech. note 1970–45, Lincoln Lab., Lexington, Mass.

Kanai, K., and Tanaka, T., 1961. On microtremors VIII: Bull. of the Earthquake Res. Inst., v. 39, p. 97–114.

Katz, L. J., 1976, Microtremor analysis of local geological conditions: SSA Bull., v. 66, p. 45–60.

Lacoss, R. T., Kelly, E. J., and Toksöz, M. N., 1969, Estimation of seismic noise structure using arrays: Geophysics, v. 34, p. 21–38.

Longuet-Higgins, M. S., 1950. A theory of the origin of microseisms: Phil. Trans. Royal Soc. London, ser. A., v. 243, p. 1–15.

Luongo, G., and Rapolla, A., 1973, Seismic noise in Lipari and Vulcano Islands, Southern Thyrrenian Sea, Italy: Geothermics, v. 38, p. 29–31.

McDonough, R. N., 1974, Maximum-entropy spatial processing of array data: Geophysics, v. 39, p. 843–851.

McEvilly, T. V., and Stauder, W. S. J., 1965, Effect of sedimentary thickness on short-period Rayleigh-wave dispersion: Geophysics, v. 30, p. 198–203.

Nicholls, H. R., and Rinehart, J. S., 1967, Geophysical study of geyser action in Yellowstone National Park: J. Geophys. Res., v. 72, p. 4651–4663.

Oliver, J., 1962, A worldwide storm of microseisms with periods of about 27 seconds: SSA Bull., v. 52, p. 507–518.

Oliver, J., and Ewing, M., 1957, Microseisms in the 11- to 18-second period range: SSA Bull., v. 47, p. 111–127.

Oliver, J., and Page, R., 1963, Concurrent storm of long and ultralong period microseisms: SSA Bull., v. 53, p. 15–26.

Robertson, H., 1965, Physical and topographic factors as related to short-period wind noise: SSA Bull., v. 55, p. 863–877.

Sass, J. H., Lachenbruch, A. H., Monroe, R. J., Greene, G. W., and Moses, T. H., 1971, Heat flow in the western United States: J. Geophys. Res., v. 76, p. 6376–6413.

Savino, J., McCamy, K., and Hade, G., 1972, Structures in earth noise beyond twenty seconds—a window for earthquakes: SSA Bull., v. 62, p. 141–176.

Sax, R. L., and Hartenberger, R. A., 1965, Seismic noise attenuation in unconsolidated material: Geophysics, v. 30, p. 609–615.

Sorrells, G. G., McDonald, J. A., Der, Z. A., and Herrin, E., 1971, Earth motion caused by local atmospheric pressure changes: Geophys. J. R. Astr. Soc., v. 26, p. 83–98.

Whiteford, P. C., 1970, Ground movement in the Waiotapu geothermal region, New Zealand: Geothermics, special issue on proceedings of the U.N. Symps. Dev. Util. of Geothermal Resources, 2, part III, p. 478–486.

——— 1975, Studies of the propagation and source locations of geothermal seismic noise: 2nd U.N. Symps. on the Dev. and Use of Geothermal Resources, San Francisco, p. 1263–1271.

Wilson, C. D. V., 1953, The origins and nature of microseisms in the frequency range 4 to 100 c/s: Proc. R. Soc. A., v. 217, p. 176–202.

GEOPHYSICS, VOL. 46, NO. 10 (OCTOBER 1981); P. 1456–1466, 9 FIGS., 4 TABLES.

Delineation of a low-velocity body under the Roosevelt Hot Springs geothermal area, Utah, using teleseismic *P*-wave data

Russell Robinson* and H. M. Iyer‡

ABSTRACT

To assess the nature of the heat source associated with the Roosevelt Hot Springs geothermal area, we have investigated the *P*-wave velocity structure of the crust and uppermost mantle in the vicinity of the Mineral Mountains, southwest Utah, a region of late Cenozoic rhyolitic and basaltic volcanic activity. A roughly square (30 × 30 km) array of 15 seismographs, centered on the mountains, was operated for a period of 46 days, during which 72 teleseismic events were recorded with sufficient quality for calculation of *P*-wave traveltime residuals. Relative residuals, using the array average for each event as reference, show a clear pattern of azimuthal variation of up to 0.3 sec. This pattern implies the existence of a localized region of relatively low-velocity material extending up from the upper mantle to depths of about 5 km under the Mineral Mountains. A three-dimensional (3-D) inversion of the data confirms this conclusion and yields a model featuring a region of low velocity (5 to 7 percent less than the surrounding rock) centered under the geothermal area and extending from about 5-km depth down into the uppermost mantle. The near-surface velocities obtained in the inversion clearly reveal the structure of the region, part of the Basin and Range province. An azimuthally changing pattern of waveform distortion, restricted to the central Mineral Mountains, indicates the presence of a small but intensely anomalous region of low velocity and high attenuation at depths of about 15 km. Although we cannot rule out an explanation for the low velocity purely in terms of compositional changes, in view of the geothermal and volcanic manifestations found in the region we prefer an explanation in terms of abnormally high temperature and a small fraction of partial melt. A partial melt model implies a much greater heat reservoir than does a model involving only circulation along deep fault zones.

INTRODUCTION

The Roosevelt Hot Springs geothermal area, currently under proposed development for the generation of electric power, has been the focus of many geophysical studies. Seismic-refraction, gravity, magnetic, resistivity, and heat-flow investigations have all been made in the region in addition to detailed geologic and geochemical studies (for a review, see Ward et al, 1978). As a result, the relatively shallow (2–3 km) structure of the area is known to some degree, but the deeper structure of the crust has yet to be investigated. With the view of elucidating the nature of the heat source responsible for the near-surface thermal activity, we examined this deeper structure using teleseismic *P*-wave traveltime variations. This technique has proved very useful in understanding the structure of other geothermal areas at depth, for example, at Yellowstone National Park, Wyoming (Iyer, 1979), and in California, in the Geysers-Clear Lake region (Iyer et al, 1979), at Long Valley (Steeples and Iyer, 1976), and in the Coso geothermal area (Reasenberg et al, 1980).

GEOLOGIC AND GEOPHYSICAL SETTING

The Roosevelt Hot Springs geothermal area lies on the western flank of the Mineral Mountains in southwest Utah, a horst composed mainly of Tertiary granitic rocks (10–14 m.y. old) and flanked by alluvial valleys typical of the Basin and Range province (Milford Valley and Beaver Valley). The transition to the Colorado plateau physiographic province is immediately east of Beaver Valley (Figure 1).

Both basaltic and rhyolitic volcanic activity have occurred repeatedly in the vicinity of the Mineral Mountains since middle Tertiary time (related at first to the emplacement of the granitic rocks themselves), as it has in much of the Basin and Range—Colorado plateau transition zone (Smith, 1979). The most recent episode of activity resulted in rhyolite flows and domes along the crest of the Mineral Mountains 0.5 to 0.8 m.y. ago. Basaltic or andesitic flows occurred on the northeast flank of the mountains and more extensively slightly farther northeast near Cove Fort. These latter flows cover part of the northern Beaver Valley.

Large-scale seismic-refraction studies of the easternmost Basin and Range province (Braile et al, 1974; Prodehl, 1970) have shown that the crust is thin (about 25 km thick) and the P_n velocity low (about 7.5 km/sec). It has been suggested that a regional low-velocity layer exists in the upper crust between 5- and 15-km depth (Smith et al, 1975; Müller and Mueller, 1979). These observations have implied a high regional geothermal gradient (Smith et al, 1975).

Refraction studies near the Roosevelt Hot Springs geothermal area itself (Gertson and Smith, 1979) indicate that the Milford Valley has a maximum depth to basement of about 2 km, the deeper fill consisting of Tertiary sediments with a *P*-wave velocity

Manuscript received by the Editor April 21, 1980; revised manuscript received March 23, 1981.
*Geophysics Division, DSIR, Box 1320, Wellington, New Zealand.
‡U.S. Geological Survey, 345 Middlefield Road, Menlo Park, CA 94025.

of about 4.0 km/sec, the shallower fill consisting of more recent sediments with velocity of 1.8 km/sec. Gertson and Smith (1979) suggest that high-velocity Precambrian (?) metamorphic rocks, exposed along the western flank of the Mineral Mountains, extend westward under Milford Valley. The granitic rocks of the Mineral Mountains, beneath a surface low-velocity weathered layer, have a velocity of approximately 5.5 km/sec.

Microearthquake studies of the Roosevelt Hot Springs region (Olson and Smith, 1976) have shown that the level of activity near the Mineral Mountains is low, while 30 km to the northeast near Cove Fort, the level is much higher and of a swarm-like nature. Depths of microearthquakes were found to be mostly less than 10 km.

Many hot spring areas in the Basin and Range province are assumed to be caused by abnormally deep penetration of circulating groundwater along range-bounding fault zones (Hose and Taylor, 1974). In the case of the Roosevelt Hot Springs geothermal area, however, analyses of the heat-flow data by Ward et al (1978) indicate that this mechanism is insufficient to account for the observed heat flux. They showed that the total heat loss of about 70 MW, obtained by integrating the high heat-flow values (100 to 1000 mW m^{-2}) around the Roosevelt Hot Springs, cannot be explained by hydrologic discharge and recharge in an equivalent area characterized by typical regional heat-flow values (75 to 100 mW m^{-2} for western Utah). Hence, they suggest a heat source at depth, probably associated with the Mineral Mountains pluton, at a temperature near the granite solidus.

THE DATA

The concept of using teleseismic traveltime residuals (observed arrival time minus that calculated on the basis of a standard earth model) to study the velocity structure of the crust is simple. If a sufficiently distant earthquake is observed with a closely spaced array of seismographs, changes in residual from station to station can be taken as due to velocity variations near the array. This is true because the raypaths back toward the source converge and so are increasingly unlikely to sample different velocity structures as the distance from the receivers increases. Changes in the pattern of residual variation with changes in source azimuth are particularly useful in determining the local velocity structure.

In order to carry out our study of the crust beneath the Mineral Mountains region, the recording array of 15 seismograph stations

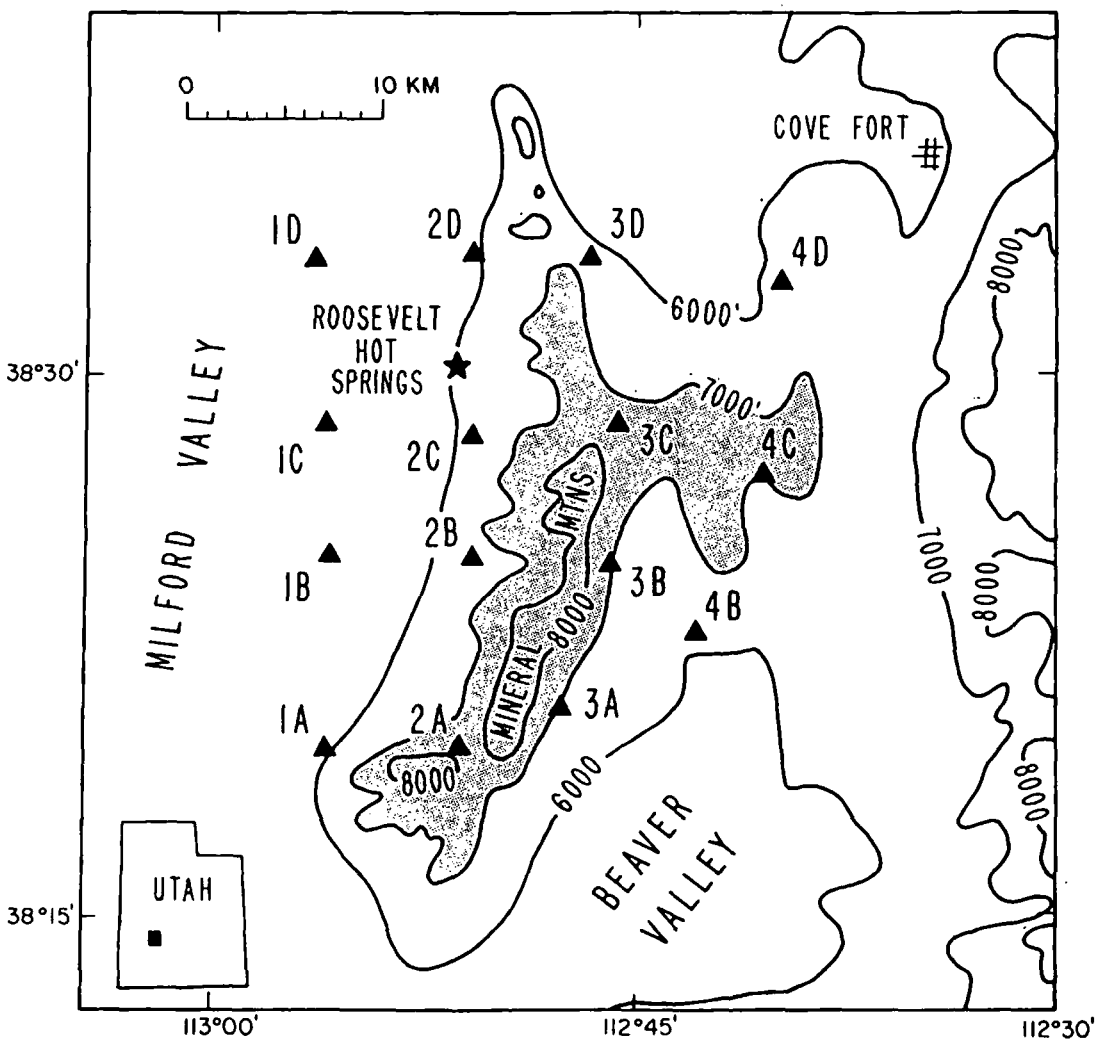

FIG. 1. The Mineral Mountains region, southwest Utah. Seismograph stations used in this study are shown by triangles. The star indicates the location of the Roosevelt Hot Springs geothermal area. Contour interval is 1000 ft, the shaded region representing the Mineral Mountains.

Table 1. Station information.

Station	Latitude (N)	Longitude (W)	Elevation (m)	Reduction velocity (km/sec)	Elevation correction (sec)	Lithology
1A	38°19.54′	112°56.05′	1722	4.5	0.38	Granite
1B	25.04	56.00	1606	3.0	0.54	Alluvium
1C	28.59	56.06	1574	2.0	0.79	Alluvium
1D	33.13	56.54	1507	2.0	0.75	Alluvium
2A	38°19.64′	112°51.32′	2201	5.4	0.41	Granite
2B	24.93	50.97	1923	4.5	0.43	Granite
2C	28.34	50.86	1905	4.5	0.42	Granite
2D	33.26	50.80	1780	4.5	0.40	Granite
3A	38°20.73′	112°47.70′	2091	4.5	0.46	Granite
3B	24.75	46.01	2152	4.5	0.48	Granite
3C1	28.58	45.77	2297	4.5	0.51	Granite
3C2	29.04	45.30	2146	4.5	0.48	Granite
3D	33.14	46.65	1853	4.5	0.41	Granite
4B	38°22.83′	112°42.95′	1929	3.0	0.64	Alluvium
4C	27.21	40.85	2115	3.0	0.71	Lava
4D	32.48	39.90	1917	3.0	0.64	Lava

was deployed (Figure 1) in a roughly square pattern 30 km wide on each side. Station coordinates and lithology are listed in Table 1. The time for seismic waves to travel vertically from sea level to the seismograph (elevation correction) was also estimated and is shown in Table 1. All stations consisted of the standard U. S. Geological Survey (USGS) three-component short-period tape recording seismograph systems described in detail by Criley and Eaton (1978). At each station, high- and low-gain data channels were recorded along with continuous radio time signals (WWVB) and the output from an internal clock. The instruments operated for a 46-day period from May 22 to July 7, 1977. Halfway through the experiment, station 3C was moved 1.07 km northeast, but in the subsequent analysis results from both sites were treated as one.

During the recording period, 72 teleseismic events were recorded sufficiently well to warrant analysis. These events are listed in Table 2 and are reasonably well distributed in azimuth. Normally in temporary seismic arrays in the United States, the recorded teleseisms are primarily from three approximate azimuths—south-

Table 2. Teleseismic events.

Date	Location	Distance	Azimuth	Date	Location	Distance	Azimuth
5/22/77	Fiji	83.0°	239°	6/18/77	Mexico	29.6°	138°
5/24/77	Volcano Is.	85.2	299	6/18/77	Solomon Is.	94.0	261
5/24/77	Mariana Is.	87.4	292	6/18/77	S. of Fiji	89.1	238
5/25/77	Fiji	83.1	241	6/19/77	Samoa	77.7	238
5/28/77	Sulawesi	119.1	293	6/19/77	Kuril Is.	66.8	312
5/29/77	Kazakh SSR	91.5	352	6/19/77	N. Atlantic Ridge	61.9	92
5/30/77	Fox Is.	41.3	309	6/22/77	Tonga	84.8	236
5/31/77	Santa Cruz Is.	90.0	255	6/23/77	Komandorsky Is.	55.1	316
6/01/77	Tonga	82.6	236	6/24/77	Tonga	89.1	231
6/01/77	Turkey	98.6	29	6/24/77	Tonga	84.4	235
6/03/77	Fiji	83.2	240	6/25/77	Fiji	86.0	239
6/05/77	Chile	73.7	140	6/25/77	N. Carolina	11.8	291
6/05/77	New Britain	96.9	270	6/25/77	Oregon	11.2	293
6/06/77	Dominican Rep.	42.0	104	6/26/77	Kuril Is.	67.9	311
6/06/77	Vancouver Is.	16.1	317	6/26/77	Tonga	84.4	235
6/06/77	Tonga	82.1	238	6/26/77	Dominican Rep.	42.1	104
6/07/77	N. California	8.9	291	6/26/77	N. Atlantic Ridge	63.5	91
6/07/77	Santa Cruz Is.	89.8	256	6/27/77	S. of Fiji	86.4	235
6/07/77	Argentina	79.8	141	6/28/77	Chile-Bolivia	72.8	137
6/08/77	Chile-Bolivia	73.7	136	6/28/77	Sicily	89.5	38
6/08/77	Honshu	77.5	309	6/28/77	N. Atlantic Ridge	59.3	84
6/09/77	Kamchatka	56.8	317	6/28/77	N. Atlantic Ridge	59.2	84
6/09/77	Mariana Is.	91.6	283	6/28/77	N. Atlantic Ridge	49.2	84
6/10/77	Sumatra	133.0	310	6/28/77	N. Atlantic Ridge	59.3	84
6/12/77	Hokkaido	74.7	312	6/29/77	Banda Sea	117.7	283
6/13/77	Guatemala	31.5	135	6/29/77	Andreanof Is.	45.3	309
6/13/77	Tonga	80.5	237	6/29/77	Tonga	84.3	235
6/15/77	N. Atlantic Ridge	61.4	91	6/30/77	South Pacific	74.5	172
6/16/77	Samoa	77.3	239	6/30/77	Chile	70.4	137
6/17/77	Fiji	84.9	240	6/30/77	Tonga	79.4	238
6/17/77	Mariana Is.	87.0	292	6/30/77	Chile	76.7	238
6/18/77	New Hebrides	92.5	253	7/01/77	Tonga	79.0	238
6/18/77	Fiji	84.4	239	7/02/77	Solomon Is.	93.5	260
6/18/77	Chile-Bolivia	72.1	137	7/02/77	Kamchatka	58.9	315
7/03/77	Fox Is.	39.9	309	7/06/77	Panama	42.8	133
7/07/77	Argentina	78.9	139	7/06/77	Fiji	85.3	239

east, southwest, and northwest (Iyer, 1979). However, in the Roosevelt array we were fortunate to record teleseisms from the northeast quadrant as well. *P*-wave arrival times of these events were read from paper playbacks of the recording tapes. The combined frequency response of the recording and playback systems peaked between 1 and 5 Hz. Arrival times used were almost never the first-break time because much greater timing accuracy can be obtained by using some other distinctive feature of the first-cycle waveform such as a zero crossing, peak, or trough. Generally, two or three separate picks were made on the waveform for each event (see Figure 2), and all those for which the timing error was estimated to be 0.05 sec or less were used in the analysis. Care had to be taken, however, to ensure that waveform changes from station to station did not introduce spurious time differences. For example, variations in attenuation along paths to different stations can cause waveform changes (a low-Q path producing a relatively broader signal). Although we found generally very good waveform correlation from station to station (Figure 2), some cases of significant distortion were indeed noticed; these will be discussed more fully below.

Traveltime residuals were calculated on the basis of hypocenters given in the USGS bulletins on Preliminary Determination of Epicenters using the Herrin (1968) *P*-wave traveltime tables. In order to eliminate the large effects of origin-time errors, relative residuals were then calculated by subtracting from each station residual the average residual for each event for the whole array. Using the average residual as a reference introduces some scatter in the data because the number of observations varies from event to event (see Table 3). However, the alternative of using one particular station as a reference, as is often done, introduces the assumption of no change in residual with azimuth at that site. Given the initially unknown structure, we thought it best not to make that assumption. Plots of relative residual versus azimuth are shown in Figure 3 for sites 1C and 2A. Site 1C exhibits one of the largest azimuthal variations of residual, and site 2A one of the smallest. The scatter shown for these two sites is also typical of the others. Average relative residuals at each station, regardless of azimuth and also as functions of the four principal quadrants, are listed in Table 3 together with their standard deviations and numbers of observations. In all cases separate picks on the waveform of a single event are treated as separate (obviously, not independent) data points. If it is assumed that the residuals have a Poisson distribution about their means, the standard errors of the means are 0.02 sec or less in all cases.

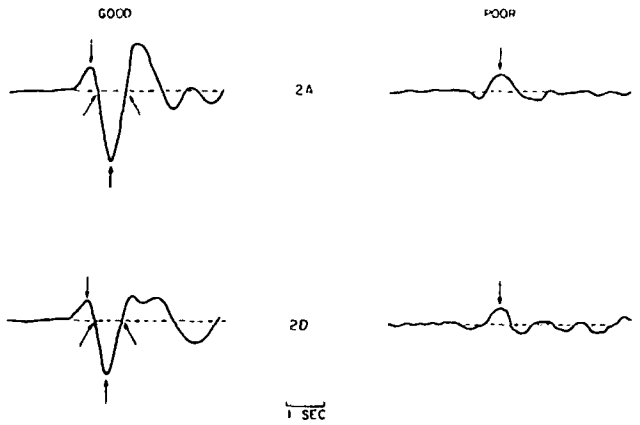

FIG. 2. Example of teleseismic *P*-wave signals at stations 2A and 2D. The arrows indicate the times used. Note the excellent waveform correlation for the first event through the first cycle of motion.

In addition to the teleseisms used above, numerous local and regional events were also recorded. Analysis of these data will be presented in detail at a later time. However, in the discussion of teleseismic results we will use arrival time data from a nuclear explosion at the Nevada test site on May 25, 1977, at a distance of 322 km and an azimuth of 242 degrees from the center of our network. For this event, the first arrivals were sharp and the first break was timed. The apparent velocity of the first arrivals indicates that they were P_n arrivals; the frequency was about 4 Hz.

ANALYSIS AND INVERSION OF THE DATA

The residuals averaged over all events for each station, listed in Table 3, reflect in only a gross way the vertically integrated velocity variations under the network because of the wide range of azimuths and incidence angles included. These results are contoured in Figure 4. (Usually in studies such as this, it is common practice to apply a correction to the residual to compensate

Table 3. Average relative residuals.

Station	All Azimuths			0–90°			90–180°			180–270°			270–360°		
	N	R	S D	N	R	S D	N	R	S D	N	R	S D	N	R	S D
1A	141	−0.23	0.06	14	−0.17	0.06	35	−0.26	0.06	35	−0.26	0.06	39	−0.21	0.07
1B	79	0.02	0.07	7	0.09	0.03	24	0.03	0.06	20	−0.05	0.05	28	0.03	0.06
1C	106	0.21	0.14	12	0.32	0.12	33	0.36	0.08	32	0.10	0.04	29	0.10	0.05
1D	96	0.17	0.14	11	0.18	0.08	32	0.34	0.07	22	0.06	0.04	31	0.09	0.07
2A	154	−0.11	0.06	15	−0.07	0.04	44	−0.16	0.05	59	−0.11	0.05	36	−0.09	0.06
2B	137	−0.05	0.10	12	0.03	0.13	38	−0.17	0.05	41	−0.10	0.06	46	0.01	0.09
2C	130	0.05	0.11	12	0.04	0.04	33	0.10	0.11	51	0.08	0.06	34	−0.03	0.14
2D	116	−0.17	0.09	15	−0.17	0.06	25	−0.06	0.06	41	−0.17	0.05	35	−0.25	0.04
3A	138	−0.02	0.06	15	0.01	0.05	34	−0.08	0.04	49	−0.02	0.04	40	0.03	0.05
3B	144	0.03	0.10	13	−0.03	0.03	41	−0.07	0.06	49	0.04	0.05	41	0.23	0.06
3C	106	0.14	0.10	9	0.04	0.04	36	0.04	0.05	56	−0.05	0.05	20	0.16	0.07
3D	149	−0.07	0.07	15	−0.07	0.06	37	−0.05	0.05	56	−0.05	0.05	41	−0.14	0.05
4B	76	0.12	0.10	1	0.06	—	29	0.02	0.09	29	0.17	0.04	17	0.19	0.07
4C	130	0.06	0.09	10	−0.04	0.05	32	−0.03	0.09	46	0.12	0.05	42	0.09	0.06
4D	90	0.10	0.08	10	0.01	0.03	23	0.03	0.07	37	0.12	0.04	20	0.16	0.06

N = number of observations; R = average residual (sec); SD = standard deviation.

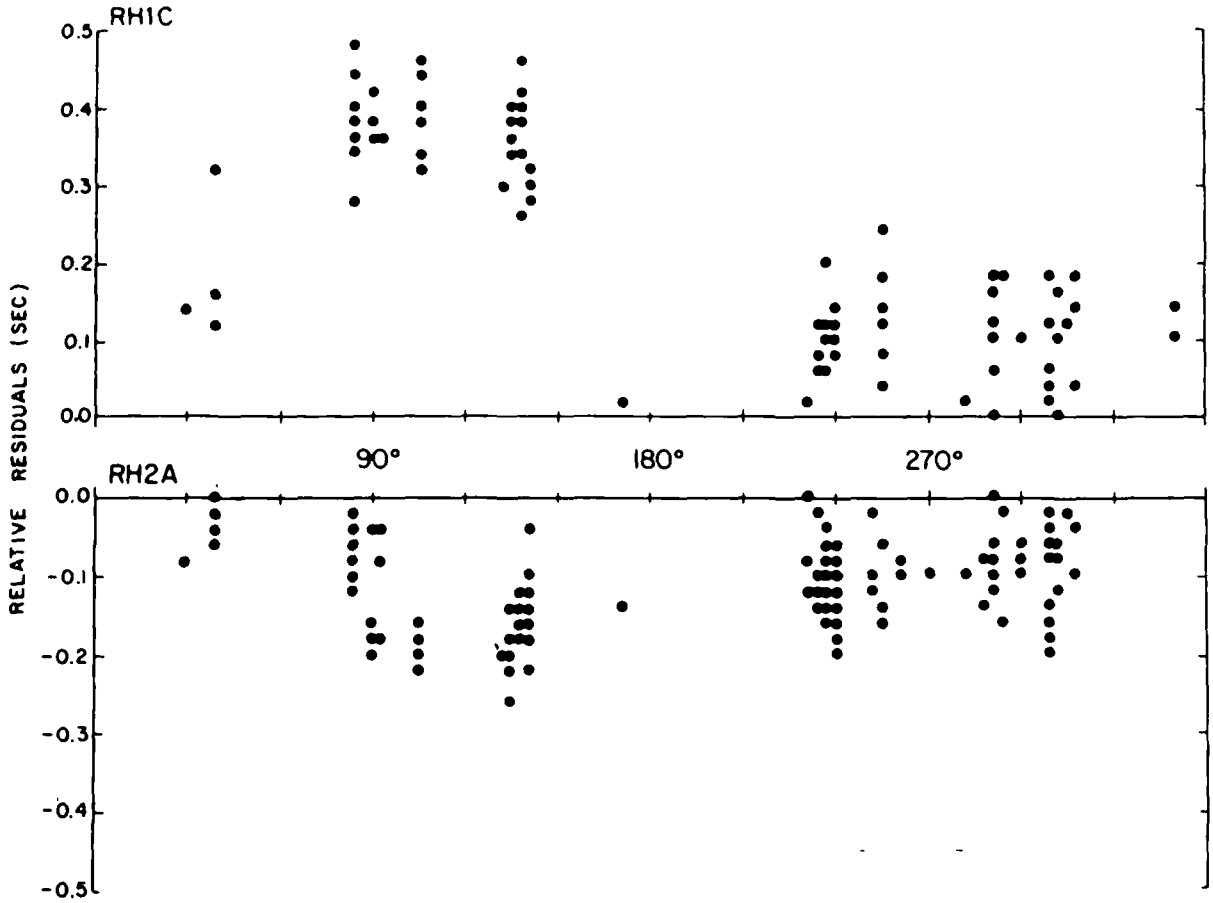

FIG. 3. Relative residuals as a function of azimuth for stations 1C and 2A.

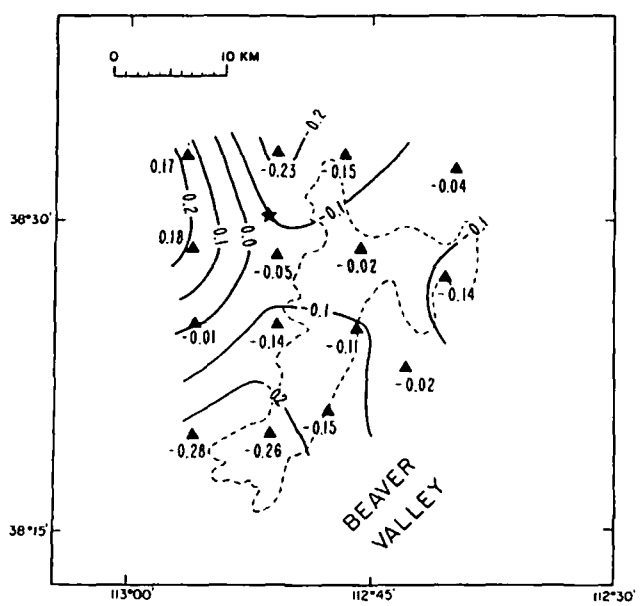

FIG. 4. Contours of average relative residual regardless of azimuth. The contour interval is 0.1 sec. Triangles represent the seismograph sites and the dotted curve outlines the Mineral Mountains. The star indicates the location of the Roosevelt Hot Springs.

for differences in station elevation. However, from Table 1 it will be seen that though elevation differences greater than 0.5 km occur, the effect of lithology is stronger than that of elevation. For example, note that stations 1C and 1D which have the lowest elevations have the largest elevation corrections. Because of this discrepancy, we did not apply elevation corrections at this point.) The basin-and-range structure is evidenced by the positive residuals at sites within Milford Valley and by the negative residuals at sites in the northern and southern Mineral Mountains. The positive residuals in Beaver Valley are not as pronounced as in the Milford Valley. Also, the residuals in the central Mineral Mountains are not as negative as they are to the north and south.

Considering the variations of residual with azimuth (Figure 3 and Table 3), it can be seen that there are significant azimuthal variations, reaching up to 0.4 sec at some of the stations. The general pattern of these variations is that the largest residuals (slowest path) occur in the direction toward the central Mineral Mountains. This effect can be seen, somewhat smoothed out, in the average residuals for the four azimuthal quadrants, shown in Figure 5. The striped areas are the regions where the relative residual is 0.1 sec or greater. It is clear that there is an azimuthally shifting "shadow zone." Such a pattern of residual variation cannot be explained simply by near-surface velocity variations since the angles of incidence, measured from vertical, of the teleseismic waves at the surface are generally 25 degrees or less

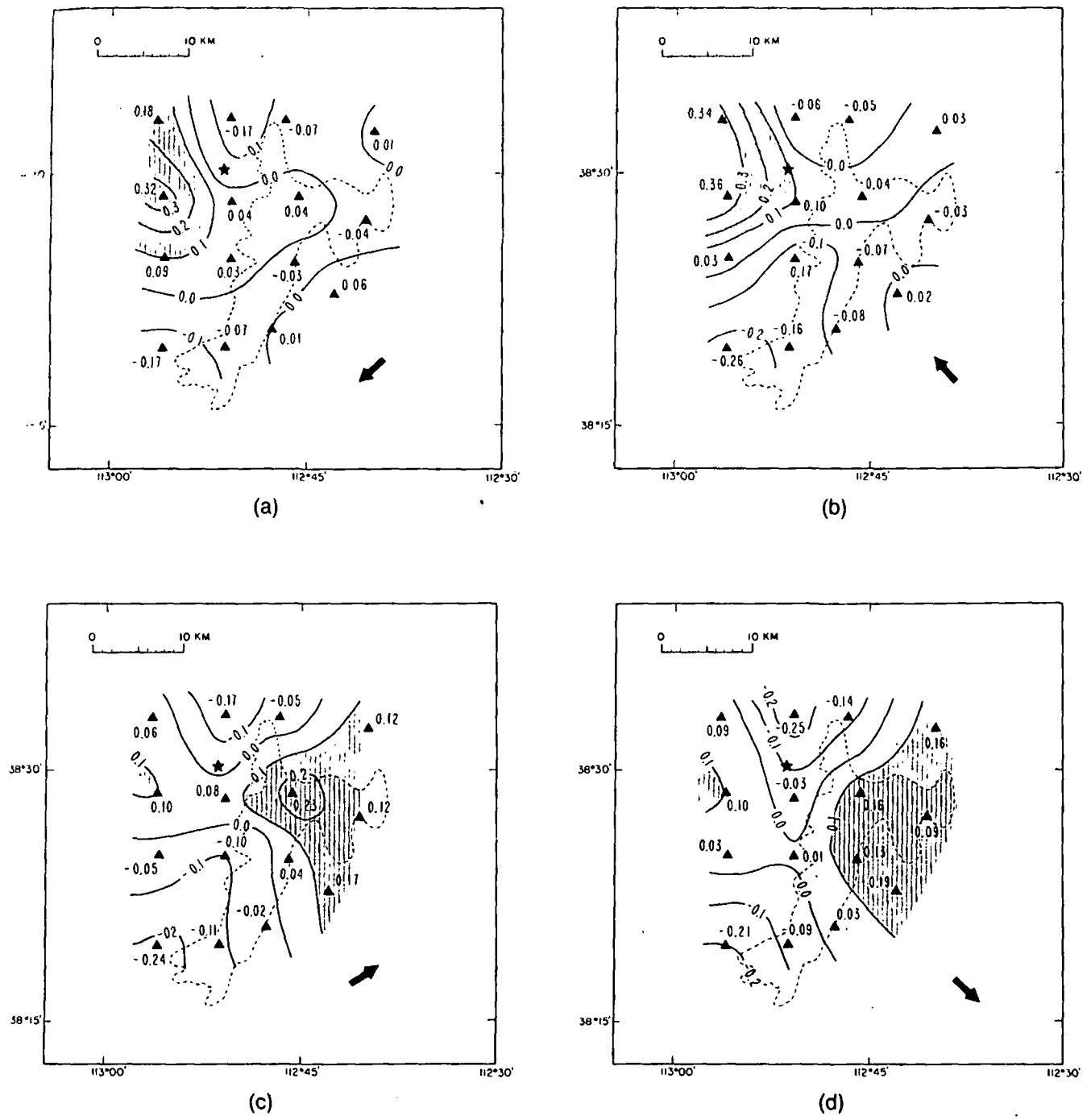

FIG. 5. Contour of average relative residual for the four principal azimuth quadrants. The shaded areas are zones where the relative residual is 0.1 sec or greater. The contour interval is 0.1 sec. Triangles represent the seismograph sites. The star indicates the location of Roosevelt Hot Springs. (a) 0–90 degrees; (b) 90–180 degrees; (c) 180–270 degrees; (d) 270–360 degrees.

(Steeples and Iyer, 1976). Ray tracing indicates that a possible cause of such a variation is a zone of relatively low velocity centered under the central Mineral Mountains in the middle and lower crust. For example, the major features of the data can be explained roughly by a sphere of radius 10 km and velocity 5.4 km/sec embedded in a half-space of velocity 6.0 km/sec at a depth of 20 km. Such a model is, however, only the simplest and not the best.

To be more quantitative and to take account of the more subtle changes in residual, we used a 3-D inversion procedure developed by Aki et al (1977). In this procedure a portion of the earth is subdivided into horizontal layers, each layer being divided in turn into a number of rectangular blocks. The initial uniform velocity assigned to each layer is modified in each block so as to minimize the variance of the resulting residuals, the needed changes obtained by finding a damped solution of a system of linear equations. The assumptions are that the velocity in each layer outside the model is uniform, that outside the model the earth is horizontally uniform, and that geometrical ray theory is applicable. A complete description of the use of this technique in a context very similar to ours can be found in Reasenberg et al (1980).

We adopted a four-layer model, each layer being 67.5 km square and subdivided into 9 × 9 blocks 7.5 km on each side. The top layer was 5 km thick and the lower ones 10 km thick. The lateral extent of the station array puts a limit on the model's maximum depth. Considering the typical wavelength of the teleseismic arrivals (5–10 km), a subdivision into smaller blocks is not warranted. The initial velocity model, shown in Table 4, is based on the seismic-refraction results discussed earlier. These initial velocities are not critical, however, since the results of the inversion procedure are in terms of the percent change in velocity within a layer, not absolute velocities. Absolute velocity values cannot be obtained from relative residual data.

Results of one inversion of the data are shown in Figure 6. These results are percent changes in velocity (positive values indicate a higher velocity). A value of 0 indicates that too few rays (<5) passed through that block for a meaningful change to be calculated. Underlined values are those for which the resolution is not as good (Reasenberg et al, 1980); all values for layer 1 are well resolved. The treatment for layer 1 was different from the deeper layers: a change in velocity was assigned to each station rather than to individual blocks. That avoided the problem of two or more stations with substantially different near-surface velocity structures overlying the same block in the model. Elevation was included in the treatment of the first layer. In this inversion, variance of the original data (0.0294 sec^2) was reduced by 91 percent to 0.0027 sec^2, close to what would be expected due to reading errors.

Table 4. Initial inversion model.

Layer	Thickness (km)	P-wave velocity (km/sec)
1	5.0	4.5
2	10.0	5.5
3	10.0	6.5
4	10.0	7.5

LAYER 1 (0 – 5 KM)

1A	7.3	3A	1.9
1B	−2.7	3B	3.6
1C	−13.1	3C	0.4
1D	−17.0	3D	5.9
2A	6.5	4B	−7.6
2B	7.9	4C	−1.1
2C	4.8	4D	−4.9
2D	9.5		

LAYER 2 (5 – 15 KM)

0	0	0	0	0	0	0	0	0
0	0	0	0	0	0	0	0	0
0	0	1.7	2.5	0.7	-1.6	-0.1	1	0
0	0.1	0.7	-1.4	-2.4	-1.7	2.3	0	0
0	0	-2.3	-5.1	-4.2	-0.5	3.9	0	0
0	0	0.1	0.9	1.0	1.8	-0.6	0	0
0	0	1.7	4.0	1.8	0.2	0	0	0
0	0	0	0	0	0	0	0	0
0	0	0	0	0	0	0	0	0

LAYER 3 (15 – 25 KM)

0	0	0	0	0	0	0	0	0
0	-0.8	-1.0	0.0	0	0	0	0	0
0.1	0.9	3.3	-1.3	0.4	-2.4	0.7	0	0
-0.7	0.9	2.2	-5.1	-3.8	0.2	1.1	0.1	0
-0.4	0.0	-0.6	-5.1	-2.8	0.8	2.3	0.1	0
-0.5	2.3	0.5	-2.0	-1.1	-0.9	0.6	-0.4	0
0	0	0.9	-1.2	2.0	0.0	3.8	0	0
0	0	0	1.5	3.4	1.7	0	0	0
0	0	0	0	0	0	0	0	0

LAYER 4 (25 – 35 KM)

2.0	0	0	0	0	0	0	0	0
-0.3	-0.6	0.0	-0.1	-0.6	0.7	0	0	0
-0.2	-0.3	3.1	0.4	-5.2	-1.4	0.6	0	0
1.0	0.5	1.6	-0.3	-3.0	-1.4	1.1	-0.8	0.5
-0.2	3.3	2.3	-2.8	-4.0	-1.6	-0.5	0.6	0.5
0	0.4	-0.9	-3.6	-4.8	-0.2	0.6	0.9	0
0	0.8	1.1	-1.2	-2.0	1.8	4.7	-1.1	0
0	0.6	-0.5	-0.5	1.2	3.6	0	0	0
0	0	0	0	0	0	0	0	0

FIG. 6. Results of one inversion of the residual data. Values are the percentage change in velocity for the corresponding block. Underlined values are less well resolved from nearby values. A 0 indicates insufficient data for a value to be calculated.

The results (shown in Figure 6) suffer to some degree from the necessarily coarse modeling due to the size of the blocks. In order to smooth out these effects, we did a second inversion with the block boundaries displaced one-half block width diagonally. Final values of the velocity changes were then calculated at a grid of points using a four-point average. These values are contoured in Figure 7 and will form the basis of the following discussion.

DISCUSSION OF THE RESULTS

Considering first the results for layer 1 (0–5 km depth), it can be seen that the basin-and-range structure dominates the results. A ridge of relatively high velocity is associated with the Mineral Mountains, although it is displaced to the west of the crest, perhaps reflecting the presence of the high-velocity metamorphic rocks along the western flank of the range. If these high-velocity rocks extend west under the Milford Valley, their effect on the results is hidden by that of the low-velocity valley fill which reaches a maximum near site 1D. These results are in good agreement with the refraction and gravity studies discussed previously. Simple models based on these studies suggest a velocity contrast of about 15 percent between sites in the Milford Valley and the Mineral Mountains for a layer 5-km thick, similar to that found

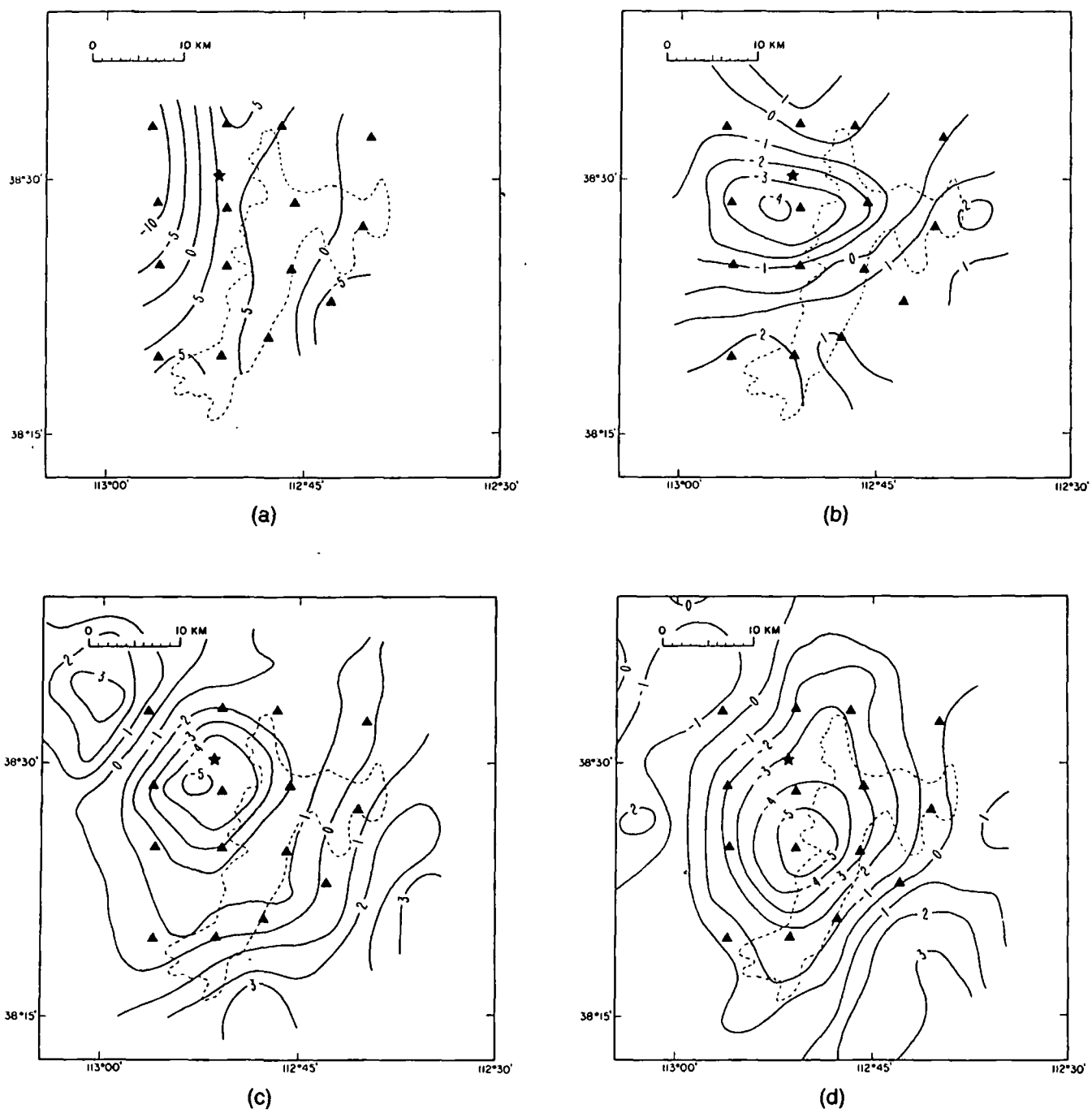

FIG. 7. Contours of the smoothed velocity changes. For the first layer the contour interval is 2.5 percent; for the others, it is 1.0 percent. Triangles represent seismograph sites. The star indicates the location of Roosevelt Hot Springs. The outlined area represents the Mineral Mountains. (a) Layer 1: 0–5 km; (b) Layer 2: 5–15 km; (c) Layer 3: 15–25 km; (d) Layer 4: 25–35 km.

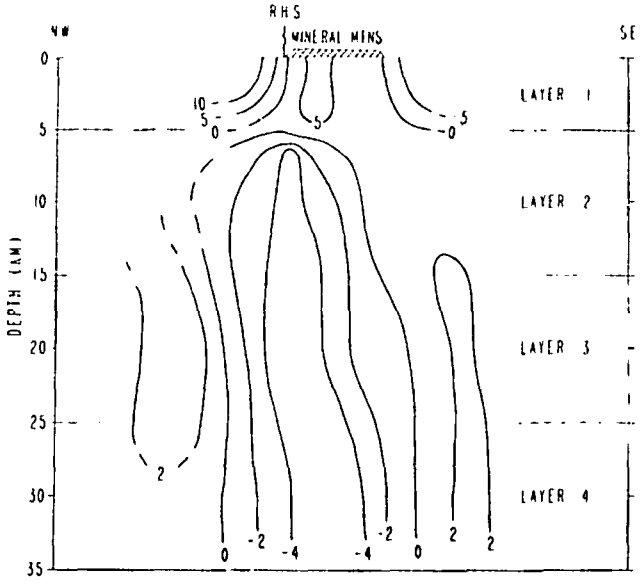

FIG. 8. A highly schematic northwest-southeast cross-section through the central Mineral Mountains based on the results shown in Figure 7. The vertical exaggeration is 2:1. Contours represent the percentage of lateral velocity contrast within the layers.

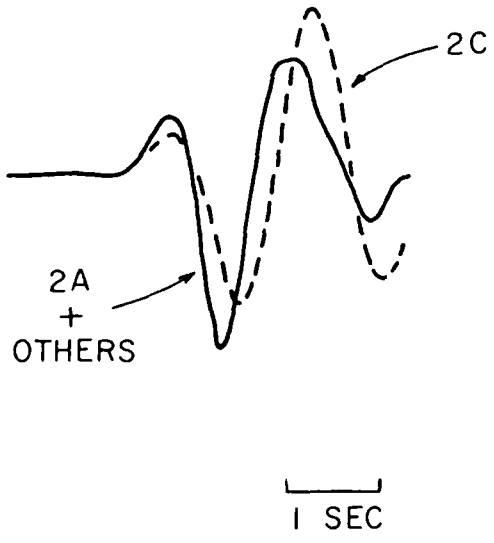

FIG. 9. An example of the waveform broadening as discussed in the text. The solid curve is the signal at site 2A and is similar to that at all other sites except, in this case 2C, which is shown by the dashed line. The event is at a southwest azimuth (Chile-Bolivia). For other azimuths other stations exhibit the broadening (see text).

here. To the east, in the area covered by stations 4B, 4C, and 4D, the average seismic velocity in this layer is lower than in the Mineral Mountains by 5 to 10 percent, reflecting the unconsolidated sediments in the Beaver Valley (less thick than in Milford Valley) and their extension north under the basalt flows near sites 4C and 4D.

Results for the second layer (5–15 km) are in sharp contrast to those above. They indicate a region of relatively low velocity (about 5 percent contrast; note the change in contour interval in Figure 7) centered near site 2C and also near the area of high heat flow associated with the Roosevelt Hot Springs geothermal area. This region of low velocity seems to extend west of the Mineral Mountains, although this may be due in part to imperfect resolution from the overlying low velocities of the Milford Valley in this region. It is important to note here that results such as this imply lateral contrasts in velocity and are not the same as the regional low-velocity zone inferred from refraction results in this depth range.

The results for the third layer (15–25 km) are similar in exhibiting a center of relatively low velocity near site 2C, but this region also extends more to the north and south. The results for layer 4 (25–35 km) in the uppermost mantle are again similar but show a shift south from the center of low velocity; the north-south elongation is still present. The velocity contrast in these deeper layers is somewhat greater, about 7 percent.

Overall, the results suggest a pipe-like feature of approximately 5–7 percent velocity contrast extending from about 5-km depth down at least as far as the uppermost mantle, centered near the Roosevelt Hot Springs geothermal area but extending to the north and south at depth. A highly diagrammatic northwest-southeast cross-section through Roosevelt Hot Springs is shown in Figure 8.

To see if this velocity structure derived from teleseismic data is in accord with data derived from regional earthquakes, the arrival-time data from a Nevada test site nuclear explosion were examined. The significance of this test is that it provides comparison between teleseismic residuals (computed using waves in the frequency band of 0.5 to 2 Hz) and residuals associated with higher frequencies characteristic of regional events. The event was approximately 310 km west of Roosevelt Hot Springs. Traveltime residuals for the explosion were calculated using the initial four-layer model and compared with those calculated on the basis of the final teleseismic inversion model. When this was done, it was found that the variance was reduced from 0.029 sec^2 (the same as for the teleseismic data) to 0.006 sec^2, an improvement of about 79 percent. The improvement in the variance using only the velocity structure determined for layer 1 is 68 percent. Thus, although the near-surface effects are clearly the most important (as they are for the teleseismic data also), the deeper structure also has an appreciable effect in reducing the variance. Still, it is clear that given the high accuracy in timing the nuclear blast arrivals (better than 0.05 sec), there remains a good deal of unexplained variance. Eventually a more detailed study of this event and other regional events may refine the rather coarse results obtained here on the basis of relatively low-frequency teleseismic data alone and perhaps provide some information on frequency-dependent effects.

Examination of waveforms of teleseismic signals provides some evidence for the presence of a small region of severe attenuation within the low-velocity body. As was mentioned above, during the process of reading the teleseismic arrival times, instances of significant waveform distortion were observed. These effects are very systematic and consistent among events from the same azimuth. For events at southeast azimuths, the waveform at station 2C was significantly broader than at any other station (an example is shown in Figure 9). Similarly, for events at southwest azimuths, station 3C exhibited waveform broadening while all other stations (including 2C) did not. For the northeast azimuth, the limited data indicate broadening at station 2B. For the northwest azimuth, however, no station exhibited abnormal broadening.

We have no detailed explanation for these observations as yet. Ray tracing would place the location of the distorting region at a

depth of about 15 km under the region bounded by the sites 2C, 3C, and 2B, within the region of relatively low velocity but displaced from its apparent center. The fact that distortion occurs at only one of many stations spaced within 10 km of one another argues that the region causing the distortion is small, probably too small for the observed broadening to be caused by attenuation alone. One possible explanation is the existence of a small (diameter about 5 km) region of intense attenuation; diffraction effects within the geometrical shadow zone could then explain the observed broadening (Matumoto, 1971). Such a region then would not produce a significant traveltime delay. Another possibility is a frequency-dependent focusing effect.

The interpretation of our results in terms of geology is not straightforward. Iyer and Stewart (1977) discussed the possible causes of low-velocity regions in the crust and upper mantle. These include lateral variation in temperature, composition, fabric, and the nature of any fluid inclusions (e.g., partial melt), in any combination. The recent volcanism certainly indicates that higher than normal temperatures are to be expected beneath the Mineral Mountains. Measurements of the temperature derivative of P-wave velocity (for references, see Iyer and Stewart, 1977) indicate that a 5 to 7 percent decrease in velocity would require a temperature increase of about 600°C to 850°C over that of the surrounding rocks. Phase diagrams for typical crustal rocks indicate that this would result in some degree of melting, especially if the regional geothermal gradient were initially abnormally high. Partial melting itself, however, leads to a much more rapid drop in velocity, so that an interpretation in terms of high temperatures needs to take this factor into account, too. Although experimental data on velocity in partially molten rocks at crustal pressures are scarce, theoretical models are well developed (e.g., O'Connell and Budiansky, 1977; Mavko, 1980). A 5 to 7 percent reduction in P-wave velocity (at a frequency of 1 Hz) can be explained by a melt fraction of only 1.5 to 4.0 percent depending upon assumptions about the pore shapes. This degree of melting would require temperatures only slightly above the solidus.

The possibility of a compositional change as the cause of the low-velocity region must be considered given the near-surface petrologic heterogeneity. A 5 to 7 percent lower velocity, for typical crustal rocks, would be associated with a density decrease of about 0.13–0.17 g/cm^3. A body of the shape of the low-velocity region with an average density contrast of 0.10 g/cm^3 would produce a broad gravity anomaly with a maximum amplitude of only about 14 mgal. It would be difficult to recognize such a long-wavelength anomaly among the stronger effects of the basin-and-range structure. [There is, however, a clear localized gravity low of 15–20 mgal in the central Mineral Mountains (Carter and Cook, 1978) that overlies the region we have hypothesized is causing waveform distortion.] Thus, a low-velocity feature such as we have found could represent something like a pipe of relatively low-density intrusive rocks, perhaps associated with the emplacement of the granitic rocks of the Mineral Mountains themselves. If so, it would then be puzzling that the extent of the low-velocity region at shallow depth (layer 2) corresponds not with the outcrop area of the granitic rocks but rather more closely with areas of thermal and volcanic activity.

It is thus our suggestion that the low velocity reflects abnormally high temperature and the presence of a small fraction of molten rock. However, the possibility that it is caused, in part or in whole, by compositional changes cannot be ruled out. At mid-crustal and lower depths, the postulated molten fraction would most likely be of basic composition (viz., the Quaternary basic eruptive activity on the northeast flank of the Mineral Mountains), whereas at shallower depths it would more likely be acidic and associated with the Quaternary rhyolitic activity along the crest of the mountains. The nature of the small anomalous region under the central Mineral Mountains associated with the waveform distortion remains somewhat of a mystery but it may be a region of more intense partial melt. On the basis of this model, the source of heat for the Roosevelt Hot Springs geothermal area is the region of partial melt, hydrothermal circulation serving to transport the heat to the surface. This model implies that there is a considerable heat reservoir associated with this geothermal area, much more than would be expected on the basis of a model involving only abnormally deep circulation of fluids along fault zones, a conclusion similar to that of Ward et al (1978) based on heat-flow data. An important question that remains is whether or not periodic recharge of the heat supply to shallower depths is required to maintain long-term, near-surface thermal activity and, if so, whether or not the region of partial melt would be sufficiently permeable to allow this to occur via upward flow of molten rock. In this regard, the small region of possibly more intense melt concentration may play an important role.

ACKNOWLEDGMENTS

We very much appreciate the help of the following persons in carrying out the field work and aiding in the playback and analysis of the resulting data: John Coakley, Edward Criley, Dennis Seguirant, Mary Ann Spieth, Tim Hitchcock, Dave Oppenheimer, and Allan Walter. Also the help of W. Ellsworth and P. Reasenberg was invaluable to us in applying the 3-D inversion method to our data. Reasenberg's thorough and critical review of the manuscript is very much appreciated.

REFERENCES

Aki, K., Christoffersson, A., and Husebye, E., 1977, Determination of the three-dimensional structure of the lithosphere: J. Geophys. Res., v. 82, p. 277–296.

Braile, L., Smith, R. B., Keller, G. R., Welch, R., and Meyer, R. P., 1974, Crustal structure across the Wasatch Front from detailed seismic refraction studies: J. Geophys. Res., v. 79, p. 1295–1317.

Carter, J. A., and Cook, K. L., 1978, Regional gravity and aeromagnetic surveys of the Mineral Mountains and vicinity, Millard and Beaver counties, Utah: Final rep. v. 77-11, DOE/DGE contract EY-76-S-07-1601, Univ. of Utah, 179 p.

Criley, E. E., and Eaton, J. P., 1978, Five-day recorder seismic system: U.S.G.S., open-file rep. 78-266.

Gertson, R. C., and Smith, R. B., 1979, Interpretation of a seismic refraction profile across the Roosevelt Hot Springs, Utah and vicinity: Topical Rep. IDO/78-1701.a.3, DOE contract DE-AC07-78er28392, Univ. of Utah, 120 p.

Herrin, E., 1968, Seismological tables for P: SSA Bull., v. 58, p. 1196–1219.

Hose, R. K., and Taylor, B. E., 1974, Geothermal systems of northern Nevada: U.S.G.S. open-file rep. 74-271.

Iyer, H. M., 1979, Deep structure under Yellowstone National Park, U.S.A.: A continental "hot spot": Tectonophys., v. 56, p. 165–197.

Iyer, H. M., and Stewart, R. M., 1977, Teleseismic technique to locate magma in the crust and upper mantle, *in* Magma genesis: H. J. B. Dick, Ed., Oregon Dept. of Geol. and Min. Ind. Bull. 96, p. 281–299.

Iyer, H. M., Oppenheimer, D. H., and Hitchcock, T., 1979, Abnormal P-wave delays in the Geysers—Clear Lake geothermal area, California: Science, v. 204, p. 495–497.

Matumoto, T., 1971, Seismic body waves observed in the vicinity of Mount Katmai, Alaska, and evidence for the existence of molten chambers: GSA Bull., v. 82, p. 2905–2920.

Mavko, G. M., 1980, Velocity and attenuation in partially molten rocks: J. Geophys. Res., v. 85, p. 5173–5189.

Müller, G., and Mueller, S., 1979, Traveltime and amplitude interpretation of crustal phases on the refraction profile Delta-W, Utah: SSA Bull., v. 69, p. 1121–1132.

O'Connell, R. J., and Budiansky, B., 1977, Viscoelastic properties of fluid saturated cracked solids: J. Geophys. Res., v. 82, p. 5719–5736.

Olson, T. L., and Smith, R. B., 1976, Earthquake surveys of the Roosevelt Hot Springs and Cove Fort areas, Utah: Final rep., v. 4, NSF grant GI-43741, Univ. of Utah, 83 p.

Prodehl, C., 1970, Seismic refraction study of the western United States:

GSA Bull., v. 81, p. 2629–2646.
Reasenberg, P., Ellsworth, W., and Walter, A., 1980, Teleseismic evidence for a low-velocity body under the Coso geothermal area: J. Geophys. Res., v. 85, p. 2471–2483.
Smith, R. B., 1979, Seismicity, crustal structure, and intraplate tectonics of the interior of the western Cordillera: GSA memoir 152, p. 111–144.
Smith, R. B., Braile, L., and Keller, G. R., 1975, Crustal low velocity layers: Possible implications of high temperatures at the Basin and Range—Colorado Plateau transition: Earth and Plan. Sci. Lett., v. 28, p. 197–204.
Steeples, D. W., and Iyer, H. M., 1976, Low-velocity zone under Long Valley as determined from teleseismic events: J. Geophys. Res., v. 81, p. 849–860.
Ward, S. H., Parry, W. T., Nash, W. P., Sill, W. R., Cook, K. L., Smith, R. B., Chapman, D. S., Brown, F. H., Whelan, J. A., and Bowman, J. R., 1978, A summary of the geology, geochemistry, and geophysics of the Roosevelt Hot Springs thermal area, Utah: Geophysics, v. 43, p. 1515–1542.

so measured will also locate distinctive radiation sources. With sufficient knowledge of the wave nature of the microseisms and a reasonably accurate velocity-depth model, a fixed nonaliased array can be used in a beam-steering mode to define the source region of radiated noise. Both approaches, as used in typical surveys, suffer greatly when data are contaminated by nongeothermal seismic noise, by interfering seismic wave trains, or by improper temporal and spatial data sampling. These pervasive problems have combined to render noise analysis at best a qualitative geophysical method and have substantially limited the acceptance of the seismic noise survey as an integral element in geothermal exploration.

This study attempts to avoid such problems through careful analysis of microseismic data in an evaluation of the feasibility of ground noise studies in geothermal site delineation. We report a series of investigations undertaken near Leach Hot Springs in Grass Valley, within the region of generally high heat flow in northern Nevada. We first quantify the spatial and temporal variations of ground noise in the region and find that the seismic noise spectrum is strongly affected by near-surface sedimentary layers at the recording site. In fact, with broadband seismic sensors in a mapping technique using amplitudes and frequencies, one can outline lateral variations in alluvial thickness. This standard mapping technique cannot differentiate noise enhancement due to shallow structure from noise enhancement due to a buried seismic source. On the other hand, we find that the mapping of wave propagation parameters provides additional information about the noise field. However, the successful application of this technique requires some understanding of the wave nature of microseisms. We used multiple-sensor arrays to study the seismic coherency as a function of frequency and spatial separation. Based on this information, an array was designed to record propagating microseismic data. The array data were processed by both the frequency domain beamforming method (BFM) and the maximum-likelihood method (MLM). From the dispersion curves obtained in the array study, it was verified that the seismic noise consists primarily of fundamental-mode Rayleigh waves.

This paper consists of several sections describing the methodology, the area studied, the data, its interpretation, and recommendations. This study together with other detailed geologic, geochemical, and geophysical studies carried out in the area provide all the ingredients, except the test wells, for a complete case history on a geothermal prospect.

GEOTHERMAL GROUND NOISE

Clacy (1968) first suggested that seismic noise increased near geothermal reservoirs. His first results northeast of Lake Taupo, New Zealand, were based on contours of total noise amplitude in the frequency band of 1 to 20 Hz. In subsequent surveys at Wairakei, Waiotapu, and Broadlands geothermal areas, he found that the local noise amplitude anomalies were characterized by a dominant frequency of 2 Hz, whereas, away from the area of the anomaly, frequencies higher than 3 Hz predominated. On the other hand, Whiteford (1970) found in repeat surveys of the same areas that neither the shape of the frequency spectrum nor its dominant frequency conformed to any regional pattern. Whiteford measured the absolute ground motion in the Waiotapu geothermal area and found that, within a distance of 1 to 2 km of the high heat flow area, the average minimum ground particle velocity was greater than 150×10^{-9} m/sec, while farther away the amplitude of the ground movement decreased by a factor of about 3 and, in addition, exhibited pronounced diurnal variations.

In the United States, a similar survey was first carried out southeast of the Salton Sea by Goforth et al. (1972) who suggested for geothermal reservoirs an empirical relationship between high-temperature gradient and high seismic noise level. Their results showed a significant increase in the noise power in the frequency band of 1 to 3 Hz at sites above the reservoir. They estimated the power spectrum at each site from ten 200-sec data segments taken over eight hours of nighttime recording. The contour map of the total power in the frequency band of 1 to 3 Hz was similar to the temperature gradient contour map. Douze and Sorrells (1972) conducted a similar survey over the nearby East Mesa area, where they found that the total seismic power in the 3 to 5 Hz band exhibited spatial variations similar, in general, to gravity and heat flow fields. East Mesa was later surveyed by Iyer (1974) with significantly different results. Iyer measured seismic noise by averaging 20 of the lowest values of the root-mean-square (rms) amplitude in several narrow frequency bands, using data blocks of 81.92 sec selected from four hours of digital data. He did not find an anomaly in seismic noise associated with geothermal activity but only the noise from canals and freeway traffic.

The seismic pulsation associated with several geysers in Yellowstone National Park is believed to be indicative of the heating of water in the under-

ieated system. Nicholls and Rinehart (1967) e studied the seismic signature of several geysers ı the park and inferred that their predominant pulse frequencies are quite similar, in the range of 20–60 Hz, presumably due to steam action. The very low-frequency seismic pulses recorded at Old Faithful, Castle, Bead, Plume, and Jewel geysers are believed to be associated with some type of water movement. The maximum amplitude of seismic pulses recorded in Yellowstone Park is 5.08×10^{-5} m/sec. At Old Faithful Geyser, the maximum amplitude is 2.54×10^{-5} m/sec at 30–50 Hz.

Iyer and Hitchcock (1974) also found good correlation between geothermal activity and high seismic noise levels in the 1 to 26 Hz range in the Park. The ground noise level in nongeothermal areas of the Park is approximately 13 to 15×10^{-9} m/sec at 1 to 26 Hz. In the Lower and Upper Geyser Basins where there are numerous geysers and hot springs, the average noise level is in general higher than $50 \times$

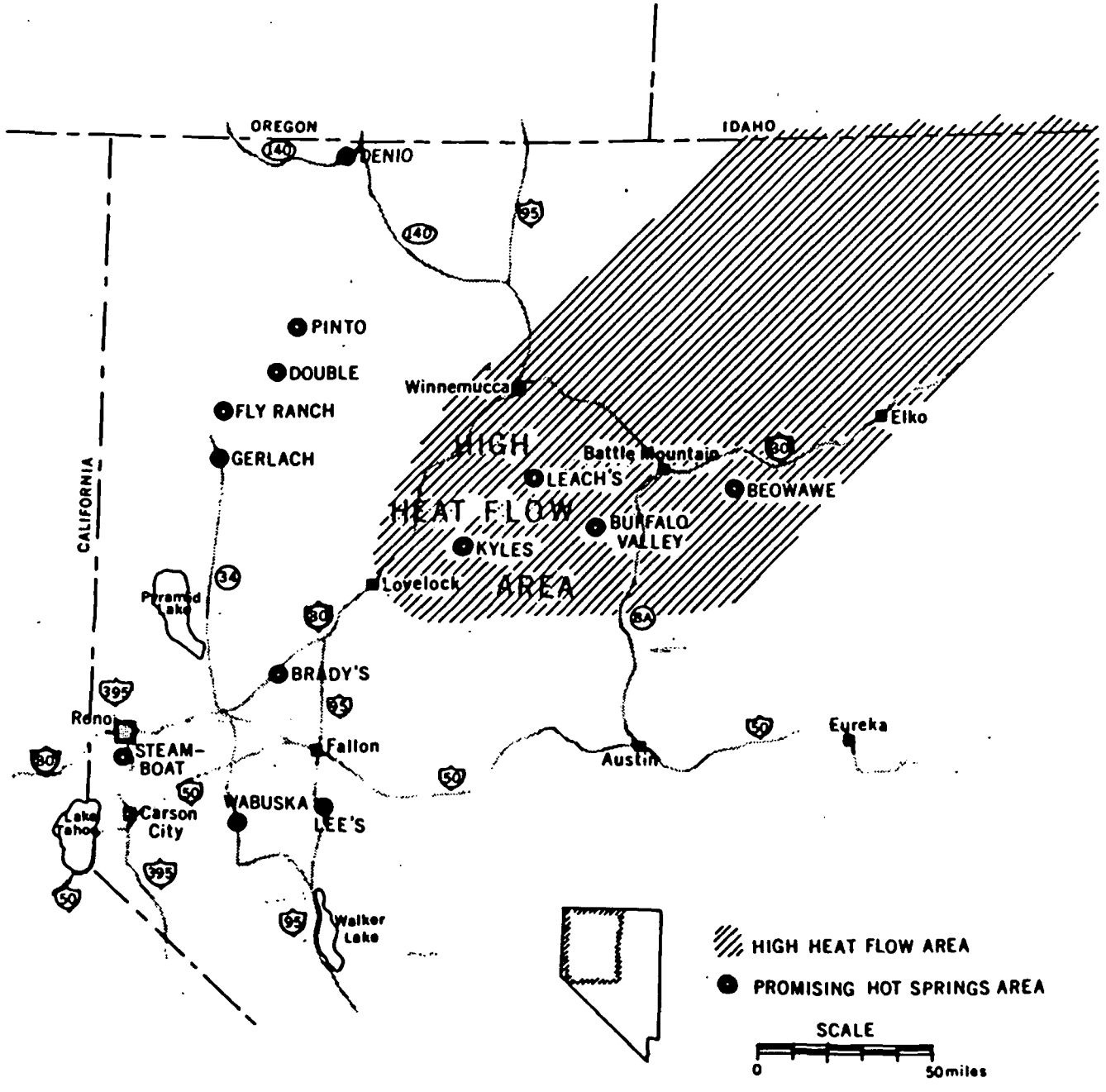

FIG. 1. Prominent thermal springs areas and the Battle Mountain high heat flow region in Northwestern Nevada. Shaded area indicates high heat flow area.

m/sec and reaches a value of 672×10^{-9} m/sec near Old Faithful. In the Norris Basin, another highly active geyser basin in the Park, the noise level varies from 50 to 500×10^{-9} m/sec. Part of the observed noise in the Lower, Upper, and Norris Geyser Basins is no doubt generated by the hydrothermal activity at the surface. The measurements near Old Faithful indicate that high-frequency noise, in the 8 to 16 Hz band, is generated during geyser eruptions; the noise level of lower frequencies is not affected by the eruption cycles. Noise levels around Mammoth Hot Springs are two to five times higher than in the surrounding area. There is no geyser or fumarole here, and the geothermal water is relatively cooler than at Norris and the other geyser basins. Hence, it is very unlikely that the seismic noise observed here is generated near the surface. The noise anomaly observed in the area between Lower Falls and Mud Volcano could be caused by ground amplification effects in the soft sedimentary deposits.

Correlations have also been reported between geothermal activity and high seismic ground noise in the Vulcano Islands, Italy (Luongo and Rapolla, 1973), the Coso geothermal area, China Lake, California (Combs and Rotstein, 1975), and Long Valley, California (Iyer and Hitchcock, 1976). High-frequency noise ($f > 8$ Hz) in the vicinity of geysers, fumaroles, and hot springs is associated with hydrothermal activity near the surface and during the geyser eruption. Low-frequency noise ($f < 8$ Hz) is not affected by geyser eruption cycles and is probably generated at depth.

It is evident that a noise power anomaly may result not only from an active seismic source, but also from lateral variation in near-surface velocity, particularly where low-velocity alluvium is involved. In order to identify a buried radiating source, the direction of propagation and the apparent phase velocity of the coherent noise field must be utilized. Whiteford (1975) successfully located the noise source in the Wairakei area using tripartite geophone array measurements. Iyer and Hitchcock (1976) used an L-shaped array with 106-m geophone spacing in Long Valley and found that propagation azimuths for the high-velocity waves defined the area of surface geothermal phenomena, but they found that random directions of propagation were characteristic of low-velocity waves.

Azimuth and apparent velocity measurements are complicated for microseisms because of multipath arrivals and nonstationary characteristics. In addition, very short wavelengths (10–20 m) can characterize the noise field in areas of low-velocity surface materials, and these are often aliased to lower wavenumber (longer wavelengths, higher velocities) and misinterpreted if array geophone spacing is too large.

MICROSEISMS

The study of microseisms, or earth noise, has been directed primarily toward frequencies less than 0.5 Hz, where the source is either ocean waves associated with storms (Longuet-Higgins, 1950; Gutenberg, 1958; Oliver, 1962; Oliver and Ewing, 1957; Oliver and Page, 1963; Haubrich and Mackenzie, 1965; Haubrich and McCamy, 1969; Fix, 1972) or atmospheric disturbances (Sorrells et al, 1971; Savino et al, 1972). Background microseism spectra for the range 0.02 to 1 Hz are characterized by two maxima at frequencies near 0.071 and 0.143 Hz (periods of 14 and 7 sec), both apparently due to coastal storm effects. In the period range beyond about 3 sec, local atmospheric pressure changes contribute primarily to the microseisms observed.

High-frequency microseisms ($f > 0.5$ Hz) observed away from the coast are generated locally by cultural activity, traffic, wind, rivers (Wilson, 1953; Robertson, 1965; Iyer and Hitchcock, 1974), by geothermal processes, and by distant sources (Lacoss et al, 1969). Noise observed at the ground surface usually consists principally of fundamental-mode Rayleigh waves. At depths where the fundamental mode has decreased to negligible amplitude, the noise consists of Rayleigh modes of order higher than third, or of body waves (Douze, 1967). Sharp spectral peaks and troughs can be related to shallow geologic structure. Low-velocity alluvium or weathering can produce a significant amplitude increase of seismic noise over that observed at a bedrock site. Thus, the shallow section can provide a waveguide for microseisms at particular frequencies (Kanai and Tanaka, 1961; Sax and Hartenberger, 1965; Katz, 1976; Iyer and Hitchcock, 1976). Certain sources of microseisms, such as waterfalls or pipelines, can produce narrow-band radiation. Near the Owens River at Long Valley, California, Iyer and Hitchcock (1976) report that the flowing river generates noise at frequencies above 6 Hz, attenuated by about 12 dB at 1 km from the river. At East Mesa, California, the canals seem to be continuous wide-band sources of seismic noise which drops off rapidly with distance, reaching a fairly steady level at 3 km. At the power drops (small waterfalls) along the canal, however,

below the surface. Before and after a survey, all geophones were buried in a common hole to verify uniformity of their responses.

For determination of spatial variation of wavenumber, an array of 12 closely spaced geophones was emplaced at a site each evening. Data were transmitted by cable to the recording vehicle some 500 m from the array. The array configuration and its impulse response in wavenumber space are shown in Figure 4. The existence of short-wavelength noise components and the low coherence seen at large geophone separation both dictated the tight array spacing used. An array of 100-m element separation or more, commonly used in ground noise studies elsewhere, would give spurious results because spatial aliasing folds the high-wavenumber noise components (which we have seen dominant in the valley alluvium) into low-wavenumber noise components. The spatial aliasing results in the appearance of erroneously high-velocity ground noise, which is interpreted as body waves. The effect of spatial aliasing due to inadequate element separation is illustrated in Figure 5, where we processed a simulated 4 Hz plane wave with 50-m wavelength, propagating with phase velocity of 200 m/sec in the direction N60°E across four arrays. Those arrays have identical array shapes and numbers of sensors but different sensor spacing. The diameters of the arrays are 50, 75, 250, and 500 m, such that the sensor spacing for each array is proportional to the array size. Since the plane waves are propagating at an azimuth of 60 degrees, the folding effects are evident along the directions of 60 degrees and 240 degrees. Many interpretations of microseisms as body waves, based on coarse sensor separation, may well be incorrect due to aliased low-velocity surface waves as seen, for example, in Figure 5c. It is true, of course, that when the array is made small enough to accommodate the short-wavelength noise characteristics, resolution for near-vertically incident body waves is degraded seriously; however, they could be enhanced by appropriate array expansion and spatial filtering.

For determination of the spatial variation of amplitude, data were selected judiciously from the quietest recording period in the early morning hours. At least 28 simultaneously recorded blocks of data were chosen from each of the recording stations, avoiding any spurious transient signals. Each data block of 12.8 sec length was filtered and digitized. The resulting 512-point records were tapered to zero at each end over 51 points and Fourier transformed. The conjugate to produce power spectral density. The estimated power spectral density at each location is the average over at least 28 data blocks, to increase statistical confidence. The ground velocity spectral density (VSD) in $m\mu/sec/\sqrt{Hz}$ was obtained by taking the square root of the power spectral density estimate and correcting it for system response. The relative intrinsic noise level, in dB, for a particular frequency band at a station is obtained by integrating the velocity spectral density over the frequency band and normalizing by that quantity at the reference station.

For estimation of the frequency(f)-wavenumber (k) power spectral density, array data were processed by using both the frequency domain beam-forming method (BFM) (Lacoss et al, 1969) and the maximum-likelihood method (MLM) (Capon, 1969). The BFM estimates f-k power spectral density by the formula

$$\hat{P}(f, \mathbf{k}) = \frac{1}{N^2}\, \mathbf{a}' \cdot \hat{\mathbf{S}} \cdot \mathbf{a}, \qquad (1)$$

where $\hat{P}(f, \mathbf{k})$ is BFM f-k power spectral density estimate, N is the number of geophones in the array, $\mathbf{S}$ is the estimate of the coherent power spectral density matrix between sensors, and $\mathbf{a}'$, the conjugate transpose of $\mathbf{a}$, is given by

$$[\exp(i2\pi \mathbf{k} \cdot \mathbf{r}),\ \exp(i2\pi \mathbf{k} \cdot \mathbf{r}_2), \ldots, \exp(i2\pi \mathbf{k} \cdot \mathbf{r}_N)], \qquad (2)$$

where $\mathbf{r}_n$ is the coordinate of the nth geophone location. Each entry of $\hat{\mathbf{S}}$, $\hat{S}_{ln}(f)$, is obtained from

$$S_{ln}(f) = \frac{1}{M} \sum_{m=1}^{M} \Phi_{lm}(f)\, \Phi^*_{nm}(f), \qquad (3)$$

by the normalization

$$\hat{S}_{ln}(f) = \frac{S_{ln}(f)}{\sqrt{S_{ll}(f) S_{nn}(f)}}, \qquad (4)$$

where $\Phi_{lm}(f)$ are the Fourier coefficients of the mth block time series from the lth geophone, and * indicates complex conjugate.

BFM is commonly called a conventional method, whose operation can be seen by rearranging equation (1) to be

$$P(f, \mathbf{k}) = \frac{1}{N^2} \sum_{n=1}^{N} \sum_{l=1}^{N} \hat{S}_{ln}(f) \cdot \cdot \exp[-i2\pi \mathbf{k} \cdot (\mathbf{r}_l - \mathbf{r}_n)]. \qquad (5)$$

For BFM a uniform weighting function is applied

for a model based on P-wave velocities from a shallow refraction survey in the area. The effect of the very shallow velocity structure is illustrated clearly. Lateral variations in the upper 10 to 20 m will control the surface wave propagation characteristics. In estimating dispersion curves, we do not restrict sampling to the quiet periods, since larger microseisms are very coherent across the array. The dispersion measurements, besides providing local observations of phase velocity for shallow structure mapping, also provide a method of verifying the wave nature of the microseisms. It is clear that waves with periods of 1 sec and greater must be analyzed for structural information at geothermal target depths, if the microseisms are fundamental-mode Rayleigh waves (see, for example, McEvilly and Stauder, 1965).

CONCLUSIONS

The spatial distribution of the amplitude, frequency, and wavenumber characteristics of background microseisms, or ground noise, contains information on the variation of subsurface properties and the location of buried sources of seismic waves. Extraction of the information requires careful sampling of the microseismic field in time and space. A simple field system, utilizing FM telemetry of data to a small, trailer-mounted, central recording site, was fabricated for one- or two-man installation and operation in a study of the methodology in a potential geothermal area in Grass Valley, Nevada.

Diurnal variation in the 2–20 Hz noise field is regular. A consistent diurnal variation that repeats from day to day is due apparently to meteorological and cultural sources, with typically 15 dB variation seen from the midday high noise level to the low noise level in the early morning hours of 2–4 AM. Secular variations, due to regional weather patterns, can produce a 5–10 dB range in the early morning minimum noise levels over a duration of a few days.

For spectral stability in investigating spatial variation of noise, at least 28 quiet data blocks, each 12.8 sec long, were taken simultaneously at the network stations, and the spectra were averaged for each site. This procedure produced consistent results throughout the area, revealing a characteristically low-amplitude smooth noise spectrum at hard rock sites, a prominent peak at 4–6 Hz at valley sites, and wide-band high-amplitude noise, apparently due to very shallow sources, at hot springs sites. Contour maps of noise level, normalized to a reference site, are dominated by the hot springs noise levels outlining faults are evident when they produce a shallow lateral contrast in rock properties.

Microseisms in the 2–10 Hz band are predominantly fundamental-mode Rayleigh waves, characterized by low velocities and wavelengths as small as 20 m, requiring arrays of closely spaced geophones for adequate spatial sampling.

High-resolution f-k processing, with proper data sampling, provides a powerful technique for mapping the phase velocity and the direction of propagation of the noise field, revealing local sources and lateral changes in shallow subsurface structure.

No evidence for a significant body wave component in the noise field was found, although it becomes clear that improper spatial sampling can give a false indication through aliasing. Noise emanating from a deep reservoir would be evident as body waves and could be traced to its source given a reasonably accurate velocity model.

RECOMMENDATIONS

Conventional seismic ground noise surveys, conducted as outlined in this study, require a large number of stations for economical implementation. With 100 stations, for example, a week-long survey could provide maps of noise amplitude distribution, P-wave delay time, and microearthquake locations, as well as f-k analyses at many sites, utilizing a 2–3 man crew. It is not clear, however, that such data will be of significant value in delineating a geothermal reservoir.

The amplitude mapping of ground noise in certain frequency bands is a poor exploration technique for delineating buried geothermal systems. The results of the amplitude mapping indicate that the amplitude variations of microseisms in an area are controlled by the near-surface geology, especially lateral variations in thickness of the alluvial layer. The large amplitude surface wave generated by surface sources and propagating horizontally will mask weak seismic waves emitted from a buried source. Therefore, amplitude mapping only reveals information on the very shallow structure.

On the other hand, the technique of f-k analysis can, theoretically, map the wavenumber of the microseisms, discriminating the vertically incident body waves from the surface waves. The yet open question of whether a reservoir acts as a radiator of seismic body waves can be answered through careful f-k analyses in existent geothermal areas. The array to be used for further study must be a nonaliased array of

pansion in array size will improve the resolution around the origin of the $k_x - k_y$ diagram. This improvement would provide a more accurate estimate for power at the small wavenumbers, so that the azimuth and the apparent velocity of the long-wavelength body waves are estimated more accurately. The amplitudes of body waves radiating from a source at depth are apparently much smaller than those of the ambient surface waves. In order to extract useful information from the body waves, a sophisticated signal detection and processing scheme is required. However, the *f-k* analysis technique may fail to detect the geothermal system at depth if our assumption of body wave radiation from the reservoir is not valid, or if the emanating body waves are either attenuated or completely masked by the ambient surface waves. It is fortunate that the ambient surface waves have shorter wavelengths than the anticipated body waves; because of this, the detection of weak body waves can be improved by a more sophisticated array, as is commonly done in conventional seismic reflection surveying.

If the assumption of radiated body waves is indeed valid, and if such body waves are detectable, we can trace the recorded wavefronts to their source, given a reasonably accurate velocity model. There are two schemes which have been used for projecting waves observed at the surface back into the earth and locating the source region, and these methods may be applicable to the geothermal reservoir delineation problem.

The first method is seismic ray tracing described by Julian (1970) and Engdahl and Lee (1976). If the array diameter is much smaller than the distance to the buried source, the microseismic field propagates as a plane wave across the array. Estimation of the azimuth and the apparent velocity of the propagating noise field from *f-k* analysis, along with the knowledge of the near-surface velocity distribution, can give us the incident angle of the coherent body wave noise. Given a reasonable velocity structure in the area and simultaneously occupied array sites, we can reconstruct raypaths to each site. The intersection of these raypaths indicates the region of the radiating source.

Another approach is much like that used in a conventional reflection survey with 2-D surface coverage but without a surface-controlled source. The coherent noise fields recorded by a 2-D surface array are projected downward into the assumed subsurface model. The reconstruction of the coherent noise field propagates the wave equation migration technique, using a finite-difference approximation such as the one described by Claerbout (1976). The restriction of this approach to microseismic data is that the noise field must propagate as a spherical wavefront across the geophone array. The spherical wavefront exists in the situation where the array dimension is greater than the distance to the source. In this case, we can determine the region of radiating sources in terms of the convergent pattern of the extrapolated wave fields.

It is clear that ray tracing and the wave equation migration are applicable at different source-array distances in the application of delineating geothermal reservoirs. In a practical exploration program, we do not know the depth of geothermal reservoirs, nor do we know the shape of the wavefront across the array. One way of solving the problem is to place a non-aliased array at several sites and search for the evidence of time-invariant, high-velocity body waves. As soon as the body waves are detected, one may compare several results of *f-k* analysis, using data of identical recording periods but of different sizes of subarray. The deterioration of the resolution in the *f-k* diagrams, as we expand the size of the subarray, indicates that the plane wave assumption is violated and the wavefront migration techniques should be applied. On the other hand, if the noise fields propagate as plane waves across the large array, the resolution in the *f-k* diagrams will be improved as we expand the size of subarrays, and the *f-k* analysis with seismic ray tracing is the proper technique to locate the noise source.

Based on this study, we suggest that if the geothermal system is indeed emanating detectable body waves, the analysis of ambient ground motion or seismic noise can be applied to the delineation of geothermal reservoirs. In fact, if the radiated body waves exist, the method can be one of the most effective geophysical methods in geothermal explorations. Clearly, a few carefully executed and strategically located experiments are warranted.

ACKNOWLEDGMENTS

This study has been supported by the U.S. Energy Research and Development Administration under contract no. W-7405-ENG-48 with the Lawrence Berkeley Laboratory.

The authors are grateful to Steven Palmer, Jack Yatou, Glen Melosh, and Ernie Majer of the University of California at Berkeley and geothermal field crews of Lawrence Berkeley Laboratory for field

Seismic

Frequency-wavenumber analysis of geothermal microseisms at Norris Geyser basin, Yellowstone National Park, Wyoming

David H. Oppenheimer* and H. M. Iyer*

Microseisms were recorded by two separate arrays within 5 km of Norris Geyser basin, Yellowstone National Park, Wyoming. The data were analyzed using frequency-wavenumber (*f*-**k**) spectral techniques to investigate whether the microseisms are originating at the geyser basin and, if so, whether body waves emanating from a deep source could be distinguished from surface waves on the basis of phase velocity. Array aperture and seismometer spacing were systematically varied to examine a continuous wavenumber range of 0 to 100 cycles/km. Results from high-resolution *f*-**k** analysis show that the microseisms indeed originate at the geyser basin in the frequency range 1.5 to 6.3 Hz with phase velocities of 1.1 to 2.5 and 2.0 to 4.0 km/sec on arrays southwest and east of the geyser basin, respectively. Although we could not distinguish between surface waves and body waves originating near the surface solely on the basis of phase-velocity information, observed velocities clearly preclude the possibility that a deep hydrothermal system is responsible for body-wave microseisms in this area.

INTRODUCTION

Studies of continuous background microseisms (seismic noise) in geothermal areas have been conducted in many regions of North America, Italy, and New Zealand. Previous studies to establish whether seismic radiation is associated with geothermal systems were attempted in areas of anomalously high microseismic amplitude through the measurement of power spectra at numerous surface locations (Clacy, 1968; Whiteford, 1970; Douze and Sorrells, 1972; Luongo and Rapolla, 1973; Iyer and Hitchcock, 1976; Liaw and McEvilly, 1979). This method, though quite useful in delimiting the extent of the anomaly, cannot determine the wavenumber and apparent velocity of the microseisms, parameters essential to an understanding of the microseismic source. Because the amplitude of microseisms is related to local geology as well as to proximity of the source of emissions (Iyer and Hitchcock, 1976; Liaw and McEvilly, 1979), erroneous interpretations of microseismic data may result if these effects are not recognized and considered. Furthermore, seismic radiation from both geothermal and cultural sources may be present in the frequency range 1 to 20 Hz (Whiteford, 1970; Douze and Sorrells, 1972; Iyer and Hitchcock, 1974; Iyer, 1975; Asten, 1976), and amplitude studies cannot distinguish between these two sources.

Iyer and Hitchcock (1976) and Page (1977) postulated that seismic waves radiating from a geothermal source a few kilometers deep may propagate as body waves and thus can, in principle, be distinguished from cultural microseisms, which generally propagate as surface waves. Seismic arrays can determine the phase velocity of microseisms and can thus distinguish body waves emanating from deep sources and exhibiting high phase velocities (typically exceeding 3 km/sec) from surface waves. Conclusive evidence regarding the body-wave nature of microseisms in geothermal regions, however, is absent. Liaw and McEvilly (1979) investigated the microseismic field in Grass Valley, Nevada, using the frequency-wavenumber (*f*-**k**) technique and found no evidence of significant body-wave energy. They found that seismic radiation from hot springs at the valley edge propagates as fundamental-mode Rayleigh waves, as

Manuscript received by the Editor June 8, 1979; revised manuscript received September 27, 1979.
*U.S. Geological Survey, 345 Middlefield Road, M.S. 77, Menlo Park, CA 94025.
0016-8033/80/0501-0952$03.00. This paper was prepared by an agency of the U.S. government.

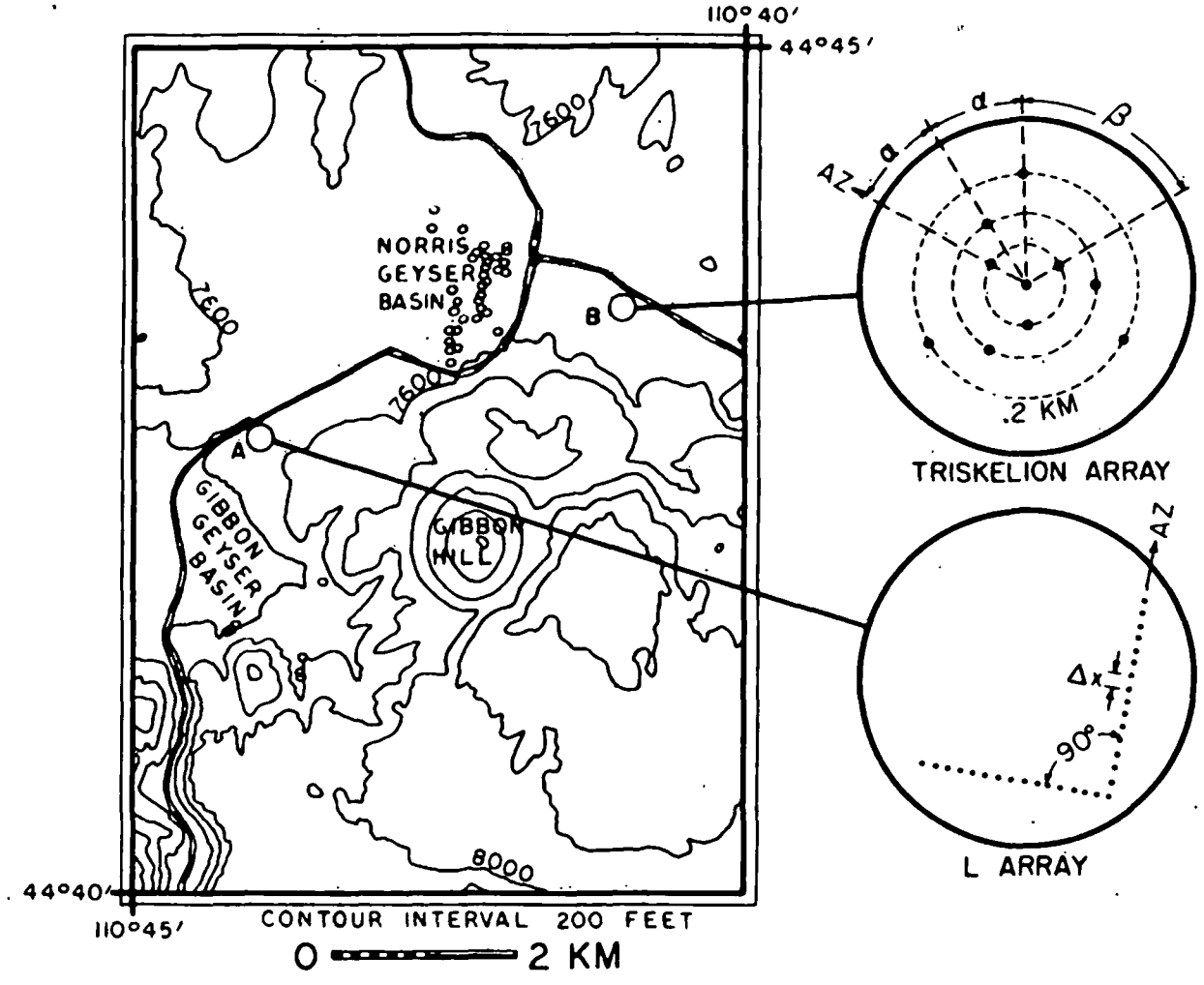

FIG. 1. Topographic map of Norris Geyser basin, depicting locations and geometries of L and Triskelion arrays at sites A and B, respectively. At site A, $\Delta x = 0.005$ km and AZ (orientation axis) = 10 degrees for small L-array; $\Delta x = 0.033$ km and $AZ = 190$ degrees for large L-array. At site B, $\alpha = 30$ degrees, $\beta = 60$ degrees, $AZ = 299$ degrees, and distance between concentric circles is 0.067 km.

do microseisms recorded in the valley center. Douze and Laster (1979), in a similar experiment at Roosevelt Hot Springs, Utah, found that during periods of cultural activity such as road traffic and trains, the microseisms consist almost entirely of Rayleigh waves. During quiet periods, data from arrays on valley fill west of the geothermal reservoir and also above the reservoir indicated the presence of a complex field of isotropic Rayleigh waves unrelated to this reservoir. A third array in the Mineral Mountains east of the reservoir detected high phase-velocity P-waves from some unknown source northeast of the array. Whether these microseisms are associated with any geothermal source has not been demonstrated.

To determine the nature of microseisms associated with an active geothermal region, the USGS recorded microseisms near Norris Geyser basin in Yellowstone National Park, Wyoming, during September, 1977. This site was chosen because earlier work by Iyer and Hitchcock (1974) showed coherent seismic radiation from the geyser basin. Our study was designed to measure phase velocities of the stationary microseismic field to detect the presence of body and surface waves and to determine the azimuth of the seismic source.

INSTRUMENTATION

Two separate arrays at sites A and B (Figure 1), respectively, were deployed to determine microseismic characteristics in several localities and to locate the seismic source. Array dimensions were systematically varied to examine a continuous wavenumber range and thus prevent misinterpretation of spatially aliased data. The spatial configuration of the seismometers in an array determines the transfer

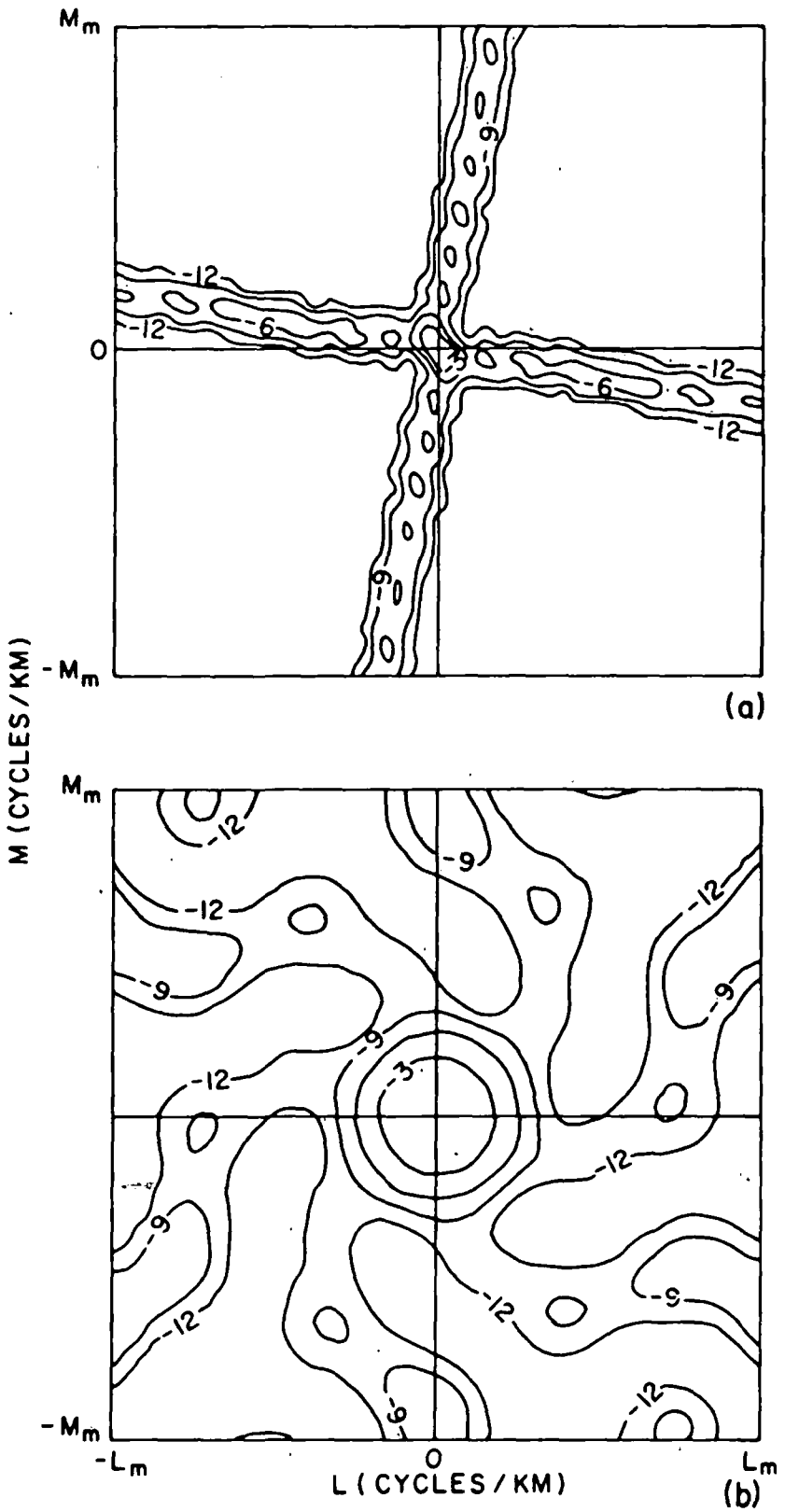

FIG. 2. Array transfer function in wavenumber space, plotted from 0 to the reciprocal of twice the minimum station spacing for (a) L-array at site A and (b) Triskelion array at site B. Contour interval is 3 dB relative to peak power value in plot.

function of the array. Increased wavenumber resolution can be achieved through optimal array design (Haubrich, 1968), but in field experiments of short duration involving a large number of instruments, deployment of complex array geometries is not feasible. Accordingly, L-shaped and Triskelion designs were selected for our experiments (Figure 1); the corresponding impulse-response functions are shown in Figure 2.

At site A, the Centipede seismic recording system, developed by Reasenberg et al (1977), was deployed in two L-shaped arrays each with 31 recording stations with spacings of 5 and 33 m, respectively. Each recording station of the Centipede system consisted of a 1-Hz vertical-component seismometer, a preamplifier, and a voltage-control oscillator. All signals were then frequency modulated, multiplexed, and recorded in AM mode on one analog magnetic tape, together with timecode and tape-speed compensation signals. The system bandwidth (−3 dB) of the Centipede is nominally 0.1 to 30 Hz, and the dynamic range is 40 dB. On playback, the data were demultiplexed, FM discriminated, and digitized at 200 samples/sec.

At site B, a Lancer digital recording system with 10 seismometers identical to those of the Centipede system was arranged in a triskelion with one center seismometer and three concentric circles, each containing three seismometers, with corresponding radii of 64, 167, and 200 m. The system bandwidth is 0.1 to 50 Hz, and the dynamic range is 90 dB. The seismic signal from each seismometer was amplified, multiplexed, digitized at 120 samples/sec, and written digitally on tape.

THEORY

The use of seismic arrays for the analysis of seismic noise makes possible the calculation of the frequency-wavenumber structure of the noise field. For a plane wave propagating at frequency f and wavenumber $\mathbf{k}$, the phase velocity $\mathbf{v}$, is given by

$$\mathbf{v} = \frac{f}{\mathbf{k}}. \tag{1}$$

For vertically incident body waves, $\mathbf{k} = 0$ and $\mathbf{v} = \infty$, and for horizontally propagating surface waves, the phase velocity is equal to the true velocity of the wave. Thus, determination of the f-$\mathbf{k}$ structure provides insight into the modes of propagation of the noise field. Capon (1969) derived in detail the estimation of the f-$\mathbf{k}$ spectrum, and Liaw and McEvilly (1979) provided an excellent discussion of the theory and its relative merits with respect to other estimation techniques. For completeness and consistency with later notation, a brief review is given here.

Consider K seismometers at positions $\mathbf{x}_j$, where $j = 1, 2, \ldots, K$ relative to some arbitrary reference point. The time series n_j recorded at each station can be divided into M nonoverlapping segments of N points. The Fourier transform of the ith segment of the jth station can be written as

$$F_{ij}(f) = \frac{1}{N} \sum_{m=1}^{N} a_m n_{j,\, m+N(i-1)} \exp(i2\pi fm), \tag{2}$$

where the a_m are the weighting coefficients. An estimate of the cross-spectral matrix averaged over M segments is given by

$$\hat{S}_{jl} = \frac{1}{M} \sum_{i=1}^{M} F_{ij}(f) F_{il}^{*}(f), \tag{3}$$

where the * denotes the complex conjugate, and j and l represent the station indices. An estimate $P(f, \mathbf{k})$ of the f-$\mathbf{k}$ power spectrum $P(f, \mathbf{k})$ is then given by

$$\hat{P}(f, \mathbf{k}) = \frac{1}{K^2} \sum_{j,\, l=1}^{K} w_j(\mathbf{k}) w_l^{*}(\mathbf{k}) \hat{S}_{jl}(f) \cdot \cdot \exp[i2\pi \mathbf{k} \cdot (\mathbf{x}_j - \mathbf{x}_l)], \tag{4}$$

where the $w_j(\mathbf{k})$ are the spatial weighting coefficients. For conventional f-$\mathbf{k}$ spectral analysis, $w_j(\mathbf{k}) = 1$. Smart and Flinn (1971) rearranged equation (4) to increase computational efficiency in the form

$$\hat{P}(f, \mathbf{k}) = \frac{1}{M} \sum_{i=1}^{M} \left| \frac{1}{K} \sum_{j=1}^{K} w_j(\mathbf{k}) F_{ij}(f) \cdot \cdot \exp(i2\pi \mathbf{k} \cdot \mathbf{x}_j) \right|^2. \tag{5}$$

If the time series is a monochromatic plane wave of frequency f_0 and wavenumber $\mathbf{k}_0$, then $P(f, \mathbf{k})$ will be a delta function at f_0, $\mathbf{k}_0$, and $\hat{P}(f_0 \mathbf{k}_0)$ will be the transfer function of the array (Figure 2).

Figure 2 shows that significant spectral leakage results from the use of a finite-element array. To suppress the effects of the beam pattern and to improve wavenumber resolution, we used high-resolution f-$\mathbf{k}$ spectral analysis (Capon, 1969). The high-resolution method is based on the inverse $\hat{q}_{jl}(f, \mathbf{k})$ of matrix $\hat{\mathbf{S}}_{jl}(f) \cdot \exp[i2\pi \mathbf{k} \cdot (\mathbf{x}_j - \mathbf{x}_l)]$ and is designed to pass a monochromatic plane wave of wavenumber $\mathbf{k}_0$ but suppress the power due to wavenumbers other than $\mathbf{k}_0$ such that $\hat{P}(f, \mathbf{k}_0)$ is an

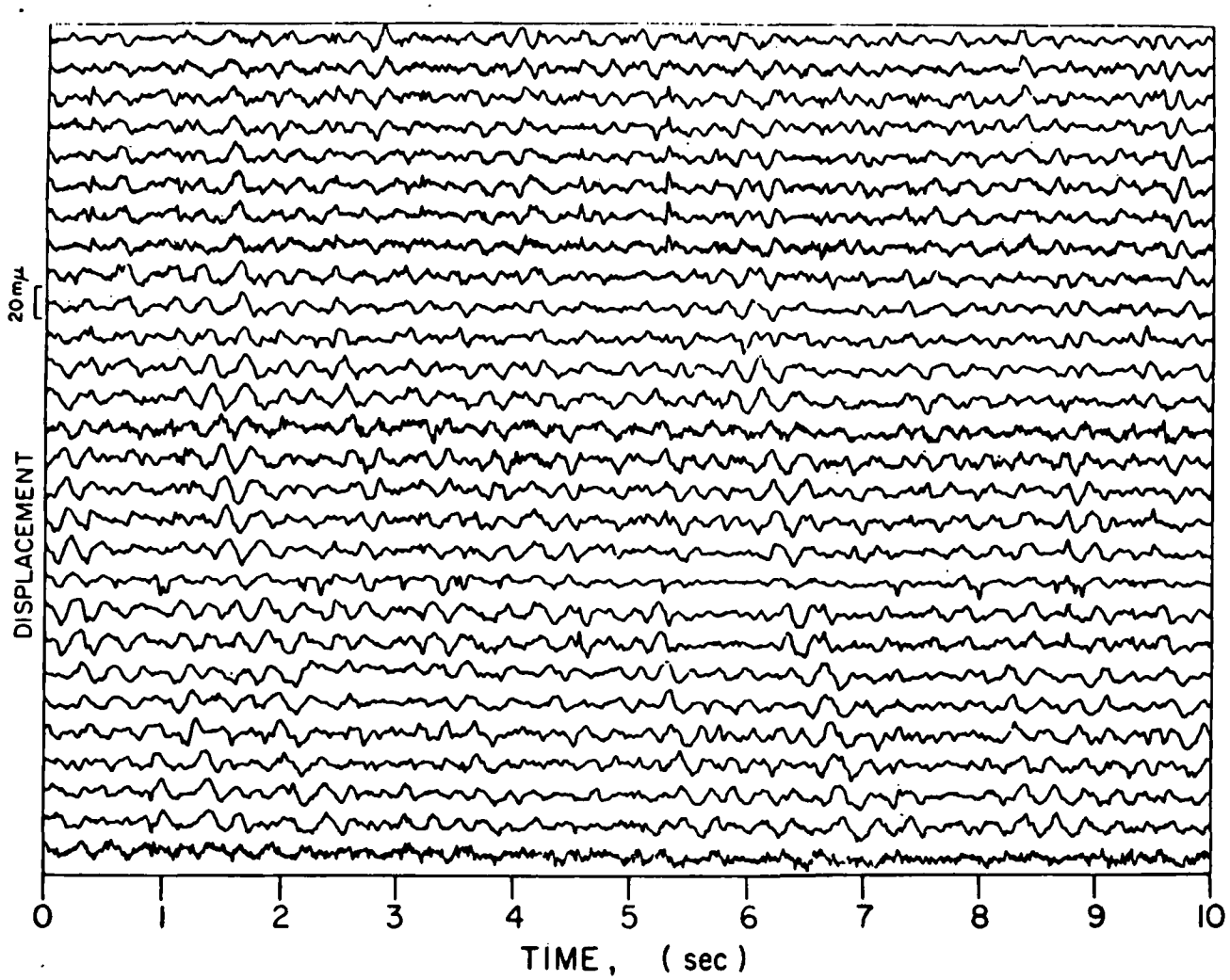

FIG. 3. Sample record of microseisms recorded by large L-array at site A. All stations were operated at same gain, and interstation spacing was 0.033 km.

unbiased minimum variance estimate of $P(f, \mathbf{k}_0)$. The high-resolution estimate of the f-$\mathbf{k}$ spectrum is given by

$$\hat{P}_h(f, \mathbf{k}) = \frac{1}{M} \sum_{i=1}^{M} \left| \sum_{j=1}^{K} A_j^*(f, \mathbf{k}) F_{ij}(f) \cdot \cdot \exp[i2\pi \mathbf{k} \cdot \mathbf{x}_j) \right|^2 \quad (6)$$

where

$$A_j(f, \mathbf{k}) = \frac{\sum_{l=1}^{K} \hat{q}_{jl}(f, \mathbf{k})}{\sum_{j,l=1}^{K} \hat{q}_{jl}(f, \mathbf{k})}. \quad (7)$$

Capon and Goodman (1970) showed that $\hat{P}_h(f, \mathbf{k})$ is a multiple of a chi-square variable with $2(M - K + 1)$ degrees of freedom. For the large L-array where $M = 32$ and $K = 28$, there are 10 degrees of freedom, and the 90 percent confidence limits are approximately 4.05 dB above and -2.62 dB below $\hat{P}_h(f, \mathbf{k})$ for $f = 0$, f_{Nyquist}. For the Triskelion array where $M = 32$ and $K = 10$, there are 46 degrees of freedom, and the confidence limits are approximately -1.35 and 1.65 dB.

A further savings in computation time can be realized through calculation of the Fisher statistic at each f-$\mathbf{k}$ point (Smart and Flinn, 1971). The Fisher statistic, a measure of the signal-to-noise ratio, is defined as

$$T(f, \mathbf{k}) = (K - 1) \frac{\hat{P}(f, \mathbf{k})}{\hat{P}(f, \mathbf{k}) - \frac{1}{K} \sum_{j=1}^{K} \hat{S}_{jj}(f)}. \quad (8)$$

Equation (8) shows that the Fisher statistic is a weighted ratio of the power at a particular frequency and wavenumber to the difference between that power and the total power at the given frequency. Thus, only

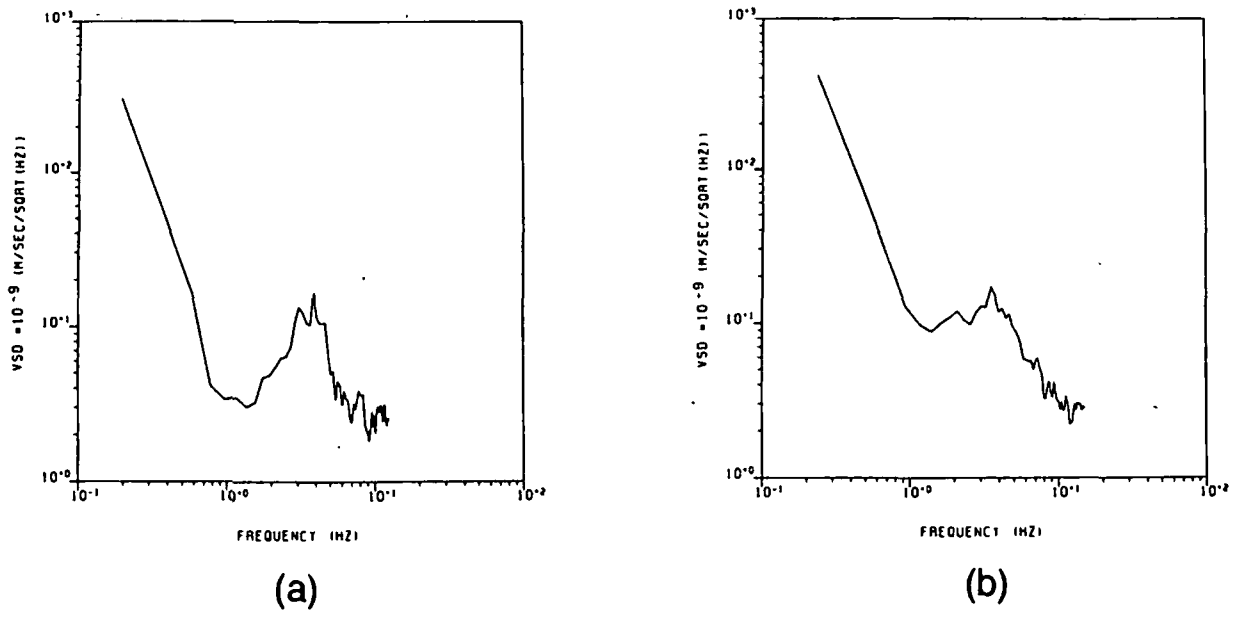

FIG. 4. Typical power spectral density plots corrected for instrument response for microseisms recorded at (a) site A and (b) site B.

when the computed Fisher value exceeds a certain threshold will signal be considered to be present and $\hat{P}_h(f, \mathbf{k})$ be computed.

OBSERVATIONS

The data used for analysis were recorded between midnight and 3:00 A.M. MST to reduce noise contributions from cultural sources. Each time series was subdivided into 32 segments of lengths 1.28 and 2.13 sec for the Centipede and Lancer data, respectively. Figure 3 shows representative microseisms recorded by the large L-array at site A; note the presence of coherent arrivals across the entire array. Figure 4 shows typical velocity spectral density plots of the microseismic field at sites A and B. All spectra were computed by tapering each time segment with a Hamming window, taking the square root of the average of the corresponding segment power spectra, and removing the instrument response. It is seen that the predominant signal occurred between 2.3 and 6.5 Hz.

Algorithms for computation of the high-resolution f-$\mathbf{k}$ filter were taken largely from Liaw (1977). The f-$\mathbf{k}$ power spectra were computed at discrete frequencies as a function of the wavenumber $\mathbf{k}$ decomposed into orthogonal components L and M, represented by a 43×43 point grid (Figures 5 and 6). Since both the Triskelion and L-arrays used in this

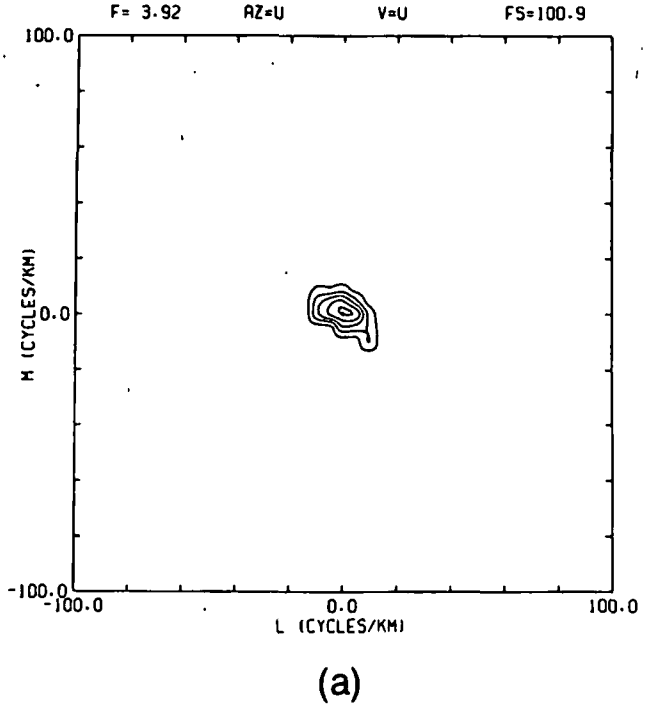

FIG. 5a. Frequency-wavenumber (f-$\mathbf{k}$) power spectral density plots for microseisms recorded at site A. Arrow points toward source of wavefront. F = frequency (Hz), AZ = aximuth (degrees), V = velocity (km/sec), FS = maximum Fisher statistic, U = undefined. Contour interval is 3 dB relative to peak power value in plot. f-$\mathbf{k}$ plot for small L-array; $f = 3.92$ Hz, maximum wavenumber = 100 cycles/km.

study were not symmetrical, the Nyquist wavenumber varies with the azimuthal angle through the $\mathbf{k}_x - \mathbf{k}_y$ domain. The maximum wavenumber examined in this study is equal to the reciprocal of twice the minimum station spacing. Accordingly, both L and M range from zero to this maximum wavenumber, and contours indicate power in decibels relative to the maximum power in the plot. All contours were computer-generated according to the method of minimum curvature (Briggs, 1974) and consequently are not unique. The arrow drawn from $\mathbf{k} = 0$ to the wavenumber point of maximum power can be interpreted as pointing in the direction of the microseismic source.

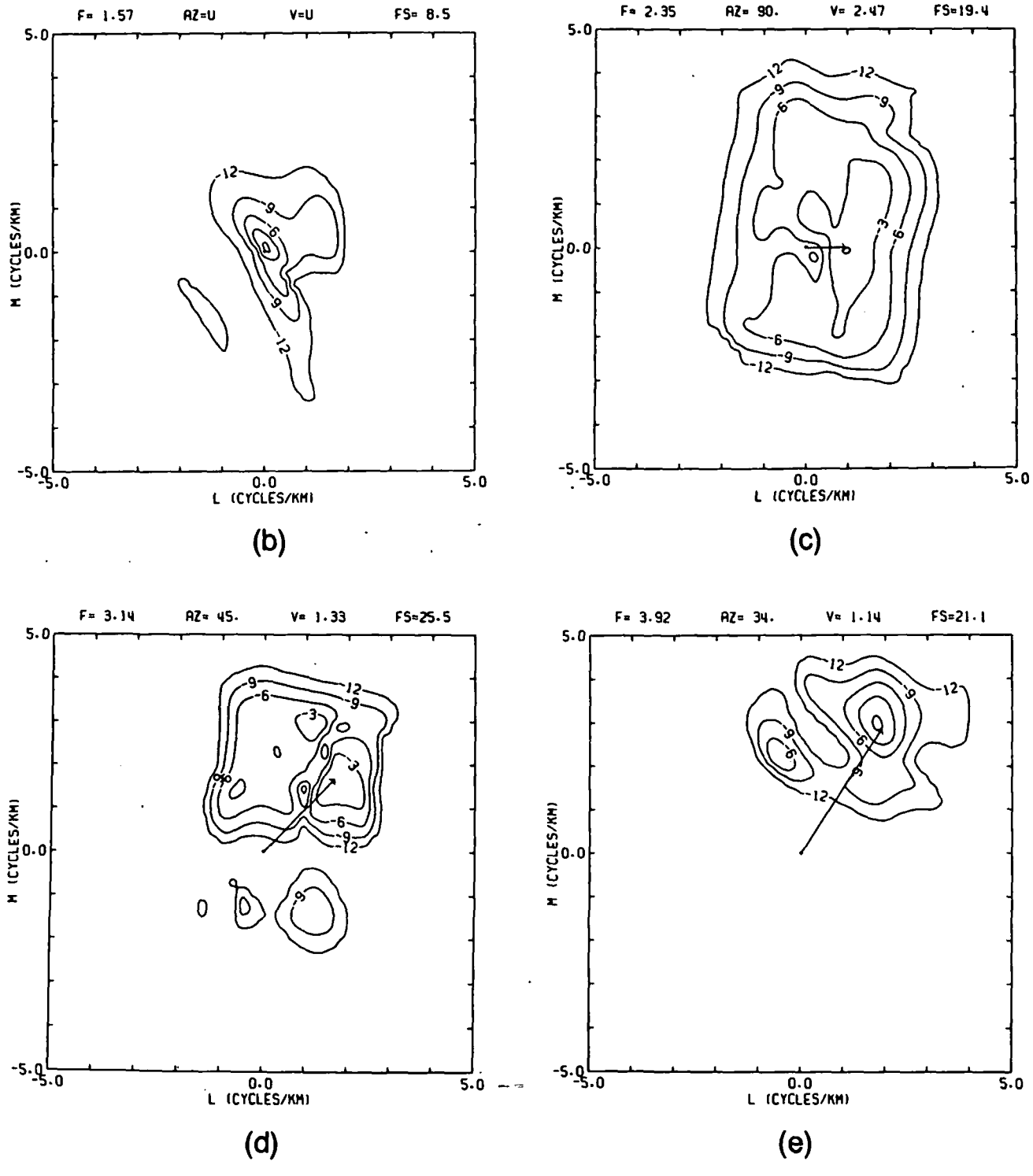

FIGS. 5b–5e. Frequency-wavenumber (f-$\mathbf{k}$) power spectral density plots for microseisms recorded at site A. Symbols are the same as in Figure 5a. f-$\mathbf{k}$ plots for large L-array; for $f = 1.57–3.92$ Hz, the maximum wavenumber = 5 cycles/km, and for $f = 4.71–6.27$ Hz, the maximum wavenumber = 15 cycles/km.

Site A—small L-array

Data from 29 of 31 stations from the small L-array were used in the computation of f-**k** spectra. The minimum interstation spacing of 0.005 km results in a maximum wavenumber of approximately 100 cycles/km. The array aperture was 0.106 km and the wavenumber increment was approximately 4.76 cycles/km. The high-resolution f-**k** power at $f = 3.92$ Hz is shown in Figure 5a. Maximum power was in the wavenumber range 0 to 4.76 cycles/km corresponding to phase velocities ranging from ∞ to 0.8 km/sec that arrived from Norris Geyser basin. Since more detailed resolution at low wavenumbers is possible with the large L-array, we defer an interpretation of these velocities until discussion of those data. However, because no significant power is present at wavenumbers exceeding 10 cycles/km, data recorded by the large L-array are considered to be essentially free from wavenumber aliasing. Similar results were observed throughout the frequency range 1.56 to 6.27 Hz.

Site A—large L-array

We used data from 28 of 31 stations from the large L-array in the f-**k** analysis. The minimum interstation spacing was 0.033 km and the array aperture was 0.707 km. For frequencies 1.57 to 3.92 Hz, a maximum wavenumber of 5 cycles/km, corresponding to a wavenumber increment of 0.24 cycles/km, was used for f-**k** analysis since no appreciable energy was observed beyond this wavenumber. For higher frequencies, a maximum wavenumber of 15 cycles/km and an increment of 0.71 cycles/km were used. The results of the high-resolution f-**k** analysis are shown in Figures 5b–5h for the frequency range 1.57 to 6.27 Hz.

At 1.57 Hz (Figure 5b), the maximum power was at a wavenumber magnitude between 0 and 0.24 cycles/km corresponding to a phase velocity from ∞

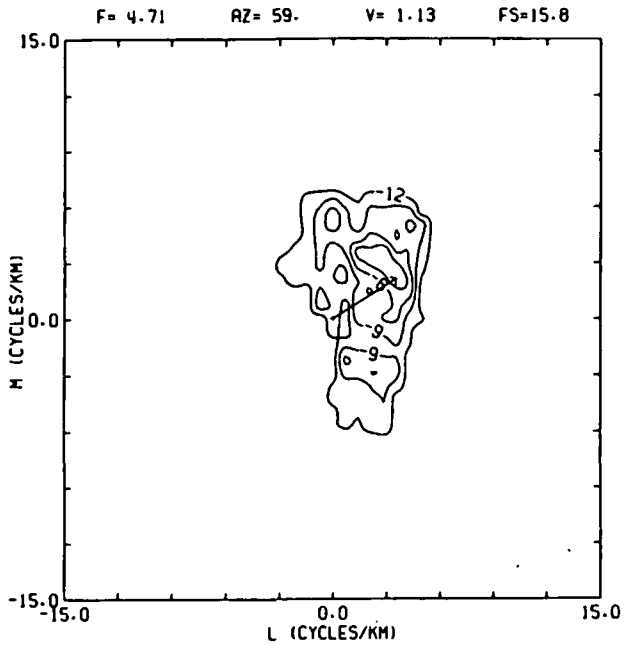

(f)

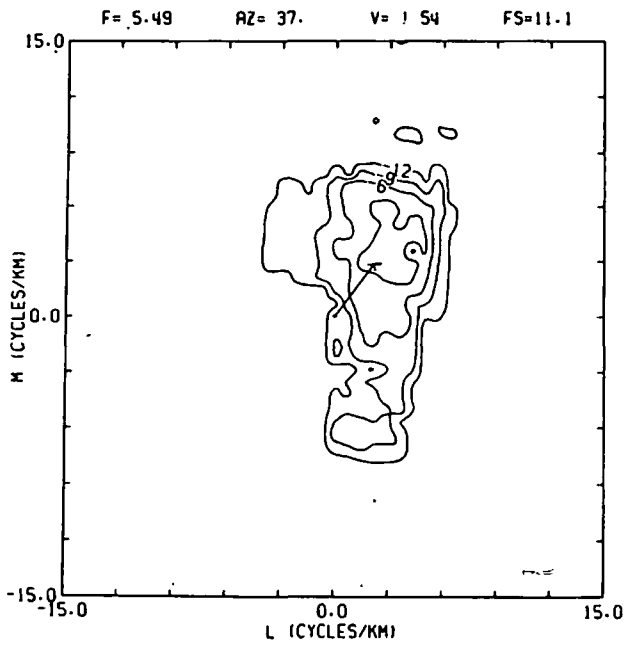

(g)

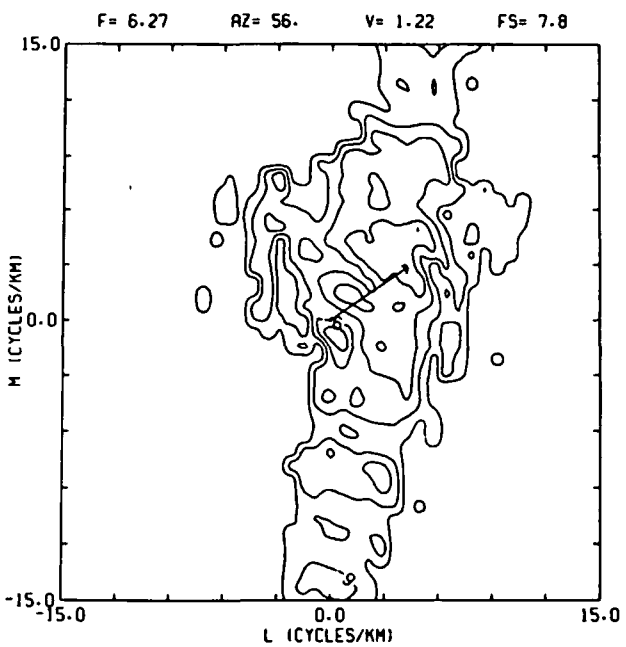

(h)

FIGS. 5f–5h. Frequency-wavenumber (f-**k**) power spectral density plots for microseisms recorded at site A. Symbols are the same as in Figure 5a. f-**k** plots for large L-array; for $f = 1.57$–3.92 Hz, the maximum wavenumber = 5 cycles/km, and for $f = 4.71$–6.27 Hz, the maximum wavenumber = 15 cycles/km.

to 6.6 km/sec; the maximum Fisher statistic was 8.5. At the next frequency interval, 2.35 Hz, the energy of the signal increased as seen in the Fisher value of 19.4 (Figure 5c). However, the −3 dB contour which approximately defines the 90 percent confidence interval indicates that statistically significant estimates of the phase velocity range from 1.0 to 3.3 km/sec. At frequencies of 3.14 to 4.71 Hz (Figures 5d through 5f), maximum energy arrived from Norris Geyser basin in the northeast azimuth at an average phase velocity of 1.20 km/sec. The broad azimuthal distribution in power is to be expected because diameter of the geyser basin exceeds 1.5 km.

At frequencies greater than 5.0 Hz, the considerable drop-off in energy of the signal (Figures 4a, 5g, 5h) resulted in a decrease of the signal-to-noise ratio and, similarly, of the Fisher statistic. At wavenumbers at which the calculated Fisher statistic is less than the Fisher threshold of 1.0, the f-**k** power value

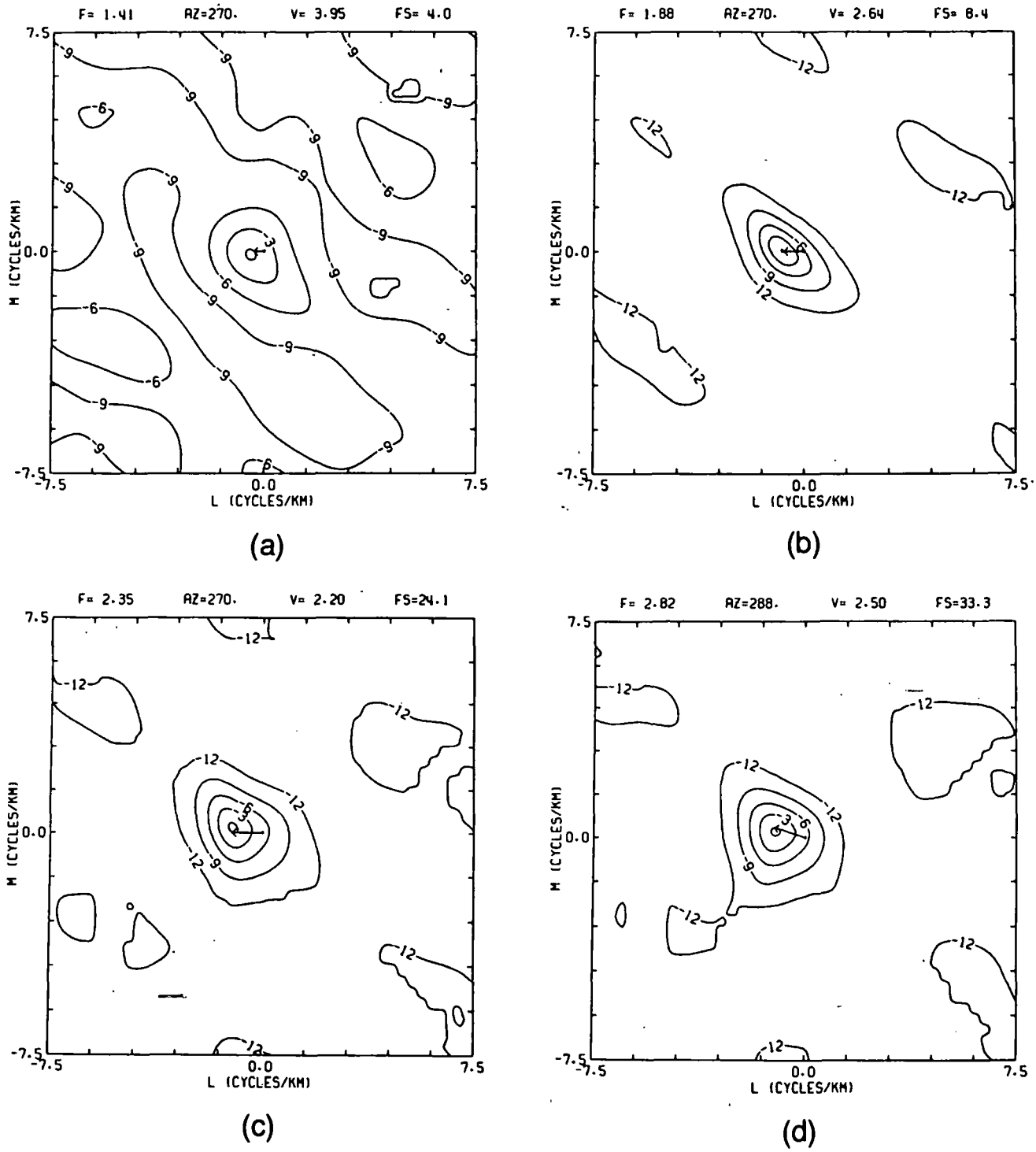

FIGS. 6a–6d. Frequency-wavenumber power spectral density plots for microseisms recorded at site B at frequencies 1.41–2.82 Hz. Maximum wavenumber is 7.5 cycles/km. Symbols are the same as in Figure 5.

was artificially set at least 40 dB lower than the computed values, where the Fisher statistic exceeded the threshold. Consequently, the elongate patterns seen at frequencies of 5.49 and 6.27 Hz (Figures 5g, 5h) are due to the restriction of high-resolution *f*-**k** processing to the side lobes of the transfer function (Figure 2b), where the Fisher statistic exceeded the Fisher threshold. The predominant signal continues to arrive at velocities and azimuths similar to those at lower frequencies. At frequencies greater than 6.27 Hz, no coherent signal was observed.

Site B—Triskelion array

All 10 stations of the Triskelion array were used in computing the *f*-**k** spectra. The minimum interstation spacing was 0.067 km and the aperture of the array was 0.346 km. The maximum wavenumber for *f*-**k** analysis was 7.5 cycles/km and the corresponding

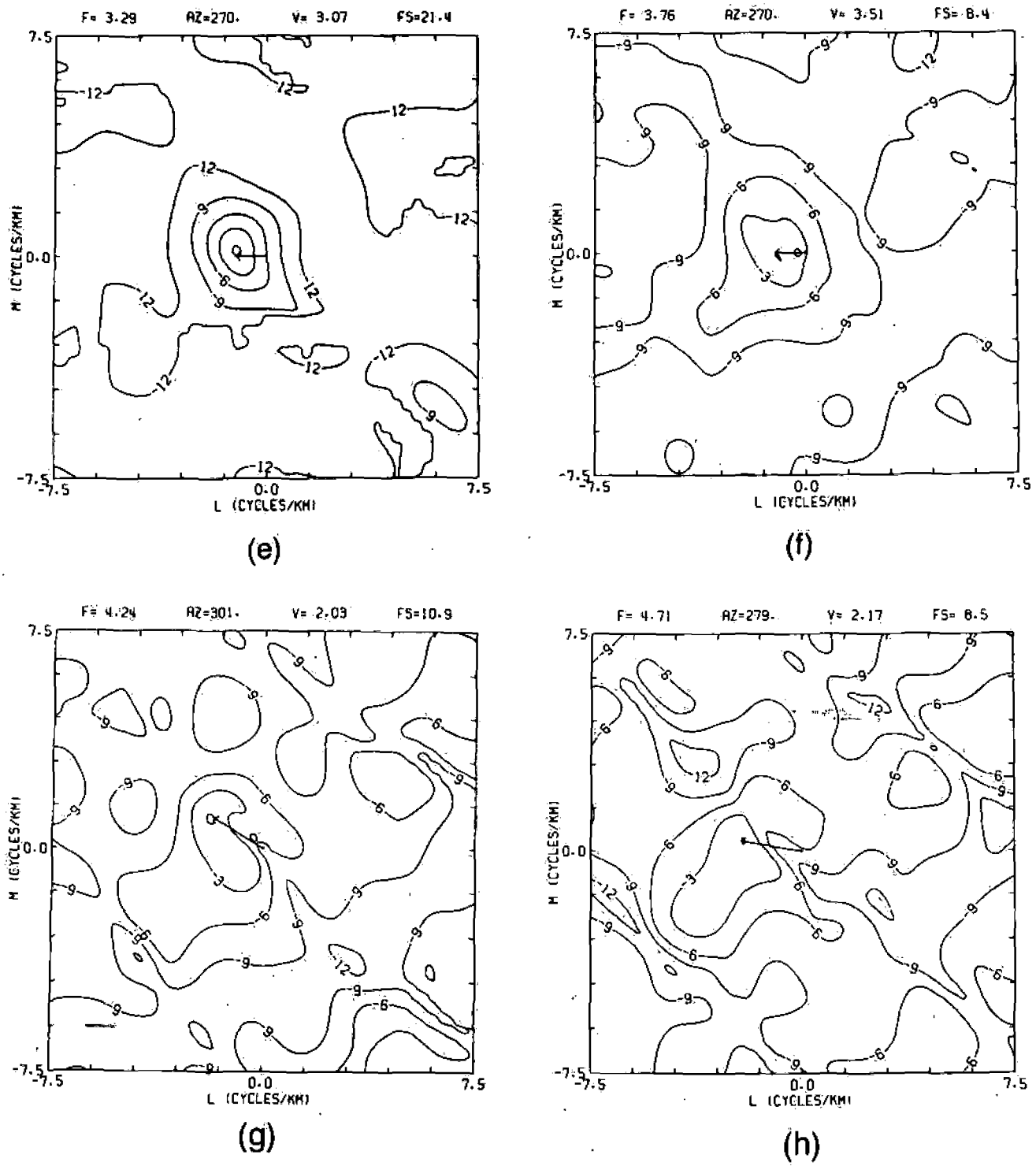

FIGS. 6e–6h. Frequency-wavenumber power spectral density plots for microseisms recorded at site B at frequencies 3.29–4.71 Hz. Maximum wavenumber is 7.5 cycles/km. Symbols are the same as in Figure 5.

wavenumber increment was 0.36 cycles/km. The high-resolution f-**k** diagrams for frequencies of 1.41 to 4.70 Hz are shown in Figures 6a through 6h.

For frequencies lower than 1.41 Hz, no coherent energy was observed. At 1.41 Hz (Figure 6a), a weak signal, as seen by a Fisher value of 4.0, arrived with an azimuth of 270 degrees and a phase velocity of 3.95 km/sec. Recalling the 90 percent confidence interval of −1.35 to 1.65 dB, significant velocities range from ∞ to 1.32 km/sec. At frequencies 1.88 to 3.5 Hz (Figures 6b through 6e), a signal arrived from the west with an average apparent velocity of 2.6 km/sec. This azimuth is consistent with the hypothesis that Norris Geyser basin is the source of the seismic radiation. The general shape of the power contours in wavenumber space at site B differs from that of the L-array owing to changes in both the f-**k** structure of the microseisms and the different response function of the array (Figure 2b). A comparison of the side lobes of the array response with the position of the seemingly random −12 dB contours in Figures 6b through 6e indicates that these contours are due to wavenumber spectral leakage.

At frequencies greater than 3.5 Hz (Figures 6f through 6h), the signal-to-noise ratio decreases similarly to that observed at site A for frequencies exceeding 5 Hz. This difference in the upper frequency of signal coherence, in addition to the differences in phase velocity magnitude observed at the two sites, suggests dissimilarities in the respective media through which the microseisms travel. Alternatively, the difference in phase velocity at sites A and B may represent a signal generated at depth that propagates at the same velocity but arrives at the two arrays with different angles of incidence due to source-receiver geometry. The predominant signal continues to arrive from the direction of the geyser basin, but confidence in the estimate of the apparent velocity has decreased as can be seen from the increase in extent of the 3 dB contour. At frequencies greater than 5 Hz, either the signal becomes incoherent or aliasing occurs in wavenumber space.

DISCUSSION

The azimuths of wave propagation, determined by two separate arrays, all point to Norris Geyser basin and leave little doubt that the microseisms originate at the basin. However, it is unclear whether these microseisms are associated with the surface geothermal phenomena, such as geysers, fumaroles, and hot springs, or due to more fundamental processes associated with the geothermal system at depth. In order to use phase velocity to distinguish between the two instances, the velocity structure of the Norris basin must be known.

The geologic structure of Norris Geyser basin comprises a densely welded tuff, the Lava Creek tuff, overlain by a thin veneer of glacial till and rubble no more than 5 m thick (Christiansen and Blank, 1972; Richmond and Waldrop, 1975). Drilling in Norris Geyser basin has shown that the tuff is at least 300 m thick (White et al, 1975). Since no detailed information exists on the velocity of shallow units in this area, a unique velocity cannot be assigned to the tuff layer. Crustal refraction studies at Long Valley caldera, California, by Hill (1976) indicated velocities of volcanic layers in the upper 1 to 1.5 km of the crust range from 2.5 to 3.5 km/sec. Accordingly, compressional waves emanating from a near-surface source would exhibit a similar range of phase velocities, whereas P-waves from a source at depth would have much higher velocities owing to the emergence angle at the array. Assuming a Poisson's ratio of 0.25 and the above P-wave velocities, fundamental Rayleigh waves propagating along the free surface would have a velocity between 1.3 and 1.8 km/sec.

The high phase velocity, exceeding 6.6 km/sec, observed by the large L-array at 1.57 Hz (Figure 5b) suggests the presence of P-wave energy originating at great depth. However, if energy indeed arrived at a wavenumber between 0 and 0.238 cycles/km, the wavelength of the signal would be at least six times the array aperture, and the array would not be able to provide adequate wavenumber resolution. Hence, the phase velocity estimate would also be poor. Although the wavenumber resolution increases with an increase of array aperture, larger apertures require greater interstation spacing for a fixed number of seismometers and increase the risk of spatial aliasing. For this experiment, we considered the risk of aliasing sufficiently important to sacrifice resolution. Furthermore, due to the distance between the arrays and the Norris basin, an array much larger than 0.5 km would have made the plane-wave assumption unreasonable. Considering the phase velocities observed at all other frequencies and the problem of wavenumber resolution, it is doubtful that this energy results from body waves from a deep source.

At 2.35 Hz (Figure 5c), recalling the range of statistically significant phase velocities, there is evidence for the presence of body waves from near-surface sources. At higher frequencies (Figures 5d–5h), the phase velocities observed at the large L-array indicate the arrival primarily of surface waves.

The velocities at the Triskelion array, while generally higher than those of the L-array, indicate a mixture of both surface waves and body waves originating near the surface.

Although we could not distinguish between surface waves and body waves on the basis of the observed phase velocities, and since there was no observable velocity dispersion, these velocities clearly demonstrate that Norris Geyser basin is the source of the microseisms. There is only a remote possibility that a deep seismic source is responsible for body-wave microseisms in this area. We suggest that hydrothermal processes associated with surface manifestations at the geyser basin are the cause of observed microseisms.

CONCLUSION

The high-resolution *f*-**k** technique used to analyze microseisms recorded at two sites near Norris Geyser basin, Yellowstone National Park, shows coherent signals propagating from the geyser basin in the frequency range 1.4 to 6.3 Hz with phase velocities of 1.0 to 4.0 km/sec. The mode of seismic transmission suggests that both surface and body waves are emanating from near-surface sources. Furthermore, such low-phase velocities preclude body waves originating from deep hydrothermal systems in Norris Geyser basin.

ACKNOWLEDGMENTS

We thank Robert Cessaro, John Coakley, and Steve Wegener of the USGS for their invaluable help during field operations and Tim Hitchcock for preparation of the figures. We also thank Jon Fletcher and William Ellsworth of the USGS who provided technical assistance with instrumentation and data processing and critically reviewed the manuscript.

REFERENCES

Asten, M. W., 1976, The use of microseisms in geophysical exploration: Ph.D. thesis, MacQuarie University, North Ryde, Australia, 178 p.

Briggs, I. C., 1974, Machine contouring using minimum curvature: Geophysics, v. 39, p. 39–48.

Capon, J., 1969, High-resolution frequency-wavenumber spectrum analysis: Proc. IEEE, v. 57, p. 1408–1418.

Capon, J., and Goodman, N. R., 1970, Probability distribution for estimators of the frequency-wavenumber spectrum: Proc. IEEE, v. 58, p. 1785–1786.

Christiansen, R. L., and Blank, H. R., Jr., 1972, Volcanic stratigraphy of the Quaternary rhyolite plateau in Yellowstone National Park: U.S.G.S. prof. paper 729-B, p. B1-B18.

Clacy, G. R. T., 1968, Geothermal noise amplitude and frequency spectra in the New Zealand volcanic region: J. Geophys. Res., v. 73, p. 5377–5383.

Douze, E. J., and Laster, S. J., 1979, Seismic array noise studies at the Roosevelt Springs, Utah, geothermal area: Geophysics, v. 44, p. 1570–1583.

Douze, E. J., and Sorrells, G. G., 1972, Geothermal ground-noise surveys: Geophysics, v. 37, p. 813–824.

Haubrich, R. A., 1968, Array design: SSA Bull., v. 58, p. 977–991.

Hill, D. P., 1976, Structure of Long Valley caldera, California, from a seismic refraction experiment: J. Geophys. Res., v. 81, p. 745–753.

Iyer, H. M., 1975, Search for geothermal seismic noise in the East Mesa area, Imperial Valley, California: Geophysics, v. 40, p. 1066–1072.

Iyer, H. M., and Hitchcock, T., 1974, Seismic noise measurements in Yellowstone National Park: Geophysics, v. 39, p. 389–400.

——— 1976, Seismic noise survey in Long Valley, California: J. Geophys. Res., v. 81, p. 821–839.

Liaw, A. L., 1977, Microseisms in geothermal exploration: Studies in Grass Valley, Nevada: Ph.D. thesis, University of California, Berkeley, 168 p.

Liaw, A. L., and McEvilly, T. V., 1979, Microseisms in geothermal exploration—Studies in Grass Valley, Nevada: Geophysics, v. 44, p. 1097–1115.

Luongo, G., and Rapolla, A., 1973, Seismic noise in Lipari and Vulcano Islands, southern Thyrrenian Sea, Italy: Geothermics, v. 2, p. 29–31.

Page, E. A., 1977, Mapping seismic activity in geothermal regions: EOS, AGU trans., v. 58, p. 1187.

Reasenberg, P., Cessaro, R., and Wilson, D., 1977, The Centipede seismic recording system: U.S.G.S. open file rep. 77-315, 81 p.

Richmond, G. M., and Waldrop, H. A., 1975, Surficial geologic map of the Norris Junction quadrangle, Yellowstone National Park, Wyoming: U.S.G.S. misc. inv. ser. map I-650, scale 1:62,500.

Smart, E., and Flinn, E. A., 1971, Fast frequency-wavenumber analysis and Fisher signal detection in real-time infrasonic array data processing: Geophys. J. Roy. Astr. Soc., v. 26, p. 279–284.

White, D. E., Fournier, R. O., Muffler, L. J. P., and Truesdell, A. H., 1975, Physical results of research drilling in thermal areas of Yellowstone National Park, Wyoming: U.S.G.S. prof. paper 892, 70 p.

Whiteford, P. C., 1970, Ground movement in the Waiotapu geothermal region, New Zealand: Geothermics, spec. issue 2, v. 2, part 2, p. 478–486.

GEOPHYSICS, VOL. 46, NO. 10 (OCTOBER 1981); P. 1456–1466, 9 FIGS., 4 TABLES.

Delineation of a low-velocity body under the Roosevelt Hot Springs geothermal area, Utah, using teleseismic *P*-wave data

Russell Robinson* and H. M. Iyer‡

ABSTRACT

To assess the nature of the heat source associated with the Roosevelt Hot Springs geothermal area, we have investigated the *P*-wave velocity structure of the crust and uppermost mantle in the vicinity of the Mineral Mountains, southwest Utah, a region of late Cenozoic rhyolitic and basaltic volcanic activity. A roughly square (30 × 30 km) array of 15 seismographs, centered on the mountains, was operated for a period of 46 days, during which 72 teleseismic events were recorded with sufficient quality for calculation of *P*-wave traveltime residuals. Relative residuals, using the array average for each event as reference, show a clear pattern of azimuthal variation of up to 0.3 sec. This pattern implies the existence of a localized region of relatively low-velocity material extending up from the upper mantle to depths of about 5 km under the Mineral Mountains. A three-dimensional (3-D) inversion of the data confirms this conclusion and yields a model featuring a region of low velocity (5 to 7 percent less than the surrounding rock) centered under the geothermal area and extending from about 5-km depth down into the uppermost mantle. The near-surface velocities obtained in the inversion clearly reveal the structure of the region, part of the Basin and Range province. An azimuthally changing pattern of waveform distortion, restricted to the central Mineral Mountains, indicates the presence of a small but intensely anomalous region of low velocity and high attenuation at depths of about 15 km. Although we cannot rule out an explanation for the low velocity purely in terms of compositional changes, in view of the geothermal and volcanic manifestations found in the region we prefer an explanation in terms of abnormally high temperature and a small fraction of partial melt. A partial melt model implies a much greater heat reservoir than does a model involving only circulation along deep fault zones.

INTRODUCTION

The Roosevelt Hot Springs geothermal area, currently under proposed development for the generation of electric power, has been the focus of many geophysical studies. Seismic-refraction, gravity, magnetic, resistivity, and heat-flow investigations have all been made in the region in addition to detailed geologic and geochemical studies (for a review, see Ward et al, 1978). As a result, the relatively shallow (2–3 km) structure of the area is known to some degree, but the deeper structure of the crust has yet to be investigated. With the view of elucidating the nature of the heat source responsible for the near-surface thermal activity, we examined this deeper structure using teleseismic *P*-wave traveltime variations. This technique has proved very useful in understanding the structure of other geothermal areas at depth, for example, at Yellowstone National Park, Wyoming (Iyer, 1979), and in California, in the Geysers-Clear Lake region (Iyer et al, 1979), at Long Valley (Steeples and Iyer, 1976), and in the Coso geothermal area (Reasenberg et al, 1980).

GEOLOGIC AND GEOPHYSICAL SETTING

The Roosevelt Hot Springs geothermal area lies on the western flank of the Mineral Mountains in southwest Utah, a horst composed mainly of Tertiary granitic rocks (10–14 m.y. old) and flanked by alluvial valleys typical of the Basin and Range province (Milford Valley and Beaver Valley). The transition to the Colorado plateau physiographic province is immediately east of Beaver Valley (Figure 1).

Both basaltic and rhyolitic volcanic activity have occurred repeatedly in the vicinity of the Mineral Mountains since middle Tertiary time (related at first to the emplacement of the granitic rocks themselves), as it has in much of the Basin and Range—Colorado plateau transition zone (Smith, 1979). The most recent episode of activity resulted in rhyolite flows and domes along the crest of the Mineral Mountains 0.5 to 0.8 m.y. ago. Basaltic or andesitic flows occurred on the northeast flank of the mountains and more extensively slightly farther northeast near Cove Fort. These latter flows cover part of the northern Beaver Valley.

Large-scale seismic-refraction studies of the easternmost Basin and Range province (Braile et al, 1974; Prodehl, 1970) have shown that the crust is thin (about 25 km thick) and the P_n velocity low (about 7.5 km/sec). It has been suggested that a regional low-velocity layer exists in the upper crust between 5- and 15-km depth (Smith et al, 1975; Müller and Mueller, 1979). These observations have implied a high regional geothermal gradient (Smith et al, 1975).

Refraction studies near the Roosevelt Hot Springs geothermal area itself (Gertson and Smith, 1979) indicate that the Milford Valley has a maximum depth to basement of about 2 km, the deeper fill consisting of Tertiary sediments with a *P*-wave velocity

Manuscript received by the Editor April 21, 1980; revised manuscript received March 23, 1981.
*Geophysics Division, DSIR, Box 1320, Wellington, New Zealand.
‡U.S. Geological Survey, 345 Middlefield Road, Menlo Park, CA 94025.

of about 4.0 km/sec, the shallower fill consisting of more recent sediments with velocity of 1.8 km/sec. Gertson and Smith (1979) suggest that high-velocity Precambrian (?) metamorphic rocks, exposed along the western flank of the Mineral Mountains, extend westward under Milford Valley. The granitic rocks of the Mineral Mountains, beneath a surface low-velocity weathered layer, have a velocity of approximately 5.5 km/sec.

Microearthquake studies of the Roosevelt Hot Springs region (Olson and Smith, 1976) have shown that the level of activity near the Mineral Mountains is low, while 30 km to the northeast near Cove Fort, the level is much higher and of a swarm-like nature. Depths of microearthquakes were found to be mostly less than 10 km.

Many hot spring areas in the Basin and Range province are assumed to be caused by abnormally deep penetration of circulating groundwater along range-bounding fault zones (Hose and Taylor, 1974). In the case of the Roosevelt Hot Springs geothermal area, however, analyses of the heat-flow data by Ward et al (1978) indicate that this mechanism is insufficient to account for the observed heat flux. They showed that the total heat loss of about 70 MW, obtained by integrating the high heat-flow values (100 to 1000 mW m^{-2}) around the Roosevelt Hot Springs, cannot be explained by hydrologic discharge and recharge in an equivalent area characterized by typical regional heat-flow values (75 to 100 mW m^{-2} for western Utah). Hence, they suggest a heat source at depth, probably associated with the Mineral Mountains pluton, at a temperature near the granite solidus.

THE DATA

The concept of using teleseismic traveltime residuals (observed arrival time minus that calculated on the basis of a standard earth model) to study the velocity structure of the crust is simple. If a sufficiently distant earthquake is observed with a closely spaced array of seismographs, changes in residual from station to station can be taken as due to velocity variations near the array. This is true because the raypaths back toward the source converge and so are increasingly unlikely to sample different velocity structures as the distance from the receivers increases. Changes in the pattern of residual variation with changes in source azimuth are particularly useful in determining the local velocity structure.

In order to carry out our study of the crust beneath the Mineral Mountains region, the recording array of 15 seismograph stations

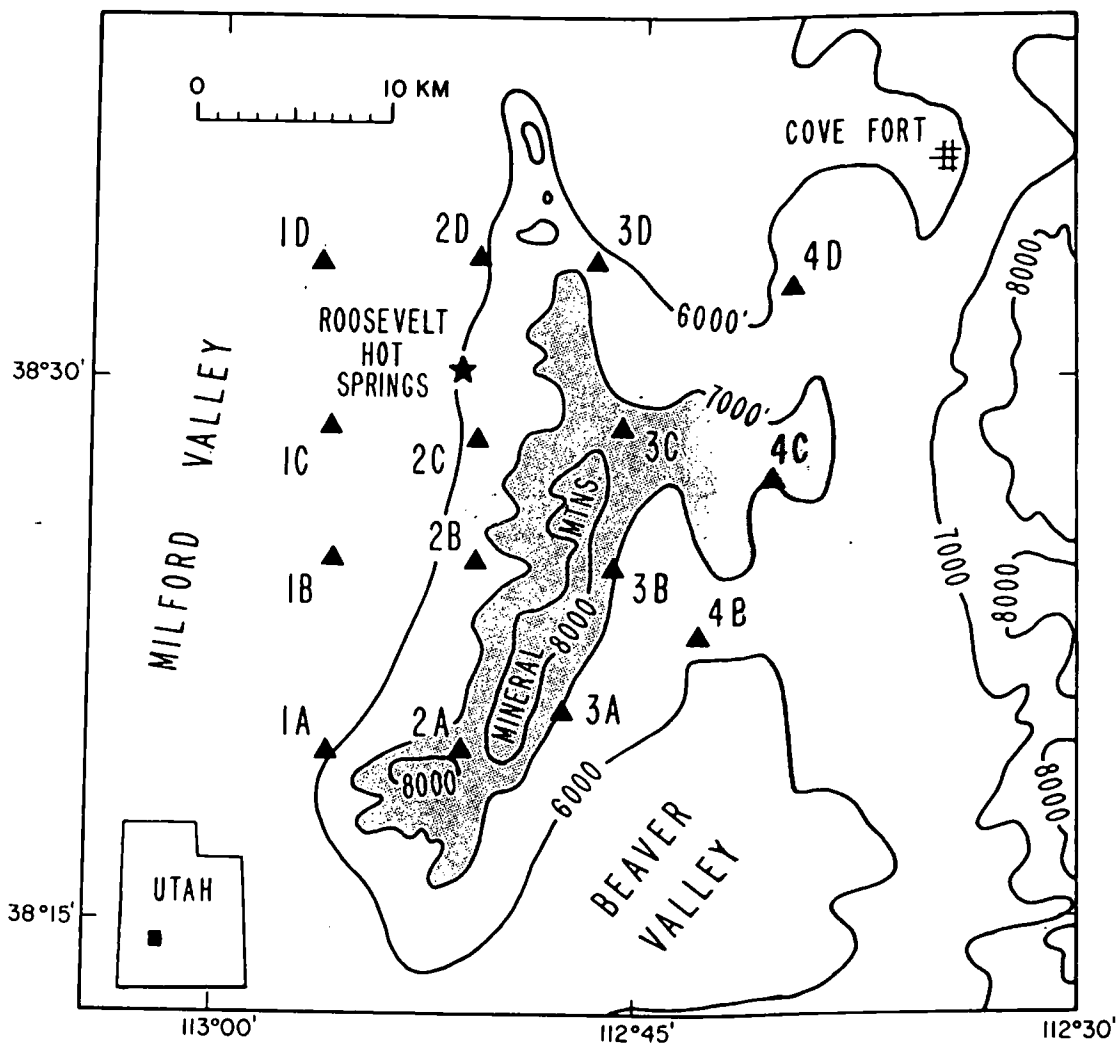

FIG. 1. The Mineral Mountains region, southwest Utah. Seismograph stations used in this study are shown by triangles. The star indicates the location of the Roosevelt Hot Springs geothermal area. Contour interval is 1000 ft, the shaded region representing the Mineral Mountains.

Table 1. Station information.

Station	Latitude (N)	Longitude (W)	Elevation (m)	Reduction velocity (km/sec)	Elevation correction (sec)	Lithology
1A	38°19.54′	112°56.05′	1722	4.5	0.38	Granite
1B	25.04	56.00	1606	3.0	0.54	Alluvium
1C	28.59	56.06	1574	2.0	0.79	Alluvium
1D	33.13	56.54	1507	2.0	0.75	Alluvium
2A	38°19.64′	112°51.32′	2201	5.4	0.41	Granite
2B	24.93	50.97	1923	4.5	0.43	Granite
2C	28.34	50.86	1905	4.5	0.42	Granite
2D	33.26	50.80	1780	4.5	0.40	Granite
3A	38°20.73′	112°47.70′	2091	4.5	0.46	Granite
3B	24.75	46.01	2152	4.5	0.48	Granite
3C1	28.58	45.77	2297	4.5	0.51	Granite
3C2	29.04	45.30	2146	4.5	0.48	Granite
3D	33.14	46.65	1853	4.5	0.41	Granite
4B	38°22.83′	112°42.95′	1929	3.0	0.64	Alluvium
4C	27.21	40.85	2115	3.0	0.71	Lava
4D	32.48	39.90	1917	3.0	0.64	Lava

was deployed (Figure 1) in a roughly square pattern 30 km wide on each side. Station coordinates and lithology are listed in Table 1. The time for seismic waves to travel vertically from sea level to the seismograph (elevation correction) was also estimated and is shown in Table 1. All stations consisted of the standard U.S. Geological Survey (USGS) three-component short-period tape recording seismograph systems described in detail by Criley and Eaton (1978). At each station, high- and low-gain data channels were recorded along with continuous radio time signals (WWVB) and the output from an internal clock. The instruments operated for a 46-day period from May 22 to July 7, 1977. Halfway through the experiment, station 3C was moved 1.07 km northeast, but in the subsequent analysis results from both sites were treated as one.

During the recording period, 72 teleseismic events were recorded sufficiently well to warrant analysis. These events are listed in Table 2 and are reasonably well distributed in azimuth. Normally in temporary seismic arrays in the United States, the recorded teleseisms are primarily from three approximate azimuths—south-

Table 2. Teleseismic events.

Date	Location	Distance	Azimuth	Date	Location	Distance	Azimuth
5/22/77	Fiji	83.0°	239°	6/18/77	Mexico	29.6°	138°
5/24/77	Volcano Is.	85.2	299	6/18/77	Solomon Is.	94.0	261
5/24/77	Mariana Is.	87.4	292	6/18/77	S. of Fiji	89.1	238
5/25/77	Fiji	83.1	241	6/19/77	Samoa	77.7	238
5/28/77	Sulawesi	119.1	293	6/19/77	Kuril Is.	66.8	312
5/29/77	Kazakh SSR	91.5	352	6/19/77	N. Atlantic Ridge	61.9	92
5/30/77	Fox Is.	41.3	309	6/22/77	Tonga	84.8	236
5/31/77	Santa Cruz Is.	90.0	255	6/23/77	Komandorsky Is.	55.1	316
6/01/77	Tonga	82.6	236	6/24/77	Tonga	89.1	231
6/01/77	Turkey	98.6	29	6/24/77	Tonga	84.4	235
6/03/77	Fiji	83.2	240	6/25/77	Fiji	86.0	239
6/05/77	Chile	73.7	140	6/25/77	N. Carolina	11.8	291
6/05/77	New Britain	96.9	270	6/25/77	Oregon	11.2	293
6/06/77	Dominican Rep.	42.0	104	6/26/77	Kuril Is.	67.9	311
6/06/77	Vancouver Is.	16.1	317	6/26/77	Tonga	84.4	235
6/06/77	Tonga	82.1	238	6/26/77	Dominican Rep.	42.1	104
6/07/77	N. California	8.9	291	6/26/77	N. Atlantic Ridge	63.5	91
6/07/77	Santa Cruz Is.	89.8	256	6/27/77	S. of Fiji	86.4	235
6/07/77	Argentina	79.8	141	6/28/77	Chile-Bolivia	72.8	137
6/08/77	Chile-Bolivia	73.7	136	6/28/77	Sicily	89.5	38
6/08/77	Honshu	77.5	309	6/28/77	N. Atlantic Ridge	59.3	84
6/09/77	Kamchatka	56.8	317	6/28/77	N. Atlantic Ridge	59.2	84
6/09/77	Mariana Is.	91.6	283	6/28/77	N. Atlantic Ridge	49.2	84
6/10/77	Sumatra	133.0	310	6/28/77	N. Atlantic Ridge	59.3	84
6/12/77	Hokkaido	74.7	312	6/29/77	Banda Sea	117.7	283
6/13/77	Guatemala	31.5	135	6/29/77	Andreanof Is.	45.3	309
6/13/77	Tonga	80.5	237	6/29/77	Tonga	84.3	235
6/15/77	N. Atlantic Ridge	61.4	91	6/30/77	South Pacific	74.5	172
6/16/77	Samoa	77.3	239	6/30/77	Chile	70.4	137
6/17/77	Fiji	84.9	240	6/30/77	Tonga	79.4	238
6/17/77	Mariana Is.	87.0	292	6/30/77	Chile	76.7	238
6/18/77	New Hebrides	92.5	253	7/01/77	Tonga	79.0	238
6/18/77	Fiji	84.4	239	7/02/77	Solomon Is.	93.5	260
6/18/77	Chile-Bolivia	72.1	137	7/02/77	Kamchatka	58.9	315
7/03/77	Fox Is.	39.9	309	7/06/77	Panama	42.8	133
7/07/77	Argentina	78.9	139	7/06/77	Fiji	85.3	239

east, southwest, and northwest (Iyer, 1979). However, in the Roosevelt array we were fortunate to record teleseisms from the northeast quadrant as well. *P*-wave arrival times of these events were read from paper playbacks of the recording tapes. The combined frequency response of the recording and playback systems peaked between 1 and 5 Hz. Arrival times used were almost never the first-break time because much greater timing accuracy can be obtained by using some other distinctive feature of the first-cycle waveform such as a zero crossing, peak, or trough. Generally, two or three separate picks were made on the waveform for each event (see Figure 2), and all those for which the timing error was estimated to be 0.05 sec or less were used in the analysis. Care had to be taken, however, to ensure that waveform changes from station to station did not introduce spurious time differences. For example, variations in attenuation along paths to different stations can cause waveform changes (a low-Q path producing a relatively broader signal). Although we found generally very good waveform correlation from station to station (Figure 2), some cases of significant distortion were indeed noticed; these will be discussed more fully below.

Traveltime residuals were calculated on the basis of hypocenters given in the USGS bulletins on Preliminary Determination of Epicenters using the Herrin (1968) *P*-wave traveltime tables. In order to eliminate the large effects of origin-time errors, relative residuals were then calculated by subtracting from each station residual the average residual for each event for the whole array. Using the average residual as a reference introduces some scatter in the data because the number of observations varies from event to event (see Table 3). However, the alternative of using one particular station as a reference, as is often done, introduces the assumption of no change in residual with azimuth at that site. Given the initially unknown structure, we thought it best not to make that assumption. Plots of relative residual versus azimuth are shown in Figure 3 for sites 1C and 2A. Site 1C exhibits one of the largest azimuthal variations of residual, and site 2A one of the smallest. The scatter shown for these two sites is also typical of the others. Average relative residuals at each station, regardless of azimuth and also as functions of the four principal quadrants, are listed in Table 3 together with their standard deviations and numbers of observations. In all cases separate picks on the waveform of a single event are treated as separate (obviously, not independent) data points. If it is assumed that the residuals have a Poisson distribution about their means, the standard errors of the means are 0.02 sec or less in all cases.

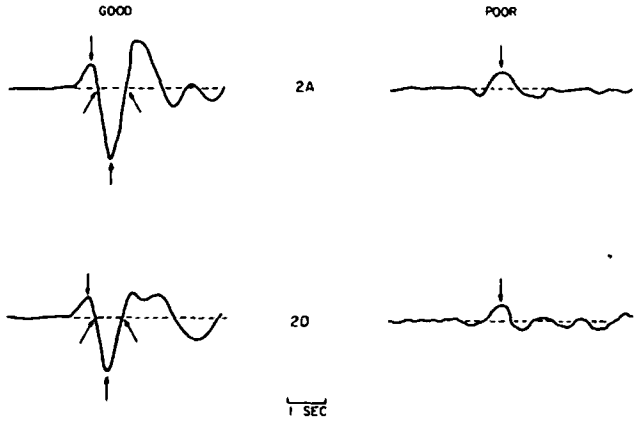

FIG. 2. Example of teleseismic *P*-wave signals at stations 2A and 2D. The arrows indicate the times used. Note the excellent waveform correlation for the first event through the first cycle of motion.

In addition to the teleseisms used above, numerous local and regional events were also recorded. Analysis of these data will be presented in detail at a later time. However, in the discussion of teleseismic results we will use arrival time data from a nuclear explosion at the Nevada test site on May 25, 1977, at a distance of 322 km and an azimuth of 242 degrees from the center of our network. For this event, the first arrivals were sharp and the first break was timed. The apparent velocity of the first arrivals indicates that they were P_n arrivals; the frequency was about 4 Hz.

ANALYSIS AND INVERSION OF THE DATA

The residuals averaged over all events for each station, listed in Table 3, reflect in only a gross way the vertically integrated velocity variations under the network because of the wide range of azimuths and incidence angles included. These results are contoured in Figure 4. (Usually in studies such as this, it is common practice to apply a correction to the residual to compensate

Table 3. Average relative residuals.

Station	All Azimuths			0–90°			90–180°			180–270°			270–360°		
	N	R	S D	N	R	S D	N	R	S D	N	R	S D	N	R	S D
1A	141	−0.23	0.06	14	−0.17	0.06	35	−0.26	0.06	35	−0.26	0.06	39	−0.21	0.07
1B	79	0.02	0.07	7	0.09	0.03	24	0.03	0.06	20	−0.05	0.05	28	0.03	0.06
1C	106	0.21	0.14	12	0.32	0.12	33	0.36	0.08	32	0.10	0.04	29	0.10	0.05
1D	96	0.17	0.14	11	0.18	0.08	32	0.34	0.07	22	0.06	0.04	31	0.09	0.07
2A	154	−0.11	0.06	15	−0.07	0.04	44	−0.16	0.05	59	−0.11	0.05	36	−0.09	0.06
2B	137	−0.05	0.10	12	0.03	0.13	38	−0.17	0.05	41	−0.10	0.06	46	0.01	0.09
2C	130	0.05	0.11	12	0.04	0.04	33	0.10	0.11	51	0.08	0.06	34	−0.03	0.14
2D	116	−0.17	0.09	15	−0.17	0.06	25	−0.06	0.06	41	−0.17	0.05	35	−0.25	0.04
3A	138	−0.02	0.06	15	0.01	0.05	34	−0.08	0.04	49	−0.02	0.04	40	0.03	0.05
3B	144	0.03	0.10	13	−0.03	0.03	41	−0.07	0.06	49	0.04	0.05	41	0.23	0.06
3C	106	0.14	0.10	9	0.04	0.04	36	0.04	0.05	56	−0.05	0.05	20	0.16	0.07
3D	149	−0.07	0.07	15	−0.07	0.06	37	−0.05	0.05	56	−0.05	0.05	41	−0.14	0.05
4B.	76	0.12	0.10	1	0.06	—	29	0.02	0.09	29	0.17	0.04	17	0.19	0.07
4C	130	0.06	0.09	10	−0.04	0.05	32	−0.03	0.09	46	0.12	0.05	42	0.09	0.06
4D	90	0.10	0.08	10	0.01	0.03	23	0.03	0.07	37	0.12	0.04	20	0.16	0.06

N = number of observations; R = average residual (sec); SD = standard deviation.

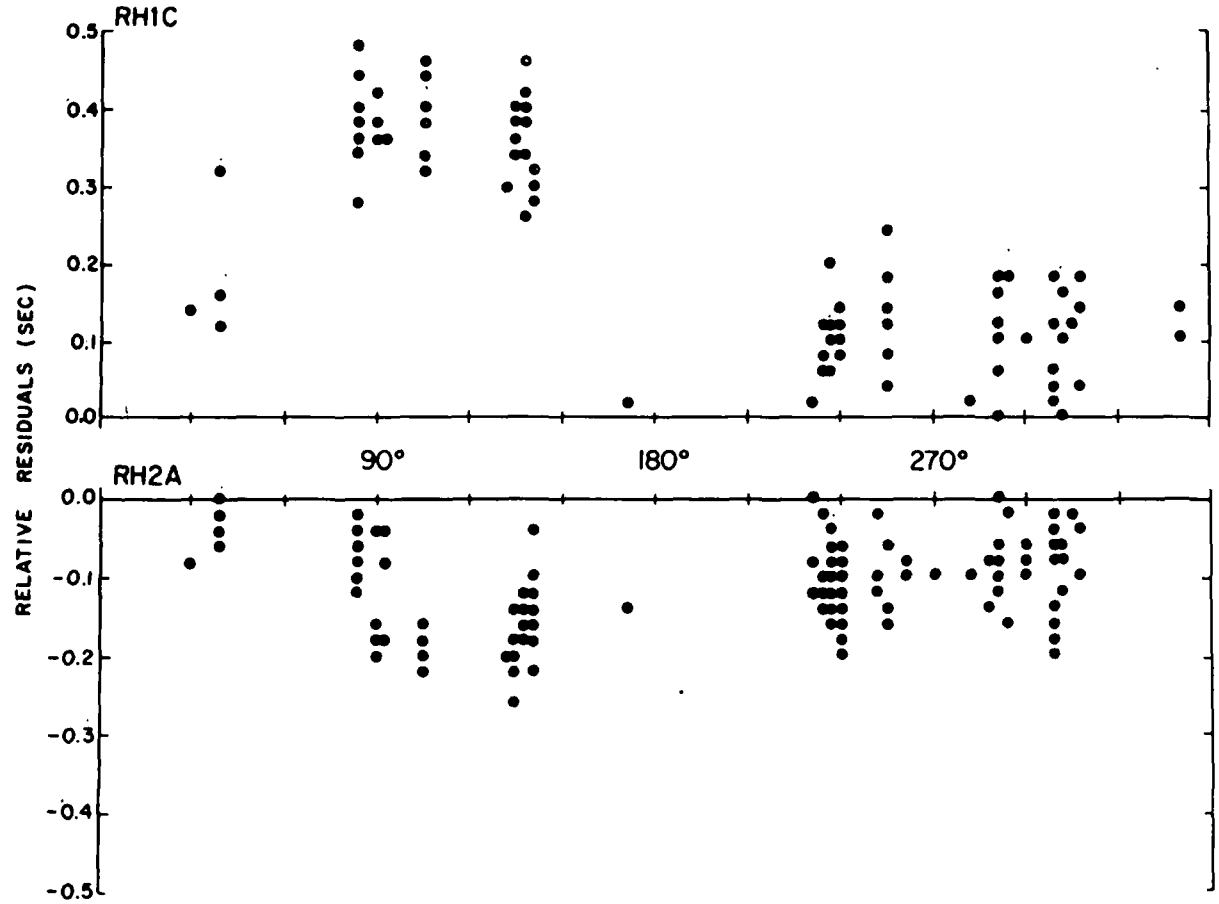

FIG. 3. Relative residuals as a function of azimuth for stations 1C and 2A.

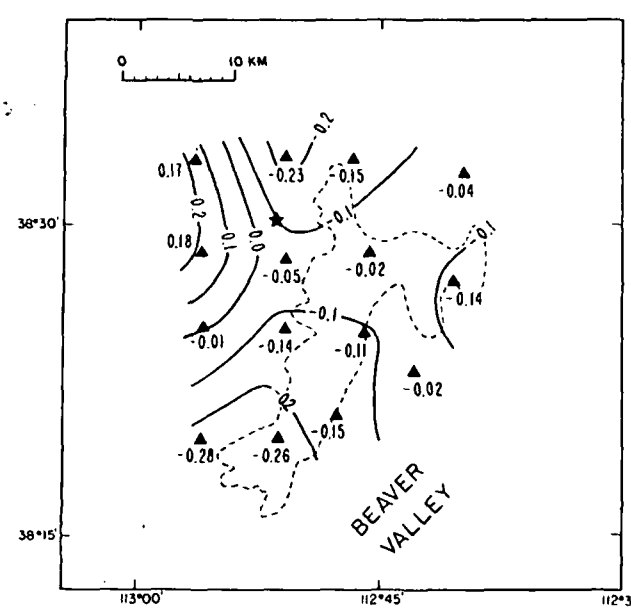

FIG. 4. Contours of average relative residual regardless of azimuth. The contour interval is 0.1 sec. Triangles represent the seismograph sites and the dotted curve outlines the Mineral Mountains. The star indicates the location of the Roosevelt Hot Springs.

for differences in station elevation. However, from Table 1 it will be seen that though elevation differences greater than 0.5 km occur, the effect of lithology is stronger than that of elevation. For example, note that stations 1C and 1D which have the lowest elevations have the largest elevation corrections. Because of this discrepancy, we did not apply elevation corrections at this point.) The basin-and-range structure is evidenced by the positive residuals at sites within Milford Valley and by the negative residuals at sites in the northern and southern Mineral Mountains. The positive residuals in Beaver Valley are not as pronounced as in the Milford Valley. Also, the residuals in the central Mineral Mountains are not as negative as they are to the north and south.

Considering the variations of residual with azimuth (Figure 3 and Table 3), it can be seen that there are significant azimuthal variations, reaching up to 0.4 sec at some of the stations. The general pattern of these variations is that the largest residuals (slowest path) occur in the direction toward the central Mineral Mountains. This effect can be seen, somewhat smoothed out, in the average residuals for the four azimuthal quadrants, shown in Figure 5. The striped areas are the regions where the relative residual is 0.1 sec or greater. It is clear that there is an azimuthally shifting "shadow zone." Such a pattern of residual variation cannot be explained simply by near-surface velocity variations since the angles of incidence, measured from vertical, of the teleseismic waves at the surface are generally 25 degrees or less

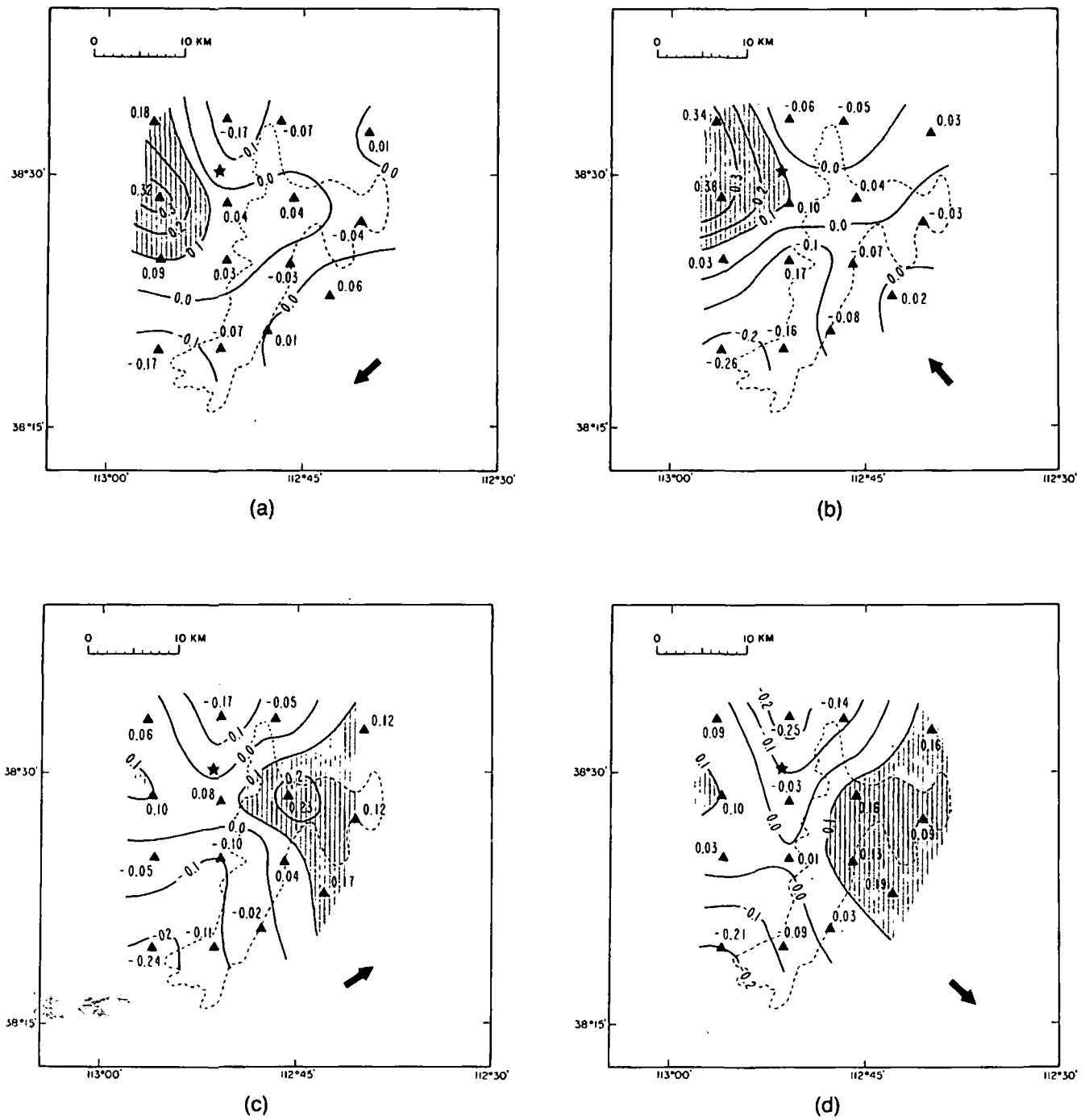

FIG. 5. Contour of average relative residual for the four principal azimuth quadrants. The shaded areas are zones where the relative residual is 0.1 sec or greater. The contour interval is 0.1 sec. Triangles represent the seismograph sites. The star indicates the location of Roosevelt Hot Springs. (a) 0–90 degrees; (b) 90–180 degrees; (c) 180–270 degrees; (d) 270–360 degrees.

(Steeples and Iyer, 1976). Ray tracing indicates that a possible cause of such a variation is a zone of relatively low velocity centered under the central Mineral Mountains in the middle and lower crust. For example, the major features of the data can be explained roughly by a sphere of radius 10 km and velocity 5.4 km/sec embedded in a half-space of velocity 6.0 km/sec at a depth of 20 km. Such a model is, however, only the simplest and not the best.

To be more quantitative and to take account of the more subtle changes in residual, we used a 3-D inversion procedure developed by Aki et al (1977). In this procedure a portion of the earth is subdivided into horizontal layers, each layer being divided in turn into a number of rectangular blocks. The initial uniform velocity assigned to each layer is modified in each block so as to minimize the variance of the resulting residuals, the needed changes obtained by finding a damped solution of a system of linear equations. The assumptions are that the velocity in each layer outside the model is uniform, that outside the model the earth is horizontally uniform, and that geometrical ray theory is applicable. A complete description of the use of this technique in a context very similar to ours can be found in Reasenberg et al (1980).

We adopted a four-layer model, each layer being 67.5 km square and subdivided into 9 × 9 blocks 7.5 km on each side. The top layer was 5 km thick and the lower ones 10 km thick. The lateral extent of the station array puts a limit on the model's maximum depth. Considering the typical wavelength of the teleseismic arrivals (5–10 km), a subdivision into smaller blocks is not warranted. The initial velocity model, shown in Table 4, is based on the seismic-refraction results discussed earlier. These initial velocities are not critical, however, since the results of the inversion procedure are in terms of the percent change in velocity within a layer, not absolute velocities. Absolute velocity values cannot be obtained from relative residual data.

Results of one inversion of the data are shown in Figure 6. These results are percent changes in velocity (positive values indicate a higher velocity). A value of 0 indicates that too few rays (<5) passed through that block for a meaningful change to be calculated. Underlined values are those for which the resolution is not as good (Reasenberg et al, 1980); all values for layer 1 are well resolved. The treatment for layer 1 was different from the deeper layers: a change in velocity was assigned to each station rather than to individual blocks. That avoided the problem of two or more stations with substantially different near-surface velocity structures overlying the same block in the model. Elevation was included in the treatment of the first layer. In this inversion, variance of the original data (0.0294 sec^2) was reduced by 91 percent to 0.0027 sec^2, close to what would be expected due to reading errors.

Table 4. *Initial inversion model.*

Layer	Thickness (km)	*P*-wave velocity (km/sec)
1	5.0	4.5
2	10.0	5.5
3	10.0	6.5
4	10.0	7.5

LAYER 1 (0 – 5 KM)

1A	7.3	3A	1.9
1B	-2.7	3B	3.5
1C	-13.1	3C	0.4
1D	-17.0	3D	5.9
2A	6.5	4B	-7.6
2B	7.9	4C	-1.1
2C	4.8	4D	-4.9
2D	9.5		

LAYER 2 (5 – 15 KM)

0	0	0	0	0	0	0	0	0
0	0	0	0	0	0	0	0	0
0	0	1.7	2.5	0.7	-1.6	-0.1	1	0
0	0.1	0.7	-1.4	-2.4	-1.7	2.3	0	0
0	0	-2.3	-5.1	-4.2	-0.5	3.9	0	0
0	0	0.1	0.9	1.0	1.8	-0.6	0	0
0	0	1.7	4.0	1.8	0.2	0	0	0
0	0	0	0	0	0	0	0	0
0	0	0	0	0	0	0	0	0

LAYER 3 (15 – 25 KM)

0	0	0	0	0	0	0	0	0
0	-0.8	-1.0	0.0	0	0	0	0	0
0.1	0.9	3.3	-1.3	0.4	-2.4	0.7	0	0
-0.7	0.9	2.2	-5.1	-3.8	0.2	1.1	0.1	0
-0.4	0.0	-0.6	-5.1	-2.8	0.8	2.3	0.1	0
-0.5	2.3	0.5	-2.0	-1.1	-0.9	0.6	-0.4	0
0	0	0.9	-1.2	2.0	0.0	3.8	0	0
0	0	0	1.5	3.4	1.7	0	0	0
0	0	0	0	0	0	0	0	0

LAYER 4 (25 – 35 KM)

2.0	0	0	0	0	0	0	0	0
-0.3	-0.6	0.0	-0.1	-0.6	0.7	0	0	0
-0.2	-0.3	3.1	0.4	-5.2	-1.4	0.6	0	0
1.0	0.5	1.6	-0.3	-3.0	-1.4	1.1	-0.8	0.5
-0.2	3.3	2.3	-2.8	-4.0	-1.6	-0.5	0.6	0.5
0	0.4	-0.9	-3.6	-4.8	-0.2	0.6	0.9	0
0	0.8	1.1	-1.2	-2.0	1.8	4.7	-1.1	0
0	0.6	-0.5	-0.5	1.2	3.6	0	0	0
0	0	0	0	0	0	0	0	0

FIG. 6. Results of one inversion of the residual data. Values are the percentage change in velocity for the corresponding block. Underlined values are less well resolved from nearby values. A 0 indicates insufficient data for a value to be calculated.

The results (shown in Figure 6) suffer to some degree from the necessarily coarse modeling due to the size of the blocks. In order to smooth out these effects, we did a second inversion with the block boundaries displaced one-half block width diagonally. Final values of the velocity changes were then calculated at a grid of points using a four-point average. These values are contoured in Figure 7 and will form the basis of the following discussion.

DISCUSSION OF THE RESULTS

Considering first the results for layer 1 (0–5 km depth), it can be seen that the basin-and-range structure dominates the results. A ridge of relatively high velocity is associated with the Mineral Mountains, although it is displaced to the west of the crest, perhaps reflecting the presence of the high-velocity metamorphic rocks along the western flank of the range. If these high-velocity rocks extend west under the Milford Valley, their effect on the results is hidden by that of the low-velocity valley fill which reaches a maximum near site 1D. These results are in good agreement with the refraction and gravity studies discussed previously. Simple models based on these studies suggest a velocity contrast of about 15 percent between sites in the Milford Valley and the Mineral Mountains for a layer 5-km thick, similar to that found

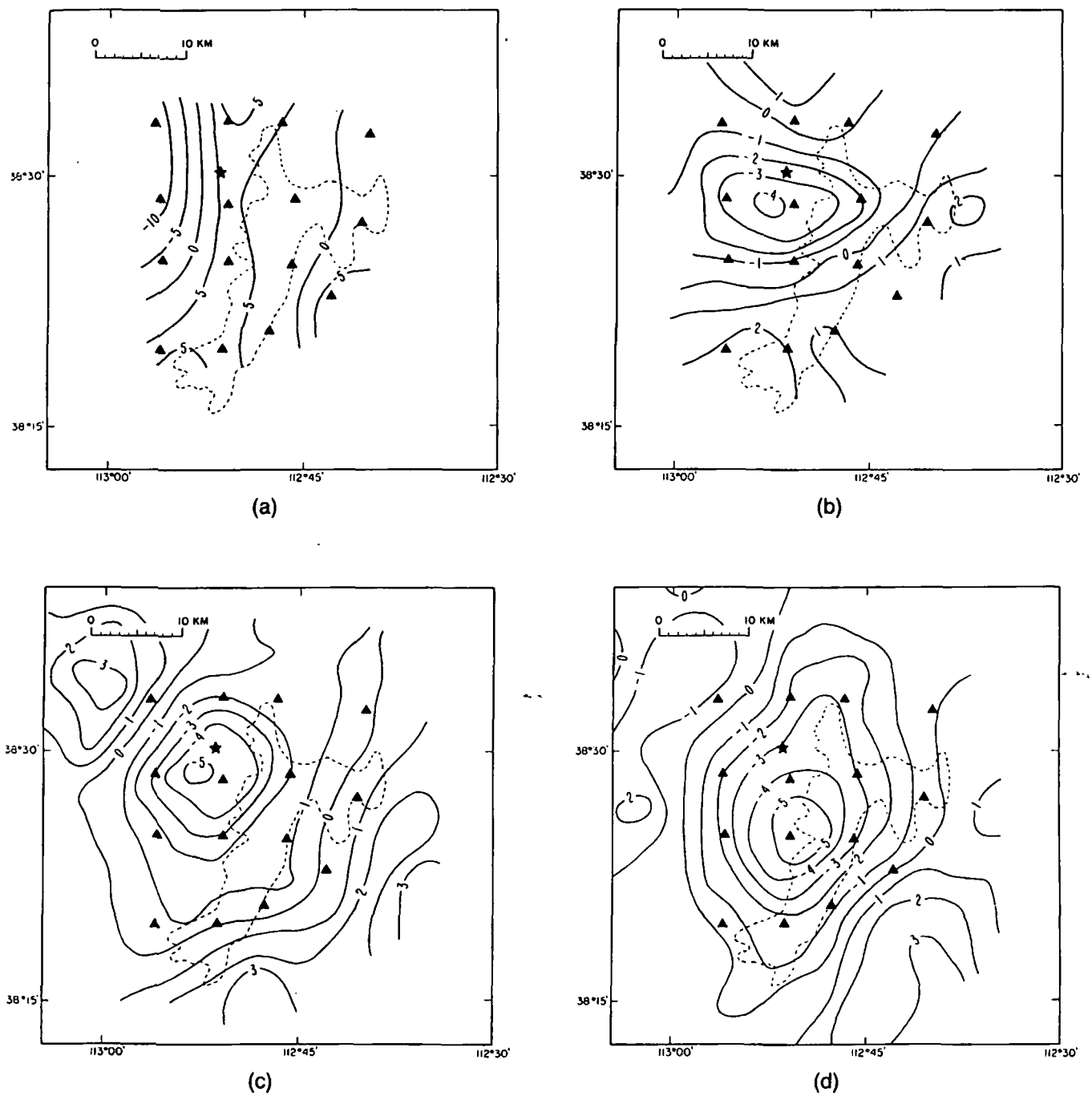

FIG. 7. Contours of the smoothed velocity changes. For the first layer the contour interval is 2.5 percent; for the others, it is 1.0 percent. Triangles represent seismograph sites. The star indicates the location of Roosevelt Hot Springs. The outlined area represents the Mineral Mountains. (a) Layer 1: 0–5 km; (b) Layer 2: 5–15 km; (c) Layer 3: 15–25 km; (d) Layer 4: 25–35 km.

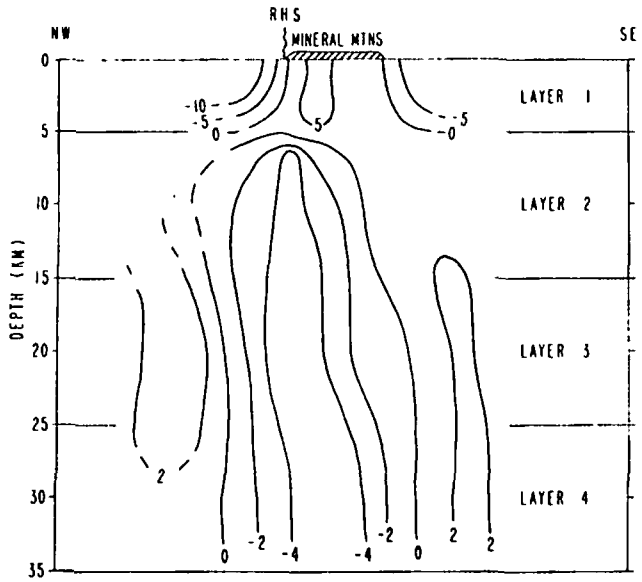

FIG. 8. A highly schematic northwest-southeast cross-section through the central Mineral Mountains based on the results shown in Figure 7. The vertical exaggeration is 2:1. Contours represent the percentage of lateral velocity contrast within the layers.

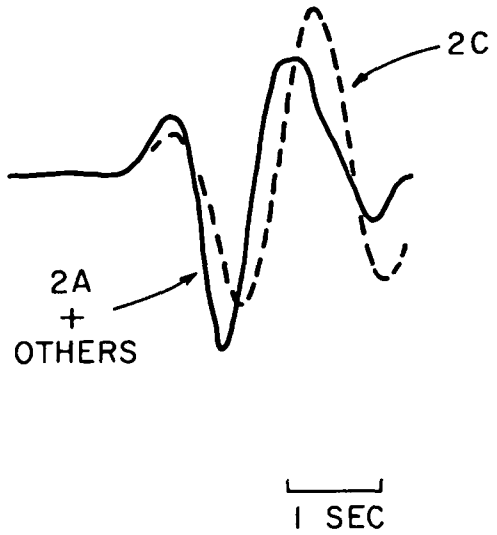

FIG. 9. An example of the waveform broadening as discussed in the text. The solid curve is the signal at site 2A and is similar to that at all other sites except, in this case 2C, which is shown by the dashed line. The event is at a southwest azimuth (Chile-Bolivia). For other azimuths other stations exhibit the broadening (see text).

here. To the east, in the area covered by stations 4B, 4C, and 4D, the average seismic velocity in this layer is lower than in the Mineral Mountains by 5 to 10 percent, reflecting the unconsolidated sediments in the Beaver Valley (less thick than in Milford Valley) and their extension north under the basalt flows near sites 4C and 4D.

Results for the second layer (5–15 km) are in sharp contrast to those above. They indicate a region of relatively low velocity (about 5 percent contrast; note the change in contour interval in Figure 7) centered near site 2C and also near the area of high heat flow associated with the Roosevelt Hot Springs geothermal area. This region of low velocity seems to extend west of the Mineral Mountains, although this may be due in part to imperfect resolution from the overlying low velocities of the Milford Valley in this region. It is important to note here that results such as this imply lateral contrasts in velocity and are not the same as the regional low-velocity zone inferred from refraction results in this depth range.

The results for the third layer (15–25 km) are similar in exhibiting a center of relatively low velocity near site 2C, but this region also extends more to the north and south. The results for layer 4 (25–35 km) in the uppermost mantle are again similar but show a shift south from the center of low velocity; the north-south elongation is still present. The velocity contrast in these deeper layers is somewhat greater, about 7 percent.

Overall, the results suggest a pipe-like feature of approximately 5–7 percent velocity contrast extending from about 5-km depth down at least as far as the uppermost mantle, centered near the Roosevelt Hot Springs geothermal area but extending to the north and south at depth. A highly diagrammatic northwest-southeast cross-section through Roosevelt Hot Springs is shown in Figure 8.

To see if this velocity structure derived from teleseismic data is in accord with data derived from regional earthquakes, the arrival-time data from a Nevada test site nuclear explosion were examined. The significance of this test is that it provides comparison between teleseismic residuals (computed using waves in the frequency band of 0.5 to 2 Hz) and residuals associated with higher frequencies characteristic of regional events. The event was approximately 310 km west of Roosevelt Hot Springs. Traveltime residuals for the explosion were calculated using the initial four-layer model and compared with those calculated on the basis of the final teleseismic inversion model. When this was done, it was found that the variance was reduced from 0.029 sec^2 (the same as for the teleseismic data) to 0.006 sec^2, an improvement of about 79 percent. The improvement in the variance using only the velocity structure determined for layer 1 is 68 percent. Thus, although the near-surface effects are clearly the most important (as they are for the teleseismic data also), the deeper structure also has an appreciable effect in reducing the variance. Still, it is clear that given the high accuracy in timing the nuclear blast arrivals (better than 0.05 sec), there remains a good deal of unexplained variance. Eventually a more detailed study of this event and other regional events may refine the rather coarse results obtained here on the basis of relatively low-frequency teleseismic data alone and perhaps provide some information on frequency-dependent effects.

Examination of waveforms of teleseismic signals provides some evidence for the presence of a small region of severe attenuation within the low-velocity body. As was mentioned above, during the process of reading the teleseismic arrival times, instances of significant waveform distortion were observed. These effects are very systematic and consistent among events from the same azimuth. For events at southeast azimuths, the waveform at station 2C was significantly broader than at any other station (an example is shown in Figure 9). Similarly, for events at southwest azimuths, station 3C exhibited waveform broadening while all other stations (including 2C) did not. For the northeast azimuth, the limited data indicate broadening at station 2B. For the northwest azimuth, however, no station exhibited abnormal broadening.

We have no detailed explanation for these observations as yet. Ray tracing would place the location of the distorting region at a

depth of about 15 km under the region bounded by the sites 2C, 3C, and 2B, within the region of relatively low velocity but displaced from its apparent center. The fact that distortion occurs at only one of many stations spaced within 10 km of one another argues that the region causing the distortion is small, probably too small for the observed broadening to be caused by attenuation alone. One possible explanation is the existence of a small (diameter about 5 km) region of intense attenuation; diffraction effects within the geometrical shadow zone could then explain the observed broadening (Matumoto, 1971). Such a region then would not produce a significant traveltime delay. Another possibility is a frequency-dependent focusing effect.

The interpretation of our results in terms of geology is not straightforward. Iyer and Stewart (1977) discussed the possible causes of low-velocity regions in the crust and upper mantle. These include lateral variation in temperature, composition, fabric, and the nature of any fluid inclusions (e.g., partial melt), in any combination. The recent volcanism certainly indicates that higher than normal temperatures are to be expected beneath the Mineral Mountains. Measurements of the temperature derivative of P-wave velocity (for references, see Iyer and Stewart, 1977) indicate that a 5 to 7 percent decrease in velocity would require a temperature increase of about 600°C to 850°C over that of the surrounding rocks. Phase diagrams for typical crustal rocks indicate that this would result in some degree of melting, especially if the regional geothermal gradient were initially abnormally high. Partial melting itself, however, leads to a much more rapid drop in velocity, so that an interpretation in terms of high temperatures needs to take this factor into account, too. Although experimental data on velocity in partially molten rocks at crustal pressures are scarce, theoretical models are well developed (e.g., O'Connell and Budiansky, 1977; Mavko, 1980). A 5 to 7 percent reduction in P-wave velocity (at a frequency of 1 Hz) can be explained by a melt fraction of only 1.5 to 4.0 percent depending upon assumptions about the pore shapes. This degree of melting would require temperatures only slightly above the solidus.

The possibility of a compositional change as the cause of the low-velocity region must be considered given the near-surface petrologic heterogeneity. A 5 to 7 percent lower velocity, for typical crustal rocks, would be associated with a density decrease of about 0.13–0.17 g/cm^3. A body of the shape of the low-velocity region with an average density contrast of 0.10 g/cm^3 would produce a broad gravity anomaly with a maximum amplitude of only about 14 mgal. It would be difficult to recognize such a long-wavelength anomaly among the stronger effects of the basin-and-range structure. [There is, however, a clear localized gravity low of 15–20 mgal in the central Mineral Mountains (Carter and Cook, 1978) that overlies the region we have hypothesized is causing waveform distortion.] Thus, a low-velocity feature such as we have found could represent something like a pipe of relatively low-density intrusive rocks, perhaps associated with the emplacement of the granitic rocks of the Mineral Mountains themselves. If so, it would then be puzzling that the extent of the low-velocity region at shallow depth (layer 2) corresponds not with the outcrop area of the granitic rocks but rather more closely with areas of thermal and volcanic activity.

It is thus our suggestion that the low velocity reflects abnormally high temperature and the presence of a small fraction of molten rock. However, the possibility that it is caused, in part or in whole, by compositional changes cannot be ruled out. At mid-crustal and lower depths, the postulated molten fraction would most likely be of basic composition (viz., the Quaternary basic eruptive activity on the northeast flank of the Mineral Mountains), whereas at shallower depths it would more likely be acidic and associated with the Quaternary rhyolitic activity along the crest of the mountains. The nature of the small anomalous region under the central Mineral Mountains associated with the waveform distortion remains somewhat of a mystery but it may be a region of more intense partial melt. On the basis of this model, the source of heat for the Roosevelt Hot Springs geothermal area is the region of partial melt, hydrothermal circulation serving to transport the heat to the surface. This model implies that there is a considerable heat reservoir associated with this geothermal area, much more than would be expected on the basis of a model involving only abnormally deep circulation of fluids along fault zones, a conclusion similar to that of Ward et al (1978) based on heat-flow data. An important question that remains is whether or not periodic recharge of the heat supply to shallower depths is required to maintain long-term, near-surface thermal activity and, if so, whether or not the region of partial melt would be sufficiently permeable to allow this to occur via upward flow of molten rock. In this regard, the small region of possibly more intense melt concentration may play an important role.

ACKNOWLEDGMENTS

We very much appreciate the help of the following persons in carrying out the field work and aiding in the playback and analysis of the resulting data: John Coakley, Edward Criley, Dennis Seguirant, Mary Ann Spieth, Tim Hitchcock, Dave Oppenheimer, and Allan Walter. Also the help of W. Ellsworth and P. Reasenberg was invaluable to us in applying the 3-D inversion method to our data. Reasenberg's thorough and critical review of the manuscript is very much appreciated.

REFERENCES

Aki, K., Christoffersson, A., and Husebye, E., 1977, Determination of the three-dimensional structure of the lithosphere: J. Geophys. Res., v. 82, p. 277–296.

Braile, L., Smith, R. B., Keller, G. R., Welch, R., and Meyer, R. P., 1974, Crustal structure across the Wasatch Front from detailed seismic refraction studies: J. Geophys. Res., v. 79, p. 1295–1317.

Carter, J. A., and Cook, K. L., 1978, Regional gravity and aeromagnetic surveys of the Mineral Mountains and vicinity, Millard and Beaver counties, Utah: Final rep. v. 77-11, DOE/DGE contract EY-76-S-07-1601, Univ. of Utah, 179 p.

Criley, E. E., and Eaton, J. P., 1978, Five-day recorder seismic system: U.S.G.S., open-file rep. 78-266.

Gertson, R. C., and Smith, R. B., 1979, Interpretation of a seismic refraction profile across the Roosevelt Hot Springs, Utah and vicinity: Topical Rep. IDO/78-1701.a.3, DOE contract DE-AC07-78er28392, Univ. of Utah, 120 p.

Herrin, E., 1968, Seismological tables for P: SSA Bull., v. 58, p. 1196–1219.

Hose, R. K., and Taylor, B. E., 1974, Geothermal systems of northern Nevada: U.S.G.S. open-file rep. 74-271.

Iyer, H. M., 1979, Deep structure under Yellowstone National Park, U.S.A.: A continental "hot spot": Tectonophys., v. 56, p. 165–197.

Iyer, H. M., and Stewart, R. M., 1977, Teleseismic technique to locate magma in the crust and upper mantle, in Magma genesis: H. J. B. Dick, Ed., Oregon Dept. of Geol. and Min. Ind. Bull. 96, p. 281–299.

Iyer, H. M., Oppenheimer, D. H., and Hitchcock, T., 1979, Abnormal P-wave delays in the Geysers—Clear Lake geothermal area, California: Science, v. 204, p. 495–497.

Matumoto, T., 1971, Seismic body waves observed in the vicinity of Mount Katmai, Alaska, and evidence for the existence of molten chambers: GSA Bull., v. 82, p. 2905–2920.

Mavko, G. M., 1980, Velocity and attenuation in partially molten rocks: J. Geophys. Res., v. 85, p. 5173–5189.

Müller, G., and Mueller, S., 1979, Traveltime and amplitude interpretation of crustal phases on the refraction profile Delta-W, Utah: SSA Bull., v. 69, p. 1121–1132.

O'Connell, R. J., and Budiansky, B., 1977, Viscoelastic properties of fluid saturated cracked solids: J. Geophys. Res., v. 82, p. 5719–5736.

Olson, T. L., and Smith, R. B., 1976, Earthquake surveys of the Roosevelt Hot Springs and Cove Fort areas, Utah: Final rep., v. 4, NSF grant GI-43741, Univ. of Utah, 83 p.

Prodehl, C., 1970, Seismic refraction study of the western United States:

GSA Bull., v. 81, p. 2629–2646.
Reasenberg, P., Ellsworth, W., and Walter, A., 1980, Teleseismic evidence for a low-velocity body under the Coso geothermal area: J. Geophys. Res., v. 85, p. 2471–2483.
Smith, R. B., 1979, Seismicity, crustal structure, and intraplate tectonics of the interior of the western Cordillera: GSA memoir 152, p. 111–144.
Smith, R. B., Braile, L., and Keller, G. R., 1975, Crustal low velocity layers: Possible implications of high temperatures at the Basin and Range—Colorado Plateau transition: Earth and Plan. Sci. Lett., v. 28, p. 197–204.
Steeples, D. W., and Iyer, H. M., 1976, Low-velocity zone under Long Valley as determined from teleseismic events: J. Geophys. Res., v. 81, p. 849–860.
Ward, S. H., Parry, W. T., Nash, W. P., Sill, W. R., Cook, K. L., Smith, R. B., Chapman, D. S., Brown, F. H., Whelan, J. A., and Bowman, J. R., 1978, A summary of the geology, geochemistry, and geophysics of the Roosevelt Hot Springs thermal area, Utah: Geophysics, v. 43, p. 1515–1542.

GEOPHYSICS, VOL. 46, NO. 10 (OCTOBER 1981); P. 1467–1468, 2 FIGS.

Short Note

A microearthquake survey at the Ngawha geothermal field, New Zealand

Russell Robinson*

A twenty day microearthquake survey of the Ngawha geothermal field, New Zealand, was undertaken in order to establish the level of preproduction seismicity and to test the usefulness of such surveys in geothermal exploration. The Ngawha geothermal field, in the far northwest of the North Island (Northland) is associated with a region of Quaternary basaltic volcanism. It is not a part of the much more extensive Taupo volcanic zone in the central North Island, site of the well-known Wairakei geothermal field, among others. Although surface thermal activity at Ngawha is limited to a few relatively small hot springs, resistivity surveys have outlined a 25–50 km^2 area of hot water at the 1-km depth level (Macdonald et al, 1977). Test bores to that depth have encountered temperatures of up to 250°C within Mesozoic graywacke. Overlying the graywacke is about 500 m of Cenozoic claystone and siltstone which forms an impermeable cap.

It is probable that the Ngawha geothermal field will be developed for electric power production. The possibility of future seismicity induced by fluid removal and/or reinjection makes it desirable to determine the present rate of local earthquake occurrence for comparison. Judging from the records of the low-gain permanent seismographs in the region and felt reports, earthquakes of magnitude 3½ or more are very rare in Northland (Eiby, 1964). Of the few events located instrumentally in Northland, the nearest was 45 km north of Ngawha. However, nothing was known previous to this study about the level of microearthquake occurrence in the region. Regarding the Ngawha area in particular, the nearest permanent seismograph station is 80 km distant so that little could be said about the occurrence of small events there.

This study was also undertaken in order to test further the utility of microearthquake surveys in geothermal exploration. Although it is often assumed that geothermal fields exhibit levels of microearthquake activity higher than the regional norm, previous studies in New Zealand have shown that this is not true in the Taupo volcanic zone (Evison et al, 1976; Hunt and Latter, 1981).

A 25-km diameter network of six portable seismographs (Kinemetrics models PS1 and PS1A) centered on the Ngawha geothermal field was operated from March 6 to March 26, 1980 (see Hunt and Latter, 1981, for a detailed description of the instruments and operating procedures). The gains of the instruments (approximately 125,000 at 10 Hz) were such that earthquakes of magnitude 0.1 or more within the field would be detected and located, as would events of magnitude 1.3 or more outside the field but within 50 km. However, *no* local earthquakes were detected, although 4 quarry blasts and 17 teleseisms or regional events were well recorded. The quarry blasts provide some in-

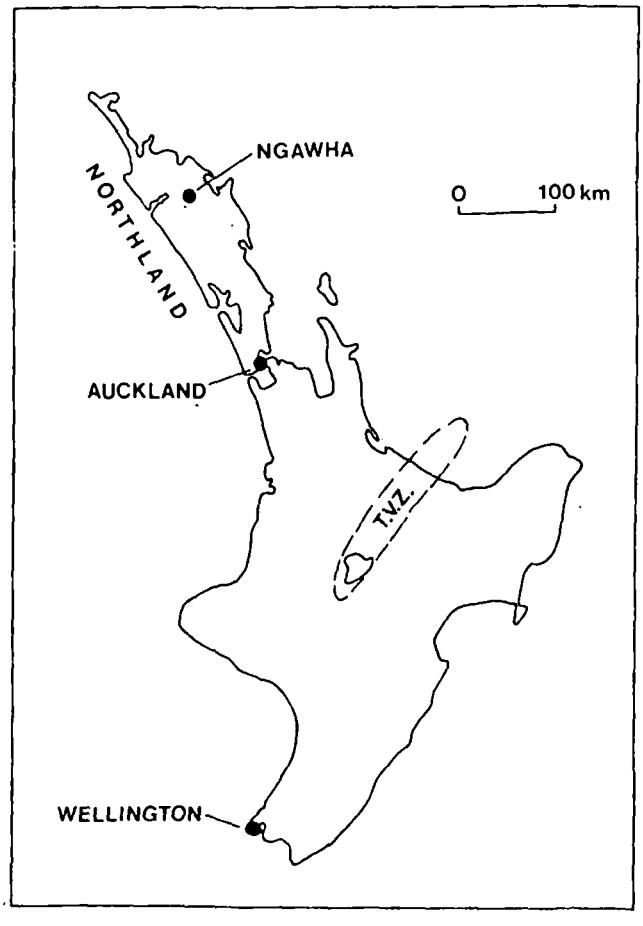

FIG. 1. North Island, New Zealand. The Ngawha geothermal area is in the far north and is not associated with the well-known Taupo volcanic zone (T. V. Z.).

Manuscript received by the Editor June 19, 1980; revised manuscript received February 18, 1981.
*Geophysics Division, Department of Scientific and Industrial Research, P.O. Box 1320, Wellington, New Zealand.

formation on the local velocity structure; more detailed experiments could make good use of future blasts to study possible variations of velocity or attenuation associated with the geothermal field.

The conclusions of this study are:

(1) The present preproduction level of microearthquake occurrence at Ngawha is nil for magnitudes greater than 0.1;
(2) microearthquake surveys of 20 days duration would have been of no use in exploration for this geothermal field.

The proviso is, of course, that earthquake activity at Ngawha is not characterized by swarms interspersed with long periods of complete quiescence. At present there are no plans for permanent microearthquake surveillance.

ACKNOWLEDGMENTS

The following persons aided in carrying out the field work: S. Ashcroft, B. Ferris, M. Lowry, D. Mutia, H. Reyner, A. Robinson, and E. G. C. Smith.

REFERENCES

Eiby, G. A., 1964, The Northland earthquakes of 1963 November-December and the seismicity of Northland: New Zealand J. Geol. Geophys., v. 7, p. 745–765.

Evison, F. F., Robinson, R., and Arabasz, W. J., 1976, Microearthquakes, geothermal activity, and structure, central North Island, New Zealand: New Zealand J. Geol. Geophys., v. 19, p. 625–637.

Hunt, T. M., and Latter, J. H., 1981, A survey of seismic activity near Wairakei geothermal field, New Zealand: J. Vol. Geotherm. Res.

Macdonald, W. J. P., Dawson, G. B., Rayner, H. H., and Hewson, C. A. Y., 1977, Geophysical investigations of the Ngawha geothermal area: Rep. 130, Geophysics Div., D. S. I. R., Wellington.

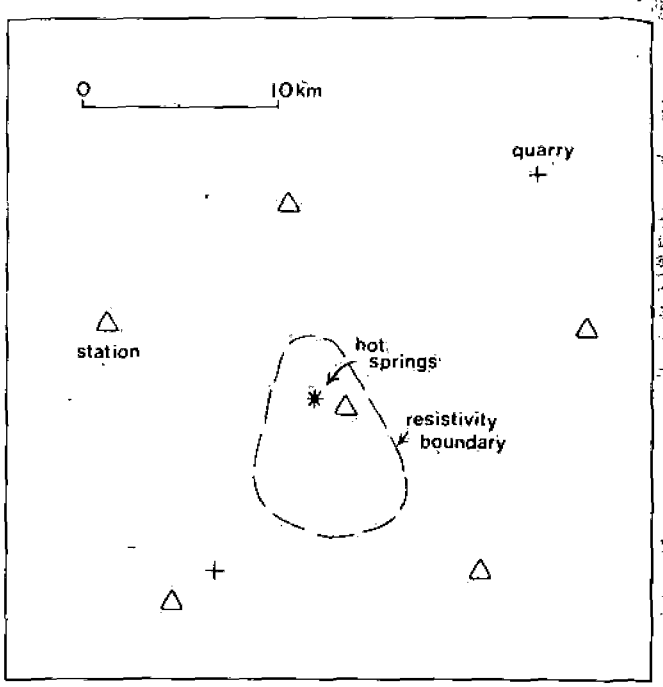

FIG. 2. Seismograph station configuration. Stations are shown by triangles; the dashed line is the resistivity boundary of the Ngawha geothermal field (1-km depth level) taken from Macdonald et al (1977).

GEOPHYSICS, VOL. 47, NO. 5 (MAY 1982): P. 819–824, 7 FIGS., 4 TABLES.

Seismic wave velocity investigation at The Geysers-Clear Lake geothermal field, California

Harsh K. Gupta*, Ronald W. Ward*, and Tzeu-Lie Lin*

ABSTRACT

Analysis of *P*- and *S*-waves from shallow microearthquakes in the vicinity of The Geysers geothermal area, California, recorded by a dense, telemetered seismic array operated by the U.S. Geological Survey (USGS) shows that these phases are easily recognized and traced on record sections to distances of 80 km. Regional average velocities for the upper crust are estimated to be 5.49 ± 0.07 and 2.98 ± 0.07 km/sec for *P*- and *S*-waves, respectively. Poisson's ratio is estimated at 23 locations using Wadati diagrams and is found to vary from 0.13 to 0.32. In general, the Poisson's ratio is found to be lower at the locations close to the steam production zones at The Geysers and Clear Lake volcanic field to the northeast. The low Poisson ratio corresponds to a decrease in *P*-wave velocity in areas of high heat flow. The decrease may be caused by fracturing of the rock and saturation with gas or steam.

INTRODUCTION

The Geysers geothermal area, with current production of 950 MW, is the largest geothermal power producing installation in the world. It is located in northern California in the vicinity of the Clear Lake volcanic system where igneous activity is believed to have occurred in the recent past (Donnelly et al, 1977). The earliest microearthquake investigations at The Geysers geothermal area were carried out by Hamilton and Muffler (1972). They located 53 microearthquakes within 10 km of The Geysers during a three-week period of operation of eight seismograph stations. Most of these earthquakes were located in a 4-km long and 1-km wide zone passing through the geothermal field with the focal depth varying from near-surface to 4 km. Marks et al (1978), using the USGS seismic array, identified two clusters of microearthquakes probably related to two independent pressure sinks resulting from steam production. They found that the earthquakes at The Geysers are confined to depths of less than 5 km, whereas earthquakes along Rodgers Creek and Mayacama faults south and west of The Geysers occur at depths greater than 5 km. In another, more recent seismic study, Bufe et al (1980) deduced tectonic stress orientation and the deep pattern of faulting. From the spatial distribution of earthquakes and their continuous occurrence in The Geysers in contrast to their episodic occurrence outside the production zone, Bufe et al (1980) strongly suggest that The Geysers's seismicity is induced. These observations are consistent with the surface deformation (Lofgren, 1978) and temporal changes in gravity (Isherwood, 1980) reported for the region.

Iyer et al (1979), on the basis of teleseismic delays, inferred molten rocks beneath Mount Hannah and a highly fractured steam reservoir beneath The Geysers. Ward and Young (1980) and Young and Ward (1981) obtained a two-dimensional (2-D) Q model of The Geysers-Clear Lake geothermal area using attenuation data of teleseismic events. They found a zone of high attenuation located in the middle crust centered southeast of Mount Hannah. Majer and McEvilly (1979) obtained a regional upper crustal *P*-wave traveltime curve extending to a distance of 45 km using data recorded from two explosions at several seismic stations operating in the vicinity of The Geysers-Clear Lake geothermal field. However, no *S*-wave velocity structure has been determined for the region. We report here our results of *P*- and *S*-wave velocity structure and estimation of the Poisson ratio using microearthquake data recorded by the USGS seismic stations.

THE DATA

The seismic stations and microearthquakes used in the present study are listed in Tables 1 and 2, respectively, and shown in Figure 1. The earthquake magnitude threshold for obtaining a hypocenter is approximately $M = 1.2$, and the location error for a blast fired south of plant no. 12 was only 200 m (Marks et al, 1978). Figure 2 shows a seismogram record section arranged at increasing epicentral distances from top to bottom for event no. 5. Figure 3, a segment of record section for event no. 6, shows *S*-phases.

Identification of *S*-phases on the vertical component instruments requires considerable care to make reliable picks. It is only possible by using dense array data and picking the clear *S*-phase arrivals on the best seismograms. It is then possible to correlate this arrival with those at other stations. The change in amplitude and/or frequency of the arrival aids in making a positive identification. The consistency of these picks for events with nearby hypocenters further supports this approach.

Manuscript received by the Editor August 14, 1980; revised manuscript received July 20, 1981.
*Center for Energy Studies, University of Texas at Dallas, P.O. Box 688, Dallas, TX 75080.
0016-8033/82/0501—819–824$03.00.

Table 1. Station parameters.

Station		Name	Latitude Degrees	Latitude Minutes	Longitude Degrees	Longitude Minutes	Elevation (m)
			North		West		
1	GCM	Cobb Mountain	38	48.45	122	45.31	1286
2	GSS	Skagg Springs	38	42.12	123	.81	282
3	GCV	Cloverdale	38	46.14	123	.89	150
4	GDC	Dry Creek	38	46.03	123	14.31	772
5	GML	McLaughlin Ranch	38	47.56	123	7.80	428
6	GMO	Moffitt Ranch	38	42.61	123	8.59	802
7	GHC	House Creek	38	36.36	123	11.81	518
8	GSM	Socrates Mine	38	46.15	122	46.87	1017
9	GGP	Geyser Park	38	45.88	122	50.65	1054
10	GHL	Highland Springs	39	2.43	123	1.12	956
11	GGL	Glenview	38	53.80	122	46.58	893
12	GPM	Pine Mountains	38	50.85	122	56.78	783
13	GBO	Black Oak	38	49.60	122	50.57	879
14	GMK	Mt. Konoctii	38	58.17	122	47.22	906
15	GSN	Snow Mountain	38	56.43	123	11.50	870
16	GHG	Hog Mountain	39	7.70	122	49.47	903
17	GAX	Alexander Valley	38	42.65	122	45.30	379
18	GRT	Round Top Mountain	38	56.32	122	40.18	619
19	GBG	Boggs	38	48.84	122	40.76	1125
20	GRM	Round Mountain	39	1.23	122	35.06	783
21	GSG	Seigler Mountain	38	52.30	122	42.58	1080
22	GAF	Pt. Arens A.F.B.	38	53.59	123	32.28	710
23	NBR	Beebe Ranch	38	15.65	122	32.99	137
24	NMW	Mi Wuk Village	38	33.03	122	43.37	134
25	NWR	Wright Ranch	38	27.42	122	53.26	50
26	NTM	Taylor Mountain	38	23.15	122	40.83	105
27	NCF	Cornfield Road	38	19.28	122	47.73	98
28	NLN	Lincoln School	38	9.15	122	42.75	120
29	NSH	St. Helena Road	38	31.20	122	36.43	328
30	NSP	Sears Point	38	10.96	122	27.20	88
31	NNX	Mix Canyon	38	24.60	122	3.44	177
32	NHM	Hamilton Ranch	38	9.28	121	48.02	65
33	NCD	Cavedale Road	38	22.19	122	27.70	620
34	CDU	Duarte Ranch	38	1.78	122	.05	168
35	NGV	Green Valley Ranch	38	16.84	122	12.89	257
36	CBW	Brookwood Road	37	55.45	122	6.40	221
37	CAC	Antioch	37	58.57	121	45.62	74
38	NFR	Fort Ross	38	31.36	123	9.66	528
39	NHB	Healdsburg	38	35.36	122	54.54	165
40	NMH	Mt. St. Helens	38	40.17	122	37.93	1311
41	NMT	Middletown	38	48.34	122	26.76	422
42	CRA	San Ramon	37	46.03	121	56.25	171
43	CNC	Norris Canyon Road	37	45.36	121	59.40	306

Table 2. Events used in study.

Event no.	Origin date	Time	Epicenter Latitude	Epicenter Longitude	Focal depth (km)	Magnitude
	(YYMMDD)		NORTH	EAST		
1	750701	1444	38°41.00′	122°48.80′	6.8	1.1
2	750912	1833	38°43.80′	122°39.00′	5.0	1.1
3	770208	1919	38°56.82′	122°35.35′	4.87	1.12
4	770303	0153	38°42.07′	122°55.40′	5.23	1.27
5	770309	1400	38°47.39′	122°58.38′	5.3	1.40
6	770521	2252	38°45.84′	122°56.56′	5.92	0.86
8	770817	0337	38°47.68′	122°39.00′	7.72	1.05
9	770831	0240	38°40.87′	122°54.15′	6.06	1.20
11	770916	1053	38°39.92′	122°46.32′	5.44	1.31
12	770918	0044	38°39.85′	122°46.30′	5.29	1.00
13	770918	0242	38°40.00′	122°46.23′	5.24	1.17
14	770920	0110	38°47.02′	122°37.85′	7.88	1.46
15	770923	1400	38°39.76′	122°46.27′	5.50	1.24
16	771012	1501	38°40.60′	122°46.25′	5.18	1.44

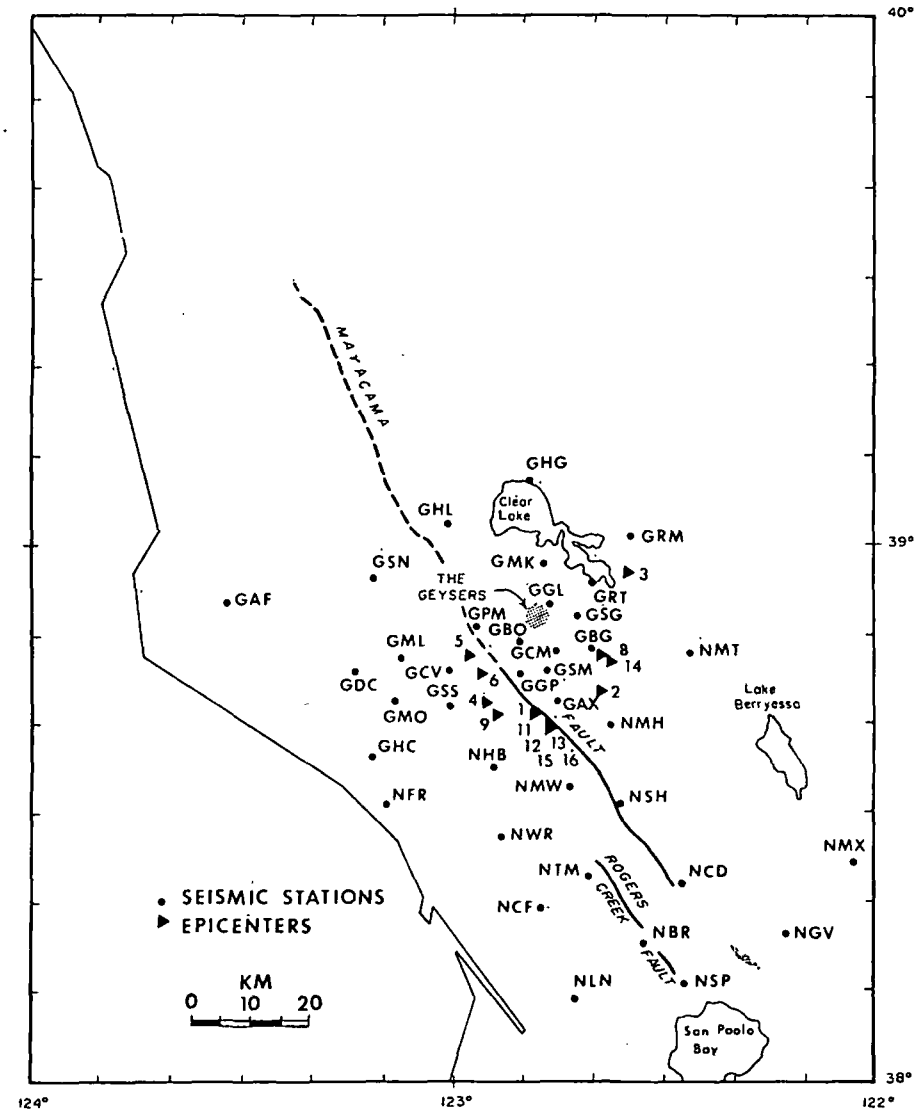

FIG. 1. *Map of seismic stations and epicenters used in this study.*

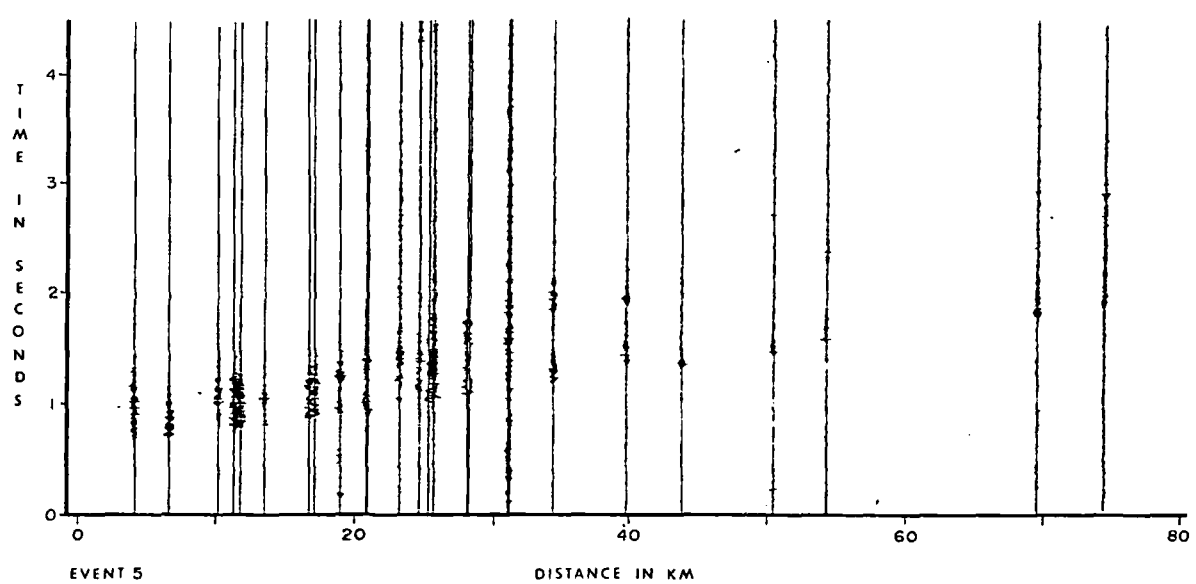

FIG. 2. Typical seismogram record section versus distance for event no. 5.

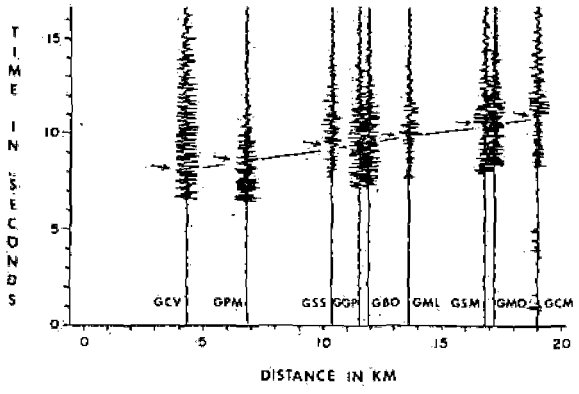

FIG. 3. Segment of seismogram record section versus distance for event no. 6 showing the clarity of the S-wave arrival.

REGIONAL P- AND S-WAVE VELOCITIES

As may be noted from Table 1, seismic stations used in the present study have a considerable variation in their elevations. The highest station NMH (Mount St. Helen) has an elevation of 1311 m, while the lowest station NWR (Wright Ranch) has an elevation of 50 m. Majer and McEvilly (1979) corrected P-wave traveltimes to various stations for elevation with respect to a reference station using 4.0 km/sec velocity. We investigated the effect of using various velocities for elevation correction of both P- and S-wave traveltimes. After a linear least-squares fit of the traveltime residuals, we found that the best results (lowest traveltime residuals) were obtained when no elevation correction was applied. Bufe (personal communication) reached a similar conclusion. Figures 4 and 5 show P- and S-wave traveltimes versus distance plots for all the events. Most of the data for P-waves (159 out of a total population of 166) and all the data for S-waves lie in the epicentral distance range of 6 to 45 km. The average velocities for P- and S-waves, obtained by linear least-squares fit (with focal depth consideration in epicentral distance calculations) are 5.49 ± 0.07 and 2.98 ± 0.07 km/sec, respectively. Majer and McEvilly's (1979) regional traveltime plot shows a break at about 15 km. We divided our traveltime data into two groups, i.e., for epicentral distances less than 15 km and greater than 15 km. Linear least-squares fits were made to these two sets of data. As can be noted in Table 3, for epicentral distances greater than 15 km, the errors are less than 0.10 and 0.12 km/sec for P- and S-waves, respectively. The large standard deviations of the velocity estimates for distances less than 15 km indicate lateral heterogeneity at shallow depths.

POISSON'S RATIO

Poisson's ratio has been estimated at a few geothermal areas. Combs and Rotstein (1976) estimated a low Poisson's ratio of 0.16 at the Coso Geothermal area, China Lake, California, and inferred that the shallow subsurface is either deficient in liquid water saturation or, more likely, the void spaces are filled with steam. Gupta and Nyman (1977) estimated Poisson's ratio at the East Mesa geothermal field, California. Majer and McEvilly (1979) reported Poisson's ratio at four seismic stations in The Geysers area varying from 0.15 to 0.27.

In this study, Poisson's ratio was estimated for a number of seismic stations using multiple events as well as at a number of hypocenters using multiple seismic station data. The technique used is the construction of a Wadati diagram of S-P traveltimes with P-wave traveltime (e.g., Majer and McEvilly, 1979). In Figure 6, S-P intervals are plotted against P-wave traveltime for event no. 5. A straight line is fitted to the data, minimizing the square error. The slope of the line $K - 1$ where $K = V_p/V_s$ gives Poisson's ratio σ by

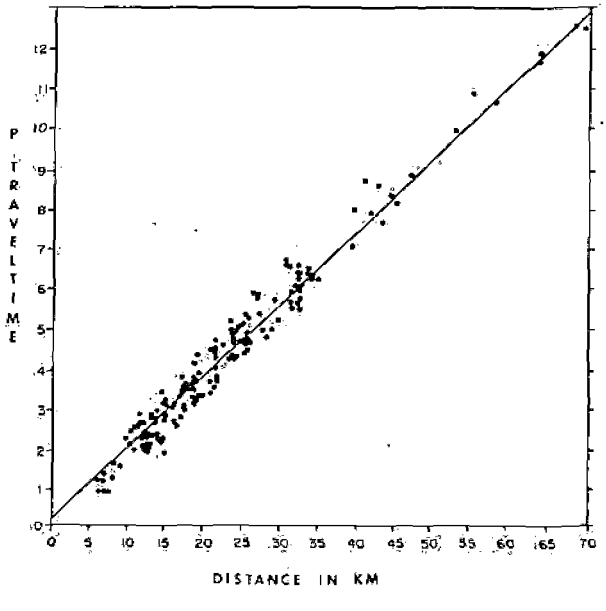

FIG. 4. P-wave traveltime versus epicentral distance for all events.

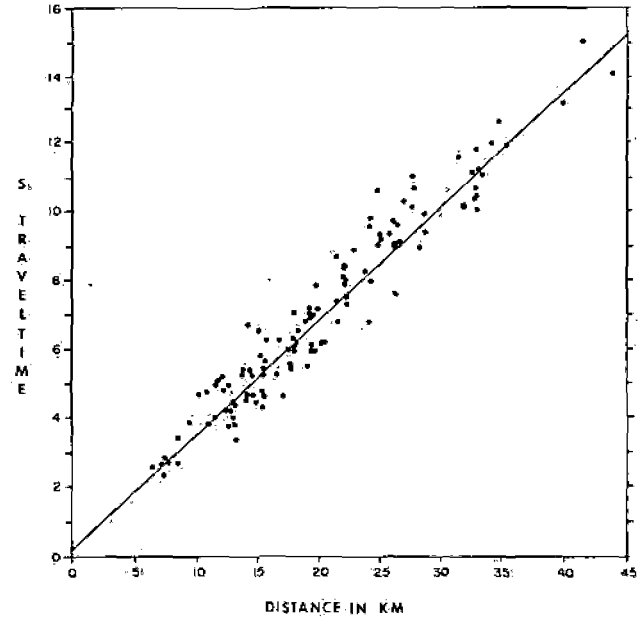

FIG. 5. S-wave traveltime versus epicentral distance for all events.

Table 3. Estimates of *P*- and *S*-wave velocities at The Geysers-Clear Lake geothermal field.

P-wave velocities (km/sec)		
Total	$\Delta < 15$ km	$\Delta > 15$ km
5.4945 ± 0.0718	5.2509 ± 0.4665	5.5894 ± 0.0973
S-wave velocities (km/sec)		
Total	$\Delta < 15$ km	$\Delta > 15$ km
2.9867 ± 0.0719	3.1542 ± 0.3392	2.9648 ± 0.1149

Note: The entire data set and subsets of epicentral distances of <15 km and >15 km were used.

Table 4. Poisson's ratio at various locations at The Geysers (Figure 7).

Location	Poisson's ratio	Location	Poisson's ratio
GSM	0.17 (0.11)	NSH	0.123 (−0.06)
GBG	0.13 (0.32)	NMW	0.32 (0.00)
GSG	0.13 (0.63)	NHB	0.28 (−0.06)
GBO	0.15 (0.68)	no. 4	0.22
GCM	0.16 (0.25)	no. 5	0.30
GGP	0.27 (−0.1)	no. 6	0.24
GAX	0.27 (−0.04)	no. 9	0.27
GSS	0.32 (−0.04)	no. 11	0.20
GPM	0.29 (0.12)	no. 12	0.28
GML	0.32	no. 13	0.26
NMH	0.30 (−0.003)	no. 14	0.26
NMT	0.22 (0.12)	no. 15	0.32
		no. 16	0.28

Note: The values within parentheses are average traveltime residuals calculated by Iyer et al (1979).

$$\sigma = \frac{K^2 - 2}{2(K^2 - 1)}$$

From Figure 6, K is found to be 1.8685, and Poisson's ratio is estimated to be 0.29 from 19 samples, with a goodness of fit of 0.947 and correlation coefficient of 0.973. Poisson's ratio is also estimated using the slope of a linear least-squares error fit of *P*- and *S*-wave traveltime data. Our results are given in Table 4, and the locations of Poisson's ratio estimates are shown in Figure 7. In general, Poisson's ratio is found to be lower at the locations close to the steam production zones at The Geysers and beneath the Clear Lake volcanic field to the northeast. Specifically, the Mercuryville fault separates the zone of low Poisson's ratio to the northeast side from the normal zone on the southwest side of the fault.

CONCLUSIONS

Several interesting and important features of *P*- and *S*-wave traveltimes in the vicinity of The Geysers are presented here. The regional *P*-wave velocity reported here (5.49 ± 0.07 km/sec) is higher than 5.04 km/sec reported by Majer and McEvilly (1979). The *S*-wave velocity for the region, reported for the first time, is 2.98 ± 0.07 km/sec. We used a set of well-distributed earthquakes for these velocity estimates. Poisson's ratios were estimated at 23 locations and found to vary from

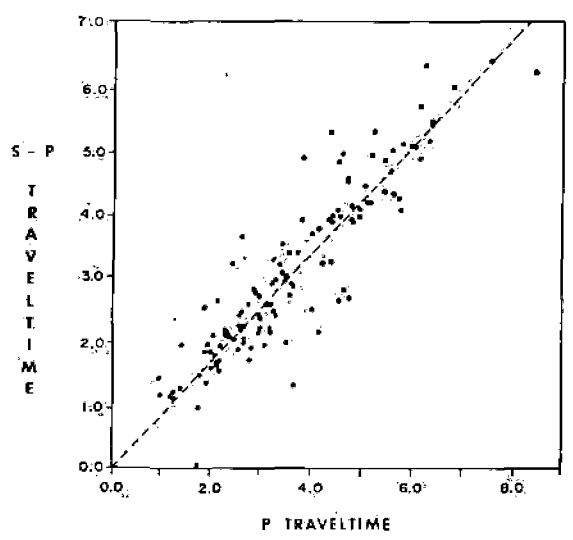

FIG. 6. Wadati diagram of *S-P* traveltime difference versus *P*-wave traveltime for event no. 5.

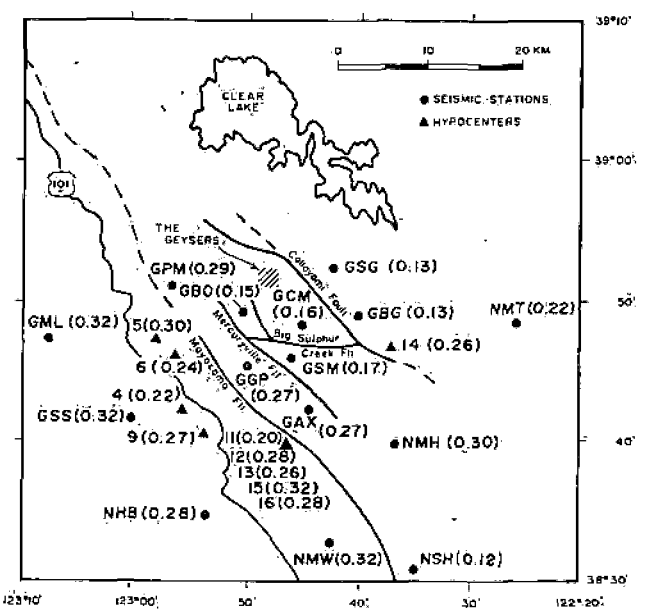

FIG. 7. Map showing Poisson's ratio estimates at seismic stations and epicenters in The Geysers-Clear Lake region.

0.13 to 0.32. Poisson's ratios at locations GBO, GSM, GCM, GSG, and GBG are low (less than 0.2), while at other locations they are normal (larger than 0.2). The low Poisson's ratios appear to be associated with zones of steam production. The Mercuryville fault appears to limit the boundary of the steam reservoir on the southwest. It is interesting to note that seismic stations having low Poisson's ratio are associated, in general, with large teleseismic *P*-wave delays, as reported by Iyer et al (1979), while stations with normal Poisson's ratios do not show significant delays (Table 4). This implies that a local decrease in *P*-velocity is probably responsible for the observed decrease in the Poisson's ratio.

A decrease in *P*-wave velocity with constant *S*-wave velocity results from a change in the compressibility of the rock. Intense fracturing of the upper crust in areas of high heat flow is a plausible explanation based upon analysis of these data. The recording of three-component, more densely spaced arrays may corroborate this preliminary interpretation of the variation of Poisson's ratio.

ACKNOWLEDGMENTS

The data analyzed in this study were provided by W. H. Bakun of the U.S. Geological Survey in Menlo Park, California. Useful discussions were held with Chuck Bufe and H. M. Iyer, also of USGS. Dr. Iyer made several useful suggestions on the manuscript. The calculations were performed at UTD on the Geosciences Program PRIME-550 computer. The assistance of Belle Koblentz, Del Hunt, Janet Garlow, and Elizabeth Partlow in preparing the manuscript is gratefully acknowledged. This research was supported by the U.S. Geological Survey, Dept. of the Interior, under USGS grant no. 14-08-0001-G-426 and the National Science Foundation grant EAR-78-23422.

REFERENCES

Bufe, C. G., Marks, S. M., Lester, F. W., Ludwin, R. S., and Stickney, M. C., 1980, Seismicity of The Geysers-Clear Lake region: U.S.G.S. open file rep.

Combs, J., and Rotstein, Y., 1976, Microearthquake studies at the Coso geothermal area, China Lake, California: Proc. 2nd UN Symp. on the dev. and use of geothermal resources, v. 2, p. 909.

Donnelly, J. M., Hearn, B. C., Jr., and Goff, F. E., 1977, The Clear Lake volcanics, California: Geol. and Field Trip Guide, p. 25.

Gupta, H. K., and Nyman, D., 1977, Short period surface wave dispersion studies in the East Mesa geothermal field, California: Geothermal Res. Council Trans. v. 1, p. 123.

Hamilton, R. M., and Muffler, L. J. P., 1972, Microearthquakes at The Geyser Geothermal Area, California: J. Geophys. Res., v. 77, p. 2081.

Isherwood, W. F., 1980, Geophysical overview of The Geysers, California: U.S.G.S. open file report.

Iyer, H. M., Oppenheimer, D. H., and Hitchcock, T., 1979, Abnormal *P*-wave delays in The Geysers-Clear Lake geothermal area, California: Science, v. 204, p. 495.

Lofgren, B., 1978, Monitoring crustal information in The Geysers-Clear Lake geothermal area, California: U.S.G.S. open file rep.

Majer, E. L., and McEvilly, T. M., 1979, Seismological investigations at The Geysers geothermal field: Geophysics, v. 44, p. 246.

Marks, S. M., Ludwin, R. S., Louie, K. B., and Bufe, C. G., 1978, Seismic monitoring at The Geysers geothermal field, California: U.S.G.S. open file report, no. 78-798, p. 26.

Ward, R. W., and Young, C. Y., 1980, Mapping seismic attenuation within geothermal systems using teleseisms with application to The Geysers-Clear Lake region: J. Geophys. Res., v. 85, p. 5227–5236.

Young, C. Y., and Ward, R. W., 1981, Attenuation of teleseismic *P*-waves in The Geysers-Clear Lake region, California: U.S.G.S. Prof. Paper, no. 1141.